Tidal Modeling of Glacier Bay, Alaska - Methodology, Results, and Applications

D.F. Hill[1]
Department of Civil & Environmental Engineering
The Pennsylvania State University
University Park, PA 16802

June 2007

[1]Contact: 814.863.7305, dfh@engr.psu.edu

Contents

List of Figures

List of Tables

Preface

The work described in this report is the result of a 10 day kayak trip in Glacier Bay during the summer of 2004 and a healthy dose of serendipity. On the way to an up-bay drop off point, the author overhead two other kayakers discussing acoustic doppler current profilers. This is decidedly *not* in the lexicon of your average kayaker and it certainly caught the ear of the author. The ensuing conversation with Dr. Lisa Etherington (then of the U.S.G.S.) and a well-timed sabbatical leave granted by the Pennsylvania State University to the author during the 2005-2006 academic year are responsible for the following pages.

The author is indebted to Dr. Etherington for her interest in and enthusiasm for a hydrodynamic study of the tides in Glacier Bay and for her provision of many useful data and reports regarding the Bay. Additional thanks are due to Jennifer Mondragon, Erika Madison, and Jennifer Fisher, all of whom provided valuable physical data to the author. This work was financially supported, in part, through a grant from the National Park Service. The author would like to also acknowledge the significant assistance he received from Lewis Sharman of the NPS. Finally, financial assistance from the U.S.G.S. allowed the author to attend and participate in the 2004 Glacier Bay Science Symposium.

This report serves two very different purposes and two very different audiences. On the one hand, it is a 'user's guide' of sorts, laying out, in rather extensive detail, the steps involved in running simulations of the tidal flows in Glacier Bay. These steps involve extensive pre-processing, parallel computations on a Linux cluster, and extensive post-processing and data visualization. The path taken by the author relied heavily on freely-available software and data and this report should assist other researchers similarly interested in conducting open-source numerical studies of tidal circulation.

On the other hand, the report serves the non-specialist who is interested in the 'big picture' of tides in the Bay. Biologists and ecologists stand to benefit from an appreciation of circulations in the bay. Model runs have produced extensive data sets which are easily queried in order to produce information on tidal elevations, water velocities, and particle trajectories.

Summary

A tidal circulation model (ADCRIC) has been adapted to Glacier Bay National Park. The model domain includes Glacier Bay proper and the outlying waters of Icy Strait and Cross Sound. A very high spatial resolution was used in constructing the model domain, allowing for the resolution of many of the small islands and tidal channels in the bay.

The model is forced with tides at the open boundaries in the Gulf of Alaska and Lynn Canal, meteorological conditions, and freshwater inputs. Presently, model runs are two-dimensional (depth integrated), allowing for accurate simulation of the water surface elevation and barotropic tidal velocities.

Model output includes time series of elevation and velocity at specified locations, global elevation and velocity output, and harmonic analysis of these fields. The simulations have been validated against tidal data and known tidal constituents and have shown very good agreement.

Specific results of interest include predictions of tidal datums, such as mean high water, tidal range, etc., at all points in the model domain. Additionally, calculations of root-mean-square tidal speed have been made and are indicative of regions of strong tidal mixing. Lagrangian particle tracking has been performed and demonstrates the dramatic variability in tidal excursions in the bay.

The ADCIRC model is open source and the pre- and post-processing tools developed by the author are also freely available. The net effect of this is a modeling package that is available to any interested scientist.

Future work on this project is centered upon extending the model to three dimensions. Given the strong freshwater inputs to Glacier Bay and the documented strong vertical stratification, this step is essential to a full understanding of the baroclinic currents in the bay.

Chapter 1

Introduction

Glacier Bay National Park (Fig. 1.1), located in southeast Alaska, attracts the attention of the public and the scientific community alike. For the public, the draw usually includes the mountains, the tidewater glaciers, and the wildlife. For the scientist, the attraction has many facets. First, Glacier Bay represents a nexus of freshwater, marine, and terrestrial environments. This variety of environment leads to a similarly rich variety in marine mammals, seabirds, and fishes.

As described by Etherington *et al.* (2007), Glacier Bay is also a unique environment due to the rapid deglaciation (Figs. 1.2-1.3) that has occurred over the past century. This rapid retreat has clearly had significant changes (for example, the bathymetry) on the estuarine environment of Glacier Bay.

Finally, the Bay's status as a national park brings with it a unique status, in terms of fisheries activity. Motivated by the desire to protect resident and sensitive species and to provide opportunities for science benefitting fisheries and marine ecosystems, legislation in the late 1990's established immediate and phased closures of the Bay proper to commercial fishing activity.

1.1 Oceanography of Glacier Bay

From an oceanographic point of view, Glacier Bay is exceptionally complex. For a full discussion of the oceanographic processes in Glacier Bay, the reader is referred to reports by Hooge & Hooge (2002) and Etherington *et al.* (2004). Several valuable reports, data, and analysis tools are found at http://www.absc.usgs.gov/glba/oceanography/index.htm.

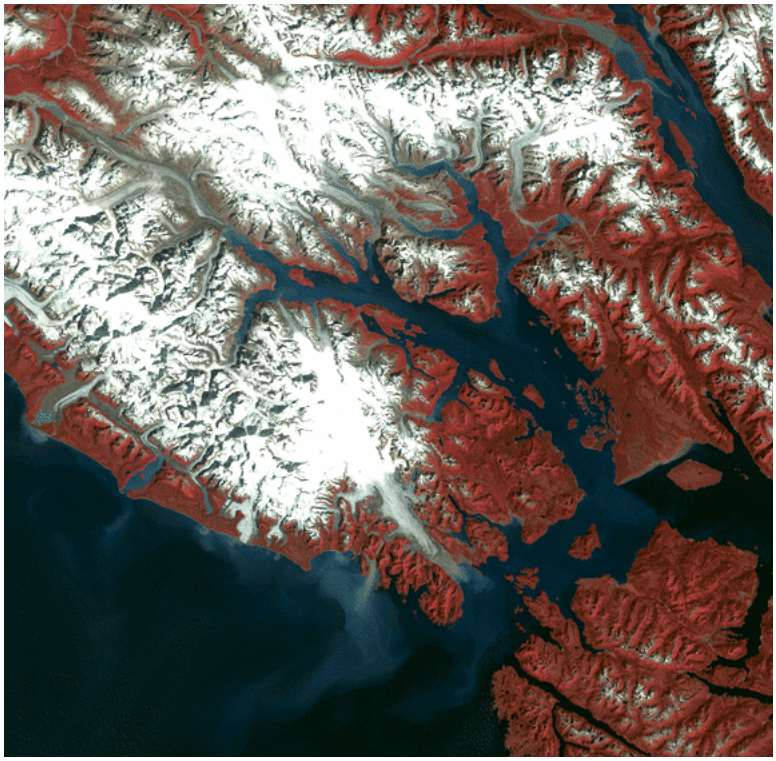

Figure 1.1: Satellite image of Glacier Bay National Park. Photo credit: NASA (http://glacier-bay.gsfc.nasa.gov/).

Briefly, Glacier Bay is a fjord estuarine system subject to large values of freshwater input, sedimentation, and tidal range. There are many deep basins, with depths on the order of 500 m, and many shallow sills, with depths on the order of 25 m. The steep gradients in bathymetry, along with the vigorous tidal currents, yield regions of significant turbulent mixing of bay waters.

In addition to the spatial complexity of the bay's physical environment, there is significant temporal complexity as well. The annual variation in precipitation, solar radiation, and (air) temperature lead to strong variations in salinity and (water) temperature, and therefore density. The annual hydrograph (runoff) is further complicated by the strong input due to meltwater. A cartoon of these and other major processes operating in the bay is given in Fig. 1.4.

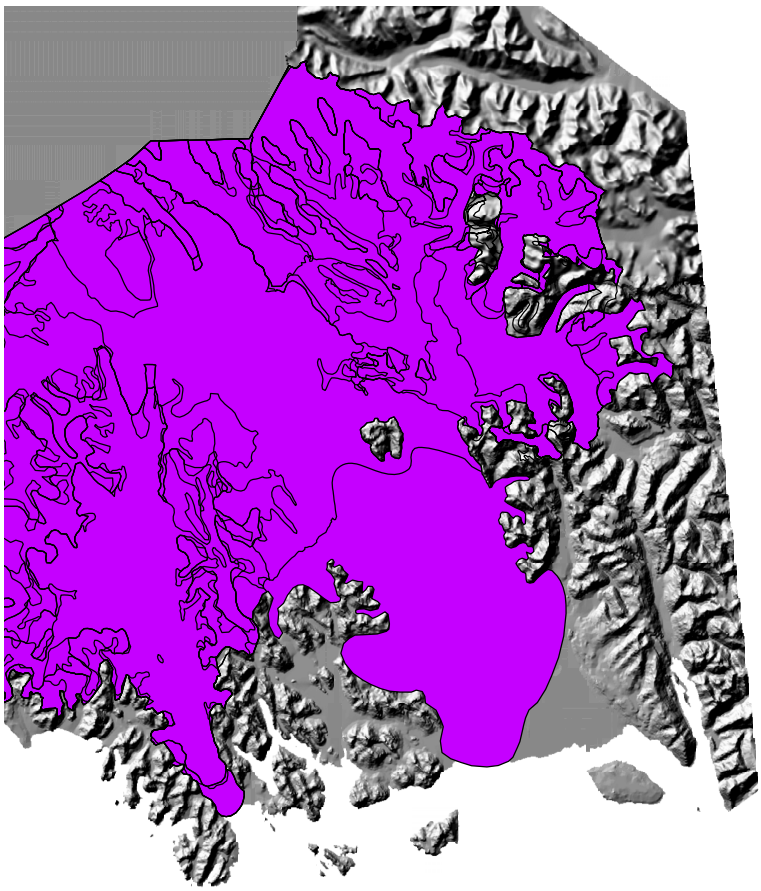

Figure 1.2: Glacier coverage in 1700; source: Glacier Bay Ecosystem CD.

1.2 Scope of Present Work

The work described in this report is intended to begin to fill an important gap in the knowledge of physical processes in Glacier Bay. As reviewed in Hooge & Hooge (2002), Etherington *et al.* (2004), and Etherington *et al.* (2007), there has been a great deal of effort invested in oceanographic data collection and analysis in the bay over the past 15 years. However, there has not been a similar effort invested in developing the ability to computationally model the tidal flows in the bay. The present report summarizes the initial steps that have been taken towards this goal.

The benefits of developing a computational model are myriad. Such a

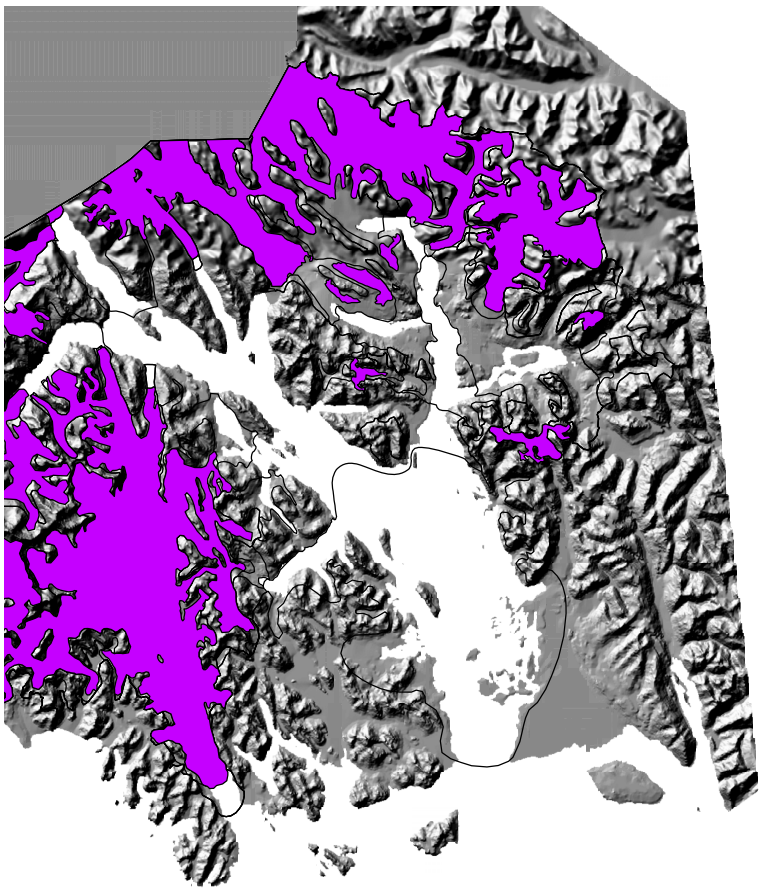

Figure 1.3: Glacier coverage in 1985; source: Glacier Bay Ecosystem CD.

model will allow park managers to obtain information about physical conditions in park waters at temporal and spatial resolutions that would be prohibitive, in terms of data collection. Additionally, a computational model allows the user to computationally explore the linkages between input and output variables, thereby helping to better understand what variables are of primary controlling importance. Finally, a model will allow users to make and test hypotheses based upon expected future conditions in the bay. For example, if glacial retreat (and hence freshwater input) accelerates, what effect will this have on tidal elevations and current patterns in the bay?

The development of a computational tidal model in no way diminishes the importance of or serves to replace regular data collection. First of all,

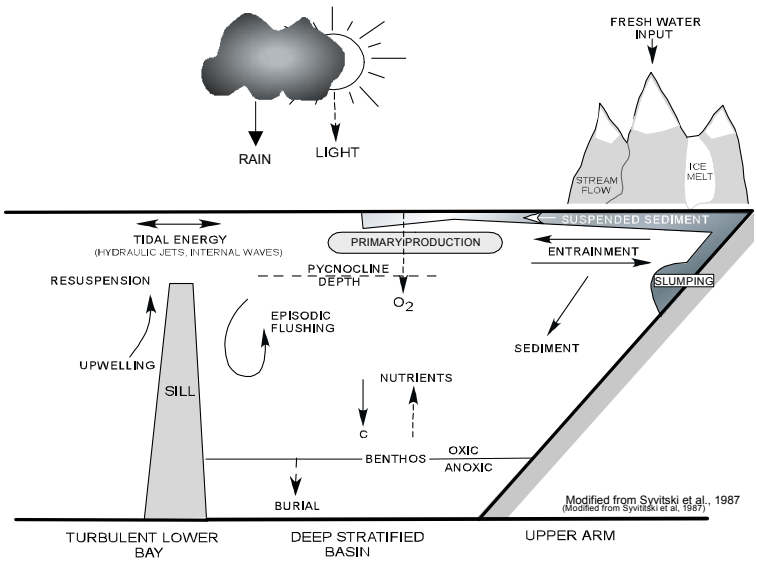

Figure 1.4: Conceptual model of the major oceanographic processes in Glacier Bay. Figure is reproduced from Hooge & Hooge (2002), and is based upon a figure from Syvitski *et al.* (1987).

data are required in order to validate the output of models. Second, no model will ever capture the entire range of processes in the bay. In order to keep computational costs reasonable, it is inevitable that compromises (for example, in how well resolved the bathymetry and coastline are) are made. An important point to keep in mind is that the data are the true picture of the bay's environment and that any model will be, at best, an approximation to this reality.

1.3 Study Approach

The approach taken by the author has been one of striking a balance between accuracy, pragmatism, and accessibility. The ultimate goal, or course, would be a low-cost computational model that fully resolves all of the fine-scale bathymetric and topographic features of the bay. In addition, the model is desired to be fully three-dimensional and baroclinic (resolving the vertical density profile). Finally, the model would be forced with spatially variable

meteorological input and freshwater inflows.

The reality is that this would be an excessively onerous computational task and would result in a product that the author, but perhaps no one else, would be able to make use of. The author has therefore taken steps to keep computational requirements modest and to make the end product accessible to a generalist. One aspect of this is the choice between commercial and open-source software. The core model used by the author (and discussed in the following chapter) is available as part of a commercial and expensive software package. The chief benefits of this package are useful graphical user interfaces (GUIs) for pre- and post-processing. However, the 'engine' itself (the tidal hydraulics code) is open-source and is distributed freely (without the GUIs) for research purposes. Therefore, the author has taken the approach of working with the freely-available code and developing Matlab-based supporting tools to aid the user.

To summarize the present capabilities of the tidal model:

1. Determination of tidal stage and two-dimensional (depth-averaged) velocities.

2. Inclusion of meteorological (wind and pressure) forcing.

3. Inclusion of freshwater input.

4. Harmonic analysis (this allows for the determination of tidal datums such as mean higher high water (MHHW), mean sea level (MSL), etc.).

5. Two-dimensional dispersion of passive tracers.

6. Calculation of pathlines (this traces the path taken by a surface drifter buoy, for example).

7. A domain that includes the bay proper, as well as Icy Strait and Cross Sound.

Chapter 2

ADCIRC Model - Overview, Compilation, and Execution

This chapter deals directly with the ADCIRC model, which is the underlying tidal hydraulics model used by the author. It gives a brief overview of the model's capabilities, which should be of interest and accessible to the generalist. Additionally, this chapter provides highly specific details on how to access, compile, and run ADCIRC. This information will be of interest only to individuals interested in running ADCIRC themselves. As will be discussed in detail later, ADCIRC can be run in a 'serial' fashion on a single computer or in a 'parallel' fashion on a cluster of computers. The details on parallel operation will necessarily be specific to the high-performance computing resources found at Penn State.

2.1 Model Overview

The source code for the ADCIRC model, along with a user's manual, theory report, an email listserv, and other resources are all available online at http://www.adcirc.org. The development of ADCIRC is generally attributed to Luettich & Westerink (1991). Since that time, many modifications and upgrades to the model have been made and ADCIRC presently enjoys very wide use among the academic community and federal agencies such as the Army Corps of Engineers, NOAA, and the Naval Research Laboratory.

2.1.1 Features and Capabilities

ADCIRC presently has the ability to operate in two-dimensional and three-dimensional barotropic (vertical density profile not resolved) mode. A three-dimensional baroclinic (vertical density profile resolved) is under development. In barotropic mode, the model solves for water elevation and water velocity.

The model uses an unstructured finite-element mesh to represent the domain. This approach is optimal for complex bathymetry and coastline boundaries as elements of varying size can be incorporated as needed (Fig. 2.1).

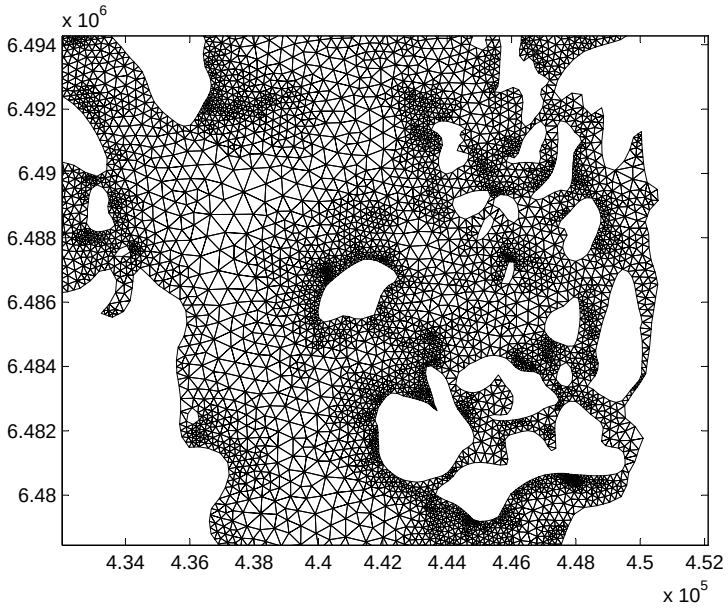

Figure 2.1: Finite element mesh of the region near the Beardslee Islands.

ADCIRC is a Fortran program which requires, at a bare minimum, two input files to run:

1. fort.14: this file describes the structure of the finite element mesh (see Chapter 3).

2. fort.15: this file is a parameter file that describes the particulars of the current ADCIRC run (see Chapter 4). This file is highly customizable

depending upon which features the user wishes to incorporate.

In addition to these files, there are many optional files that may or may not have to be present, depending upon which features the user wishes to incorporate into a particular run. For example, note that the ADCIRC model can be 'forced' by the following:

1. Gravity / tidal potential. These effects are dominant in most simulations. For a closed basin, such as one of the Great Lakes, tides will be forced due to the gravitational attraction on the water in the closed basin. For domains that have an 'open boundary,' tidal information must be specified on these open boundaries.

2. Meteorological conditions. One of the primary applications of ADCIRC is to storm surge predictions during large storm events. Users wishing to incorporate meteorological forcing will need to develop a fort.22 file (see Chapter 6).

3. Freshwater inflows. ADCIRC has the ability to incorporate freshwater inputs, i.e. rivers, into its simulations. Users wishing to models domains with river inflows will need to develop a fort.20 file (see Chapter 5).

One additional 'optional' input file is associated with the transport of passive scalars. Users wishing to study the dispersal of such tracers in the water column will need to provide a fort.10 file, which simply describes the initial concentration field in the domain. This feature may be of particular interest to biologists interested in the dispersal of the larvae of any number of species.

2.1.2 Model Output

Regarding the output of the model, ADCIRC provides for great flexibility. For example, the user can specify that water surface elevations and velocities be written only at selected points in the domain (fort.61 and fort.62 files, respectively). Alternatively, output at *all* points in the domain can be requested (fort.63 and for.64, respectively, for elevation and velocity output).

An additional feature of ADCIRC is that it has the ability to perform harmonic analysis of the elevation and velocity fields. In other words, ADCIRC, following a sufficiently long run, is able to determine the tidal constituents (amplitudes and phases) at either selected points in the domain (fort.51 and

fort.52, respectively, for elevation and velocity) or at all points in the domain (fort.53 and fort.54, respectively, for elevation and velocity). These files provide valuable information about the tides and currents at all points in a model domain. Presently, knowledge of this information is limited to very sparse NOAA tidal stations or tidal databases such as the Eastern Pacific Tidal Database (http://www.unc.edu/ims/ccats/tides/tides.htm), which does not cover Glacier Bay proper.

2.2 Model Compilation

In this section, specific instructions on compiling the ADCIRC source code (Fortran) into an executable are provided. When the source code is downloaded and unzipped, a file folder structure as shown in Fig. 2.2 is obtained.

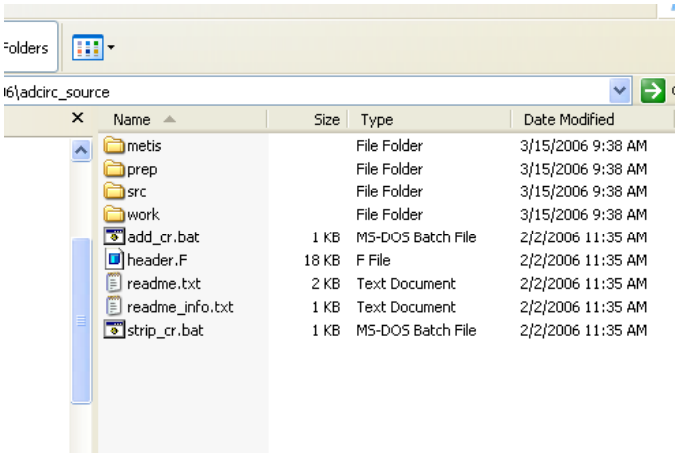

Figure 2.2: File folder structure obtained after unzipping ADCIRC source code.

2.2.1 Serial Model

Compilation of the source code is a platform dependent option. The following describes the steps required to compile a serial version of ADCIRC on the Linux clusters available at Penn State. These resources are described in detail at http://gears.aset.psu.edu/hpc/index.shtml. The web pages therein de-

scribe the different clusters, how to obtain an account, and how to access this account using the secure shell client (http://css.its.psu.edu/internet/ssh/).

With an active and connected account on one of the clusters (e.g. lionxo.aset.psu.edu), it is a simple matter to use the ssh client (Fig. 2.3) to upload the ADCIRC source files to the account.

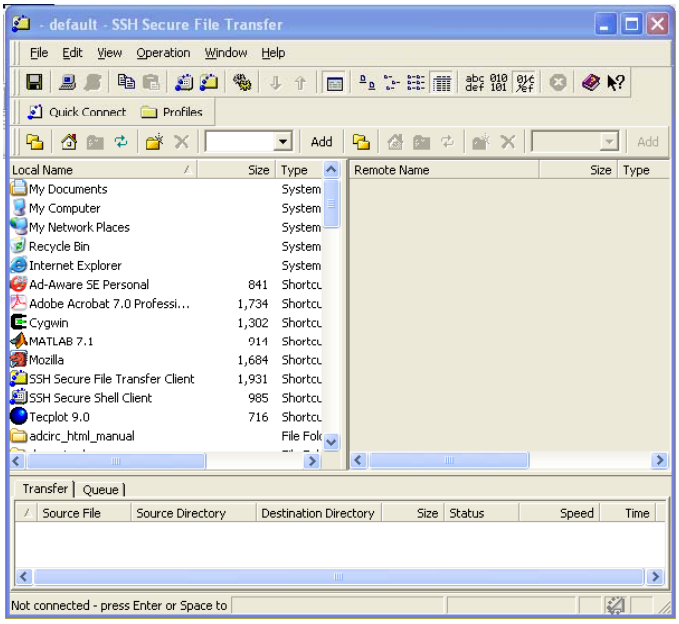

Figure 2.3: Graphical user interface of the ssh client.

Next, using a terminal window, change directories to the *work* folder. Third, before compiling, the permissions on the file *config.guess* must be changed with the command

```
>> chmod +x config.guess
```

Finally, issuing the command

```
>> make adcirc
```

will result in the creation of the executable file *adcirc*. At this point, the model is ready to run and can be executed with the simple command

```
./adcirc
```

2.2.2 Parallel Model

The ADCIRC model source code has been parallelized to run on interconnected processors. The obvious advantage of this is decreased run times. If a run can be spread out over 8 processors, it should run approximately 8 times faster. Given the large computational grid (∼80,000 elements) and the small time step (∼1 second) for the present application to Glacier Bay, this is a very real consideration.

To get ADCIRC to compile, in parallel form, on the PSU Linux cluster, change directories to the *work* folder and open the file *cmplrflags.mk*. Line 9 must be changed from the existing

```
PFC       :=  mpif90
```

to the following

```
PFC       :=  mpif90 -f90=pgf90 -config=pgf90
```

Once this is done, issuing the command

```
>> make all
```

will result in the creation of five executable files: *adcprep*, *adcprep2*, *adcirc*, *padcirc*, and *adcpost*. For a parallel run, described in the next section, the 1st, 4th, and 5th of these executables will be used.

2.3 Model Execution

Once the model has been compiled, there a variety of ways in which it can be executed. The steps for both serial and parallel runs are described below.

2.3.1 Serial Model

The simplest way to run the model is to issue the command

```
>> ./adcirc
```

from the directory in which the executable file resides. The input files fort.14 and fort.15 (and others, depending upon the run) must also be present. This approach is slightly inconvenient if one has many directories containing many different input files for simulation. In this case, the executable would have to be copied into each of these folders.

A slightly different approach is to store the executable file *adcirc* in a single location, say in the directory */adcirc_files/* created in your home directory. Then, if this location is added to the *path* variable, the executable can be accessed from any directory.

In Linux, the present path can be checked by issuing the command:

```
>> echo $PATH
```

A permanent change to the path is made by opening up the file .bash_profile, found in your home directory. There, you will find a line something like

```
PATH=$PATH:$HOME/bin
```

This line should be changed to

```
PATH=$PATH:$HOME/bin:/home2/dfh4/adcirc_files
```

where /home2/dfh4/ represents (in this case mine) the user's home directory. The next time you log in, reissue the echo $PATH command and you should see the updated path.

You can now run the *adcirc* executable from any folder simply by issuing the command

```
>> adcirc
```

As before, the necessary input files must be in the directory from which the command is issued.

Batch Runs

While ADCIRC will run successfully as described above, this 'command line' operation is only of limited use on the PSU Linux clusters. This is because jobs started in this way run on the 'login' node and are limited to only one hour of run time. As alluded to above, realistic (i.e. days to weeks long) simulations with ADCIRC will require much more than one hour of computer time.

To execute longer runs, jobs must be submitted in 'batch mode.' This is done by preparing a small script file which is then sent in to start the job. For example, the following:

```
#PBS -l nodes=1:ppn=1
#PBS -l walltime=23:00:00
#PBS -j oe
cd $PBS_O_WORKDIR
echo " "
echo "started on `hostname` at `date`"
adcirc
echo " "
echo "ended at `date`"
echo " "
```

could be saved as a file called *myjob*. The command

```
>> qsub myjob
```

submits this job to be placed in the queue. A few notes:

1. The walltime places an upper bound on the computer time that will be allocated to the job. It is therefore important that one estimate the time required in order to prevent an early program termination.

2. The nodes / ppn line, as written, requests one processor. In serial form, this is all that can be utilized.

3. Finally, the *adcirc* syntax (no preceding ./) is assuming that the path variable has been changed, as described in the previous section.

The status of your request can be reviewed at any time with the command

```
>> qstat -u dfh4
```

where, in this case, dfh4 is my account user id.

2.3.2 Parallel Model

As mentioned above, ADCIRC can run in parallel fashion, thereby greatly reducing computational times. A parallel run has three main steps. The discussion below will assume that all of the relevant executables are in a location that is in the path.

1. *adcprep* - issuing this command at the prompt the user to specify the number of processors to be utilized (say 4, 8, 16, etc.). When this program is completed, the user will note that a number (the same number entered by the user) of folders will have been created.

2. *padcirc* - while this parallel version of the ADCIRC executable can be run from the command line, it is not recommended, due to the time limits discussed above. As a result, a script file should be prepared and submitted with the qsub command. The following is an example script file:

   ```
   #PBS -l nodes=4:ppn=2
   #PBS -l walltime=8:00:00
   #PBS -j oe

   cd $PBS_O_WORKDIR
   echo "Job started at ‘date‘"
   /usr/global/bin/icmpirun padcirc
   echo "Job ended at ‘date‘"
   ```

   In this script, the first line requests 4 nodes and 2 processors per node, for a total of 8 processors. This total number *must* match with the number that was specified during *adcprep*.

3. *adcpost* - when the run is complete, the user will find 'partial' input and output files in the folders that were created during the *adcprep* run. Typing *adcpost* at the command prompt will step the user through the process of recombining these individual files into global output files.

   As an aside, the author has found that the combined file is much greater in size than the sum of the individual files. Some investigation revealed that this is due to the fact that, during recombination, 'trailing zeros' are added to each line. This does not pose any problems, in terms of post-processing / visualization of the output, but it can lead to unreasonably large file sizes.

   Discussions with other researchers have led to the following 'fix' for this problem. In the file post.f, which is found in the folder *prep* in the source code distribution, one will find lines of code like:

```
 WRITE(xx,80) OUTMSG
```

where the xx is 63, 64, or some other output file designation. If this line of code is changed to

```
WRITE(xx,*) TRIM(OUTMSG)
```

and the *adcpost* code is recompiled, the trailing zeros will be eliminated.

Chapter 3

fort.14 File - Domain Mesh

The foundation of an ADCIRC simulation is the model domain mesh. This chapter gives specific information about obtaining, formatting, and refining the data required for this mesh.

3.1 Obtaining Data

3.1.1 Coastline

In preparing the mesh for the domain, one of the key ingredients is a description of the coastline. For the present application, the Coastline Extractor program, provided by the National Geophysical Data Center, was used. This database may be accessed at http://rimmer.ngdc.noaa.gov/coast/. There, a user may identify a region of interest, using an interactive web-based program, and download, in a variety of formats, available coastline data for that region.

In the present project, data were downloaded in Matlab format. In this case, the data were given in two columns representing latitude / longitude pairs describing the coastline. Distinct segments of coastline, for example different islands, are identified in the Matlab format by beginning each segment with the line 'NaN NaN.'

During the extraction and downloading process, the user is given the option of creating a graphical plot of the accessed data. An example of this is provided in Fig. 3.1.

Note that other coastline data sources exist and may be of use. For exam-

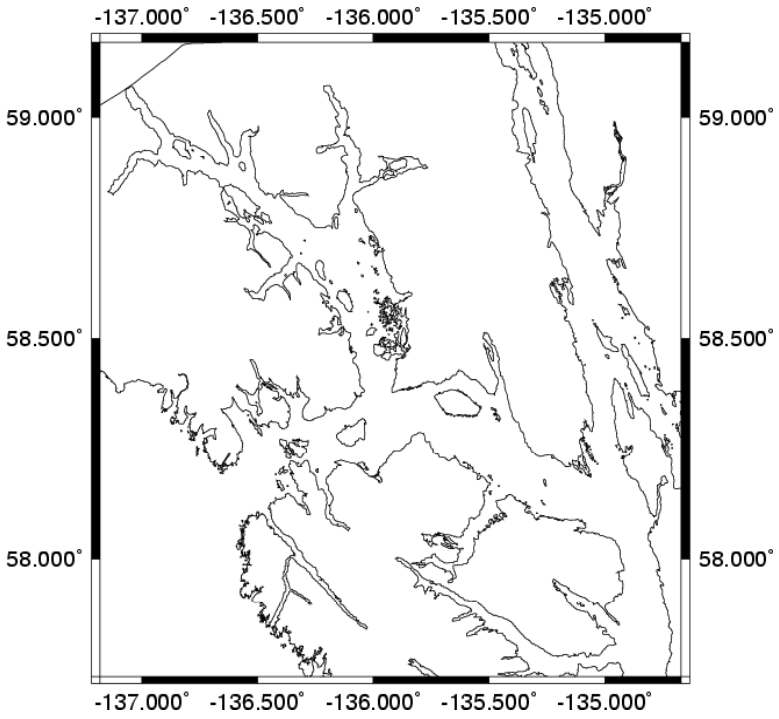

Figure 3.1: Graphical output fromt he Coastline Extractor program indicating the coastline data in the vicinity of Glacier Bay.

ple, inspection of Fig. 3.1 reveals that several of the inlets in the upper east arm of Glacier Bay appear to be truncated. This *may* be due to significant ice cover in those inlets during the time of those surveys; the exact reason is not known. Other data sources include the NOAA Shoreline Data Explorer Program, found at http://www.ngs.noaa.gov/newsys_ims/shoreline/. These additional data can be used to verify and / or fill in missing holes in the Coastline Extractor data.

3.1.2 Bathymetry Data

The other key ingredient in the construction of a finite-element mesh is the bathymetry, or depth. As with the coastline data, several excellent online sources of data exist. For example, the National Geophysical Data Center maintains a Geophysical Data System (GEODAS) that allows a user to interactively search for a wide variety of oceanographic data, including bathym-

etry. This database is found at http://www.ngdc.noaa.gov/mgg/gdas/gd_sys.html. As with the Coastline Extractor, a region of interest is identified and then the data may be downloaded in a variety of formats. Additional data can be obtained from National Ocean Service (NOS) maps and surveys at http://www.ngdc.noaa.gov/mgg/bathymetry/hydro.html.

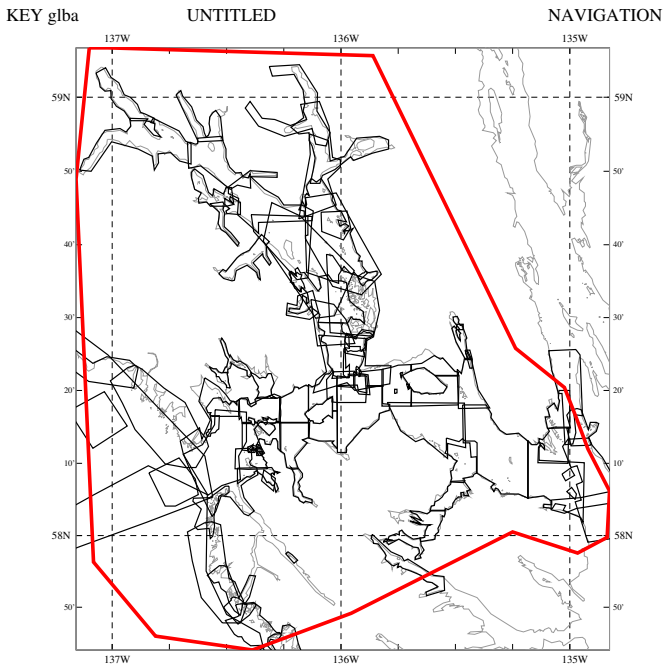

Figure 3.2: Graphical output from GEODAS indicating the bathymetry data obtained for the Glacier Bay region. The solid red line indicates the bounding polygon identified by the user. The light gray lines indicate coastlines and the heavier black lines indicate individual data sets.

Figure 3.2 shows an overview of the bathymetry data downloaded, using GEODAS, for the present application. The individual black polygons represent individual data sets from different cruises. For the present case, the data were downloaded in simple ASCII text format. In this case, each sounding is represented as a (lon, lat, depth) triplet of numbers. The datasets shown in Fig. 3.2 totalled some 800,000 soundings. A downsampled (by a factor of 20) scatter plot of the aggregated bathymetry is shown in Fig. 3.3. Here the red denotes shallow water and the blue deep water. We note in particular

the deep regions in the Alaskan Gulf, the Lynn Canal, and the upper west arm of Glacier Bay.

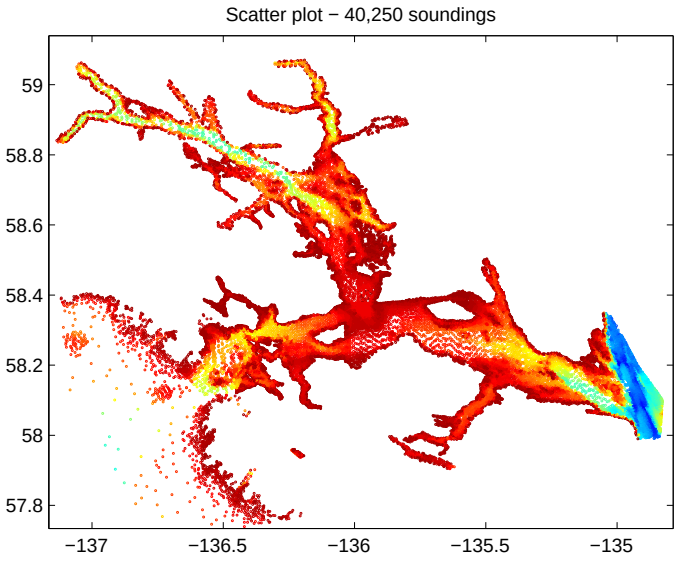

Figure 3.3: Scatter plot of domain bathymetry.

One cautionary note is illustrated in Fig. 3.4. Initial ADCIRC runs revealed unusual current patterns in the vicinity of Gustavus. A close inspection of the bathymetry data in that region revealed one survey (H08816) for which incorrect conversions appeared to have been applied. This was confirmed with NOAA and the problem was corrected both in their database and in the author's fort.14 file.

Finally, note that an inspection of the metadata from the surveys reveals that the depths are given relative to MLLW in most cases. A proper ADCIRC simulation requires depths relative to the geoid, which is well approximated by a datum such as NAVD88. The chief difficulty here is the lack of stations in Alaska where tidal datums are specified relative to a vertical datum like NAVD88. Lacking this, the adopted strategy has been to recast bathymetric depths relative to mean sea level (MSL). This was done by performing a long-term simulation with the raw bathymetric data, computing MSL and MLLW from the results, and adjusting the bathymetry. This process was iterated until satisfactory convergence was obtained.

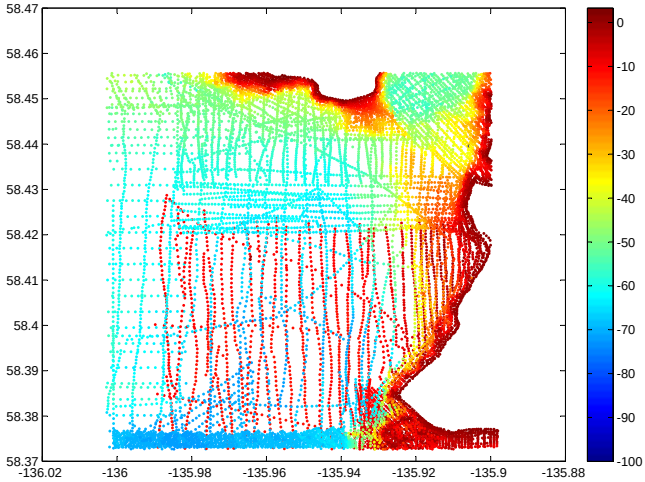

Figure 3.4: Incorrect data (red dots in the main channel) in the vicinity of Gustavus, AK.

3.2 Preparing Data

Once the necessary physical data has been assembled, the next step is conditioning this data and formatting it as required by the ADCIRC model.

3.2.1 Conditioning Coastline Data

The coastline data as obtained from the Shoreline Extractor program is not completely suitable. For example, it contains more of the coast along the Gulf of Alaska and the Lynn Canal boundaries than we require. In addition, the resolution is too fine in some spots. This, combined with the very large number of islands, many extremely small, proves prohibitive in terms of required mesh resolution. Therefore, a number of steps were taken to smooth, trim, and simplify the coastline data. These steps are enumerated below.

1. First, it was decided to run ADCIRC simulations using Cartesian coordinates, instead of latitude / longitude coordinates. This was done by using a UTM Zone 8 projected coordinate system. A free Matlab package, entitled m_map (http://www.eos.ubc.ca/ rich/map.html) makes this conversion quite straightforward.

2. Next, the raw coastline data file, as downloaded from the Shoreline Extractor, consisted of some 700 segments, some of which were mainland segments, and the bulk of which were islands. For the islands, a minimum area criterion of 2.5×10^5 m^2 was adopted, bringing the number of shoreline segments down to under 200.

3. Third, insufficient bathymetry data were found to exist in the areas of Lisianski Inlet and western Neka Bay. Therefore, the shoreline was manually edited in order to eliminate these regions from the domain.

4. Next, it was envisioned that the domain would be forced by two open boundaries, on at the west end of Cross Sound, and the other at the east end of Icy Strait. It is common, though not essential, to make open boundaries roughly semi-circular. To this end, the mainland shoreline segments along the Gulf of Alaska and Lynn Canal were 'trimmed' and then connected with semi-circles of evenly-distributed points. This is illustrated in Fig. 3.5.

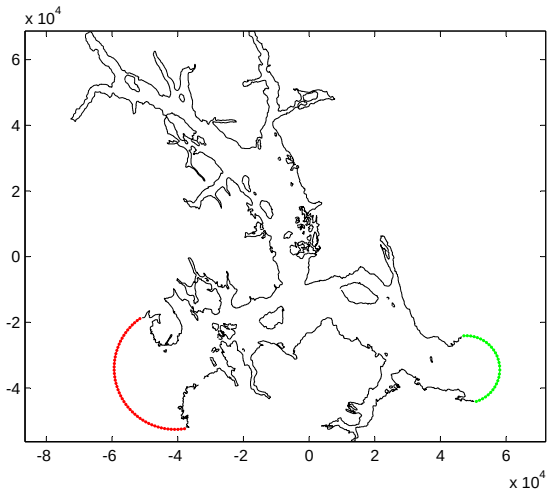

Figure 3.5: Reduced domain shoreline, with open boundaries placed at the Gulf of Alaska and the Lynn Canal.

5. Fifth, and as discussed previously, the shoreline data were inadequate in the Muir and Wachusett Inlets, artificially truncating those channels. Therefore, the shoreline data were manually edited so as to fully enclose the bathymetry data available in those locations.

6. Finally, the shoreline data, as conditioned to this point, are still irregularly spaced. Preliminary attempts at mesh generation revealed that this was very unsatisfactory, yielding very small and poorly formed elements in certain regions. As a result, the shoreline data were first evenly spaced along the shoreline, with a 400 m resolution, and then a moving window filter (in both the x and y directions) was applied to smooth the data. Figure 3.6 illustrates the before and after for a sample segment of shoreline. Clearly, this smoothing approximation results in some loss of accuracy, but this simplification is necessary if unrealistic computational demands are to be avoided. Note that many small islands do not survive this smoothing operation due to their small perimeter. The final conditioned domain shoreline therefore contains two open boundaries, two continuous mainland boundaries, and 55 islands.

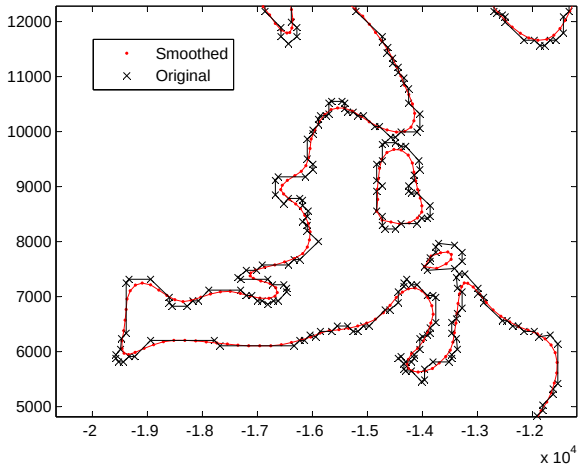

Figure 3.6: Illustration of original vs. smoothed shoreline data. Area shown is Berg Bay.

3.2.2 Conditioning Bathymetry Data

As mentioned previously, the aggregate bathymetry data from the GEODAS database consisted of some 800,000 soundings, which were downsampled to approximately 40,000. The only other required preparation to the bathym-

etry data was to convert the longitude / latitude coordinates to equivalent UTM Zone 8 projected coordinates.

3.3 Mesh Generation

Before writing the finite-element mesh information to the fort.14 file, the mesh itself must be generated. For the present project, this was accomplished using BATTRI. This is a freely-distributed (http://www-nml.dartmouth.edu/Software/battri/) graphical Matlab-based interface to Triangle. Triangle is a (C language) two-dimensional grid generator developed by Jonathan Shewchuk, presently at the University of California Berkeley. Triangle, and a complete user's manual, can be downloaded directly at http://www.cs.cmu.edu/afs/cs/project/quake/public/www/triangle.html. As a complete BATTRI manual is distributed with the software, only a brief summary of the key steps will be provided here.

3.3.1 Preliminary Steps

The use of BATTRI for mesh-generation has essentially two requirements. First, one must have bathymetry data in the form of (x, y, z) triplets, where z is the bathymetric depth. Second, one must have a .poly file, which describes the domain. More specifically, this ASCII text file describes the domain boundaries, in terms of listing the coordinates of the points on the boundaries and listing the 'edges,' in terms of describing how the boundary points link up to form continuous segments. In addition to the BATTRI manual mentioned above, a simple and useful tutorial is given by Edwards & Werner (2002).

In brief, the .poly file structure is given in Fig. 3.7. An extremely simple sample domain, containing one 'island,' and the corresponding .poly file are given in Fig. 3.8.

For a realistic application, like the present one, the boundary may be made up of thousands of points and there may be dozens to hundreds of islands. Manually assembling a .poly file in this case is not an option. Therefore, a Matlab script was written to automate this task. This script, entitled write_poly.m, and other scripts are distributed with this report and are fairly well documented with inline comments

When BATTRI is run, a number of initial choices will have to be made regarding the general display of data. Generally speaking, it is sufficient

The structure of a *poly* file is:

Line 1: nn nd natt nbm	nn:	total number of nodes (x,y pairs)
	nd:	# of dimensions (must be 2)
	natt:	# of attributes (0 in these examples)
	nbm:	# of boundary markers (0 in these examples)
Next *nn* lines: n x y	n:	node number
	x:	x-coordinate
	y:	y-coordinate
Next line: nedges nbm	nedges:	total # of land and open boundary element (node pairs)
	nbm:	# of boundary markers (0 in these examples)
Next *nedges* lines: edge na nb	edge:	number of the edge (or boundary line segment)
	na:	first node of edge
	nb:	second node of edge
Next line: nisl	nh:	number of islands (holes) in mesh
Next nh lines: isl xisl yisl	isl:	island (hole) number
	xisl:	x-coord of a point that lies within the island (hole)
	yisl:	y-coord of a point that lies within the island (hole)

Figure 3.7: Structure of the .poly file required by BATTRI.

at this point to accept the default suggestions for the parameter choices. Additionally, the .poly file will be loaded and the boundaries will be plotted on the screen.

At this point, the user is allowed to do some 'editing' of the .poly file before the mesh is created. This editing includes features such as adding, deleting, or moving points, and adding, deleting, or dividing edges into smaller segments. These features are useful in continuing to smooth and improve the boundary. Additionally, the ability to add interior points is helpful in terms of avoiding finite elements that 'span' very narrow inlets. A general example of this ability to manually add points is given in Fig. 3.9.

For the present model application, the entire domain was reviewed very carefully in this step of the BATTRI execution and points were added and deleted as needed.

3.3.2 First Cut Mesh Generation

When the manual editing of the domain boundaries is complete, a 'first cut' mesh will be generated. It is at this point that BATTRI calls the Triangle

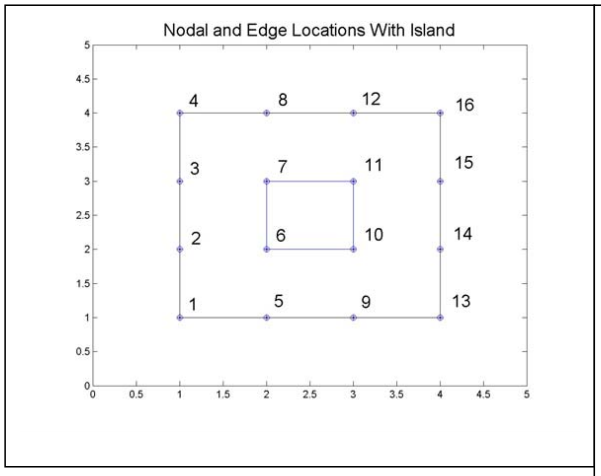


```
16 2 0 0
1   1.0 1.0
2   1.0 2.0
3   1.0 3.0
4   1.0 4.0
5   2.0 1.0
6   2.0 2.0
7   2.0 3.0
8   2.0 4.0
9   3.0 1.0
10  3.0 2.0
11  3.0 3.0
12  3.0 4.0
13  4.0 1.0
14  4.0 2.0
15  4.0 3.0
16  4.0 4.0
16  0
1    1   2
2    2   3
3    3   4
4    4   8
5    8  12
6   12  16
7   16  15
8   15  14
9   14  13
10  13   9
11   9   5
12   5   1
13   7   6
14   6  10
15  10  11
16  11   7
1
1  2.469 2.539
```

Figure 3.8: Sample domain and corresponding .poly file.

program (which runs in the background) and attempts to create a finite element mesh of the domain. The user is allowed to specify parameters such as the maximum number of nodes to add, the maximum (triangular) finite element area, the minimum interior angle allowed in each triangle, and so on. Additionally, the user can specify whether or not the boundary, as given in the .poly file can be altered / refined (by subdividing segments, for example) during the mesh generation process.

The author's experience was that significant trial and error can be expected at this step of the process. There is a fine balance to be struck since it is desired to have a mesh that is of high quality but not too large. If the former requirement is not met, the results of the hydrodynamic simulations

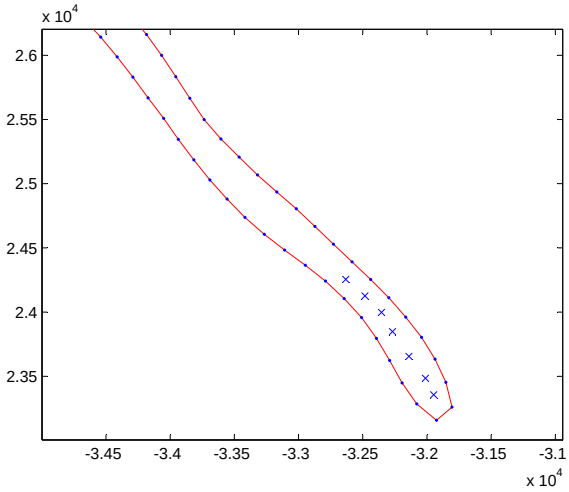

Figure 3.9: Intermediate plot output from BATTRI. The area shown is Charpentier Inlet; the blue dots and red lines indicate the boundary as specified by the .poly file, the blue x marks indicate user added interior points.

may be suspect. If the latter requirement is not met, the simulations may be prohibitively expensive in terms of computer time.

Figure 3.10 shows a representative example of what a typical 'first cut' mesh might look like. The area shown is Tarr Inlet in the West Arm. At this point, if the user is satisfied with the first cut, the bathymetry is interpolated onto the mesh. Note that this can be a very long step, depending upon the user's computer's processor speed and the size of the mesh.

3.3.3 Diagnostic Plotting

After the first cut, the user is allowed to make a number of 'diagnostic' plots. For example, the user may choose to plot the bathymetry as interpolated onto the mesh. Many of the other options have to do with subsequent mesh refinement options. For example, the user can plot the mesh element 'quality,' which is a measure of the shape of the triangles. The quality parameter ranges from a value of 0 for an extremely flat (approaching a line) triangle to a value of 1 for an equilateral triangle. Based upon experience, it is generally accepted that triangles with a quality measure less than 0.6 will cause problems with the numerical calculations.

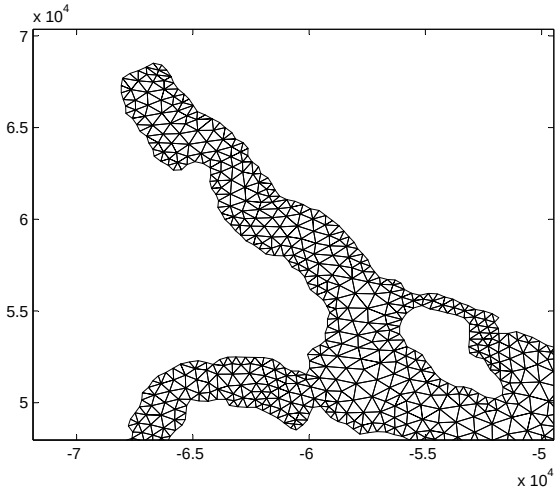

Figure 3.10: Sample mesh, as generated by BATTRI, for Tarr Inlet.

As another example, the user can plot the ratio $(\Delta h)/h$, where Δh is equal to the difference between the maximum depth of an element and the minimum depth and h is the average depth. Elements with a high $(\Delta h)/h$ value indicate regions of sharp bathymetric gradients that will need to be more finely resolved.

3.3.4 Mesh Refinement

After a first cut mesh has been generated, the diagnostic plots discussed above are helpful in determining how the mesh should be refined. The first cut is purely a two-dimensional exercise based only upon the domain boundaries; no consideration to the bathymetry is given. However, there are two very important ways in which the mesh must be refined.

1. First, there is the wavelength to grid size ratio, given by

$$\frac{\lambda}{\Delta x} = \frac{\sqrt{gh}}{\Delta x} T,$$

where λ is the tidal wavelength, Δx a measure of the linear dimension of a given element, h the mean depth of the element, and T the tidal wave period. To properly resolve the shape of the wave, it is generally sought to keep this ratio greater than 100. As tidal wavelength decreases in

shallower water, Δx must decrease as well. Therefore, this criterion has the effect of using smaller elements in shallow water and larger elements in deeper water.

2. Second, there is a criterion known as the topographic length scale criterion. This is given by the ratio

$$\frac{\Delta h}{h} = \alpha.$$

Here, Δh is maximum depth of an element minus the minimum depth and h is the mean depth. Thus, this criterion addresses the bathymetric slope, and not just the local depth. It is desired to keep α less than or equal to one.

When refining the mesh with both of these criteria, one must balance the desire to fully meet the criteria with the desire to keep element sizes from becoming too small. Thus, both criteria are generally imposed along with a minimum area criterion.

As a final step in the mesh refinement process, a 'springs relaxation' operation can be performed. Essentially, this process smooths the grid and greatly improves the element quality values.

3.3.5 Refinement in xmGredit

For the most part, the mesh generation and refinement tools available in BATTRI suffice. What BATTRI lacks, however, is the ability to go in and edit individual nodes and / or elements after the mesh has been generated. Occasionally, there will be a few problematic elements of low quality that need this type of manual editing.

As a result, the author found the program xmGredit to be extremely helpful in the preparation of the final Glacier Bay mesh. This program, available at http://www.ccalmr.ogi.edu/CORIE/software/, is a Linux / Unix based program that allows the user to create and edit two-dimensional meshes. Note that only the source code is available at the above site; interested users will have to compile this source into an executable on their own machines. A user's manual for xmGredit is available and is quite helpful.

It is fairly straightforward to take BATTRI output and route it into xmGredit for refinement. Using xmGredit has the auxiliary benefit that it

allows for the easy construction of fort.14 files, which is the goal of this section. To do this, an ASCII 'grid' file must be prepared. As described in the manual, this file simply describes the nodes and the elements of the mesh. For example, a very simple grid file might look like

```
This is a file identifer
2 4 # number of elements and number of nodes
1 0.0 0.0 1.0 # node number, x, y, depth
2 1.0 0.0 9.0 # node number, x, y, depth
3 1.0 1.0 3.0 # node number, x, y, depth
4 0.0 1.0 2.0 # node number, x, y, depth
1 3 1 2 4 # element number, number of nodes, node list
2 3 2 3 4 # element number, number of nodes, node list
```

Note that the # symbol is a comment symbol and that it and the trailing comments are optional. This sample mesh has four nodes and two elements.

To proceed, note that the final step of BATTRI creates three files of interest:

1. filename.nod - a file that describes the x and y locations of the nodes,
2. filename.bat - a file that gives a depth value for each node, and
3. filename.ele - a file that gives the node numbers (3) making up each element.

The Matlab script convert_gredit.m takes these three files and combines the information into a single .grd file, named for example grid.grd, for use with xmGredit.

Once in xmGredit, the open and mainland boundary segments must be identified and exported, say to a file named boundary.txt. If any changes are made to the mesh, it must exported, say to a file named newgrid.grd.

3.4 Final Mesh Characteristics

The final mesh for the present study of Glacier Bay is shown in Fig. 3.11, although the density of element makes it difficult to view. The final mesh has 48,144 nodes and 88,404 elements. These numbers are high given the relatively small domain and there are two reasons for this. First, the bathymetry

and the shoreline are both highly variable. Second, it was decided that a somewhat slow but accurate model was preferable to one that was fast but less accurate. Thus, the author retained as much bathymetric and coastline detail as was practical.

Figures 3.12-3.13 derive from a post-grid-generation Matlab script that was developed in order to assess the quality of the grid. In the first figure, histograms of grid size characteristics, element qualities, and time-step constraints are provided. The lattermost of these will be discussed in detail in the next chapter. Regarding the quality, note that only one element has a quality measure less than the desired 0.6 and that the vast majority of elements have qualities close to 1.0.

In the second figure, we find that the wavelength to gridsize ratio is satisfied everywhere. The TLS criterion proves to be more challenging, with many elements having $\alpha > 1$. These elements are generally found in very shallow waters and were prevented from being further refined by the minimum area criterion described above.

3.5 Writing fort.14 File

The final step is to prepare the actual fort.14 file itself. A complete description of this input file structure is given in the ADCIRC manual, which may be accessed at http://www.adcirc.org. In general, ADCIRC is highly sophisticated, allowing for a wide variety of boundary types. For example, there are open boundaries, where the tidal elevation is specified and which drive the rest of the domain. There are also no-flow boundaries, i.e. land segments. Additionally, boundary segments where the flow is specified (i.e. a river discharge) are allowed. Finally, internal and external barrier boundaries, where the normal flow is zero unless the elevation exceeds a critical value (the height of the barrier), are allowed.

3.5.1 xmGredit

For the present application, if no river inflows are considered, we have only mainland and open boundaries to contend with. In this case, xmGredit can be used to immediately create the fort.14 file. As described in the previous section, the boundary information is exported to boundary.txt and the grid information is exported to newgrid.grd. The command

```
>>cat newgrid.grd boundary.txt > fort.14
```

issued at the Linux prompt concatenates the node / element information with the descriptions of the boundaries.

If prescribed (non-zero) normal flow boundary segments (i.e. river discharges) are to be included in the ADCIRC simulation, this represents a fairly simple extension to implement. Note, first of all, that the fort.14 file structure contains, after the nodal, element, and open boundary information, the following:

```
NBOU NVEL for k=1 to NBOU
  NVELL(k), IBTYPE(k)
  for j=1,NVELL(k)
    NBVV(k,j) include if IBTYPE(k) = 0,1,2,10,11,12,20,21,22,30
    NBVV(k,j), BARLANHT(k,j), BARLANCFSP(k,j)  include if
        IBTYPE(k) = 3,13,23
    NBVV(k,j), IBCONN(k,j), BARINHT(k,j), BARINCFSB(k,j),
        BARINCFSP(k,j)  include if IBTYPE(k) = 4,24
  end j loop
end k loop
```

This section of the fort.14 file describes the boundary of the domain excluding the open boundaries. IBTYPE is a parameter that describes the boundary segment 'type.' For example, 0 refers to a no-flow external boundary, such as a piece of coastline. An IBTYPE of 1 refers to a no-flow internal boundary, or island. An IBTYPE of 2 refers to an external boundary with non-zero normal flow. Although xmGredit does not explicitly handle river discharge boundaries, they can therefore be implemented as follows:

1. In xmGredit, subdivide the external boundaries into coastline segments and river discharge segments. Then, export the boundary information and create the fort.14 file as described above.

2. Using a text editor, find the river discharge segments in the file and change the IBTYPE from 0 to 2.

3. Create, as per the ADCIRC manual and as described in Chapter 5, a fort.20 file which describes the river discharge into the domain.

3.5.2 Matlab

Another option is to prepare the fort.14 file using a Matlab script written by the present author, called write_fort14.m. There are some important points to note. First of all, the code requires the final .node, .ele, and .poly files generated from BATTRI *prior* to the optimization. As the user progresses through the mesh refinement in BATTRI, files such as filename_1.node (.poly, .ele), filename_2.node (.poly, .ele), and so on, are created. The group of three files with the highest number contain the exact same information as the (.nod, .ele, and .bat) files generated by the final optimization; the only difference is in how the nodes and elements are numbered.

Also, the text files containing the open boundary information are required. When the program is executed, the user will be prompted to provide information about the various land and open boundaries. Note that ADCIRC requires the nodes of land segments to be ordered with the 'land on the right.' This means that mainland segments are specified in a counterclockwise direction while island segments are specified in a clockwise direction. The script asks the user for help in assembling these segments in the proper order.

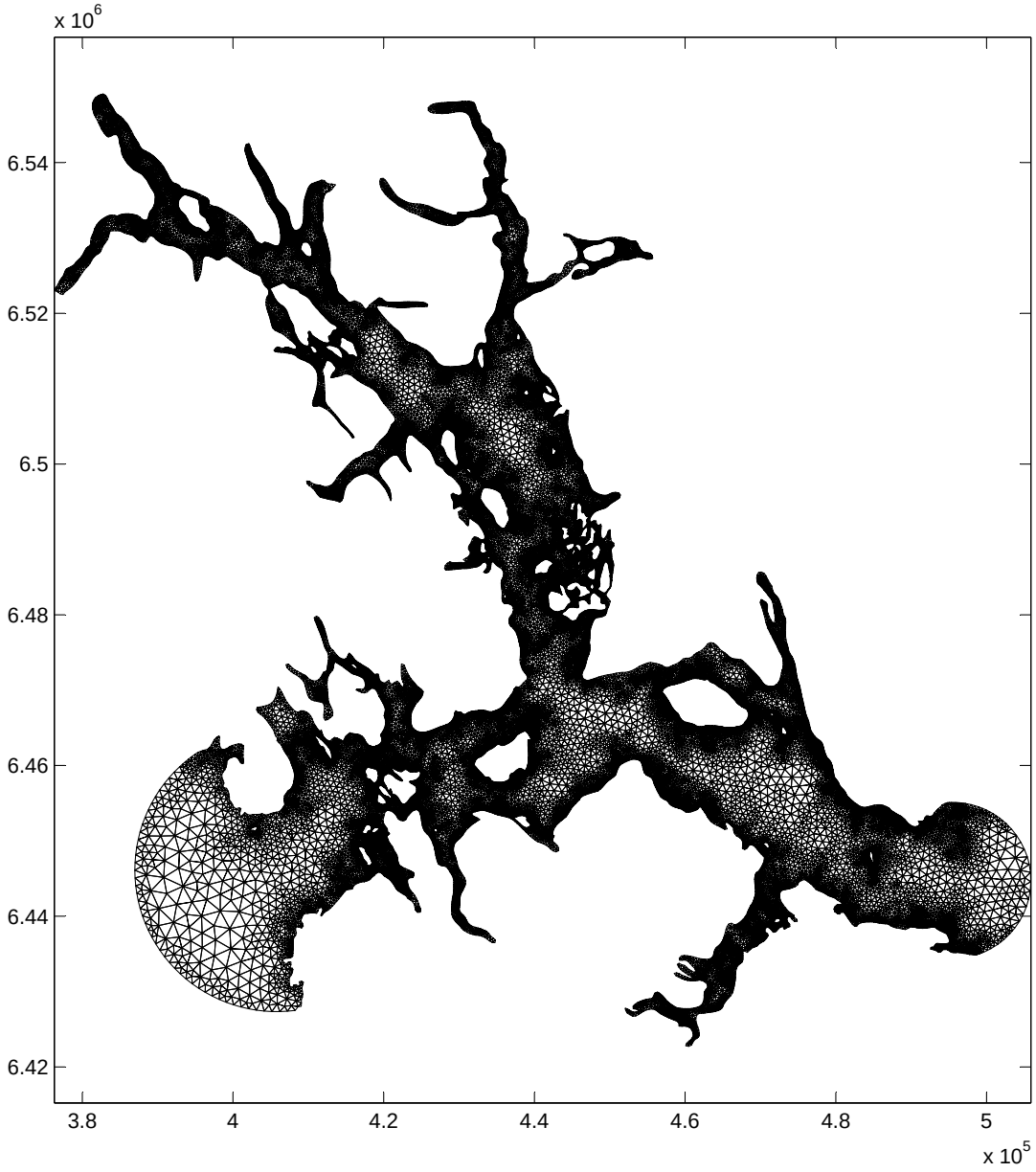

Figure 3.11: Refined (final) mesh for Glacier Bay and Icy Strait / Cross Sound.

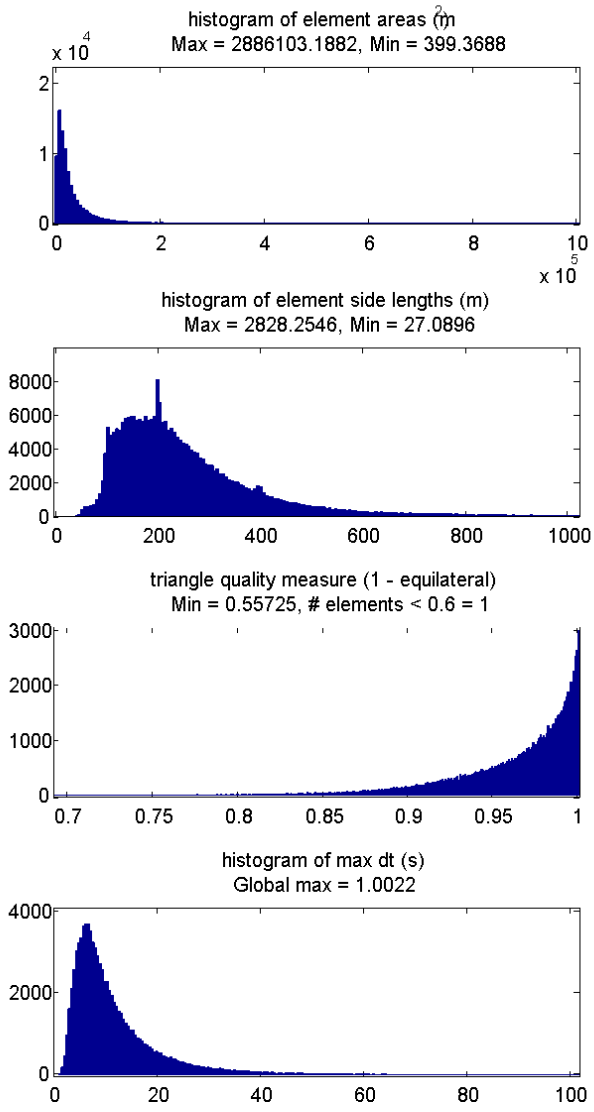

Figure 3.12: Histograms of grid element parameters.

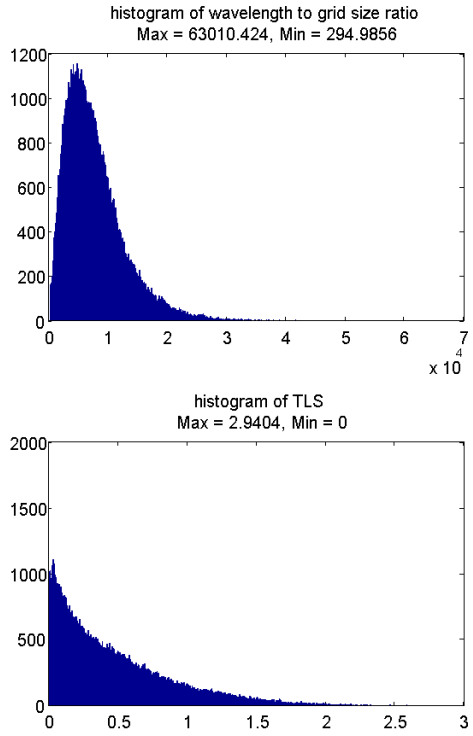

Figure 3.13: Histograms of grid element parameters.

Chapter 4

fort.15 File - Parameter File

Once a good mesh is in place, the fort.14 file becomes essentially static and does not need to be altered from simulation to simulation. The fort.15 file, on the other hand, contains many simulation-specific parameters that may need to be adjusted frequently. For a complete description of the fort.15 file, the reader is referred to the ADCIRC documentation provided at http://www.adcirc.org. Only a few items will be covered in the present chapter.

4.1 General Parameters

First of all, the beginning of the fort.15 file contains many parameters that govern how ADCIRC will be run. Is the model to be run in two-dimensional or three-dimensional mode? Are spherical (longitude, latitude) coordinates being used, or projected (x, y) coordinates?

There are some important parameters that control how nonlinearity is dealt with. For example, linear wave theory essentially ignores the wave itself and 'linearizes' the equations by using only the mean bathymetric depth at a given location. In a location like Glacier Bay, where large tidal ranges are found in shallow waters, this approximation would be quite poor. Thus, the author has been considering finite-amplitude effect by setting NOLIFA to be nonzero.

In addition to simply considering finite-amplitude effects, the ADCIRC model has the distinct advantage of being able to model wetting and drying effects. In other words, as the tide ebbs, some elements will become 'dry' as

the water contact line moves away from shore. This feature of ADCIRC is turned on by setting NOLIFA to have a value of 2.

Next, the model time step must be selected. For the sake of expediency, it is tempting to set DT to be large. However, due to the explicit way in which time derivatives are handled in ADCIRC, a too-large DT will lead to severe numerical instability. The maximum model time step is set by the lowest CFL value in the domain. The CFL (Courant-Friedrichs-Levy) constraint states that

$$\frac{\Delta t}{\Delta x}\sqrt{gh} < CFL.$$

The maximum value that the parameter CFL may have is 1.0. Thus, it is clear that exceptionally small elements may lead to prohibitively expensive computer time (very small Δt). As discussed in the previous chapter, the final Glacier Bay domain grid revealed a maximum Δt of 1 second.

4.2 Tidal Parameters

The middle section of the fort.15 file contains information about how the domain is to be forced with tides.

4.2.1 Interior Forcing

First, it is possible to force the interior of the domain via the tidal potential. In other words, a closed basin of sufficient size will generate its own tides. As the present model domain is quite small, it has been decided to use projected coordinates (x, y) and to turn off the interior forcing.

4.2.2 Boundary Forcing

Second, it is possible to force the domain by prescribing the tidal motion at the (two, in this case) open boundaries. The user has the ability to specify as many tidal constituents as desired. While there are several hundred recognized constituents, many are insignificant in amplitude and, from a practical modeling point of view, it is often sufficient to include only the top 5-10.

For each included constituent, several parameters must be specified. These include the frequency, amplitude, phase, nodal factor, and equilibrium argument. To help in explaining these terms, note that the water surface elevation

may, in general, be written as:

$$\eta(x,y,t) = \sum A_i(x,y) f_i(t_0) \cos\left[\frac{2\pi}{T_i}(t-t_0) + V_i(t_0) - \Psi_i(x,y)\right].$$

In this equation, the summation symbol merely indicates that the water surface elevation (due to the tides) is made up a number of terms (constituents). The amplitude (of constituent i) is given by A_i, the period by T_i (note that $\frac{2\pi}{T_i}$ is the angular frequency), and the phase by Ψ_i. The nodal factor is given by f_i and the equilibrium argument by V_i.

Among these terms, only the period / frequency is an absolute constant for a given constituent. The amplitudes and phases are spatially variable, temporally constant values. The nodal factors and equilibrium arguments are spatially constant, temporally variable values. Most importantly, these latter two terms are essential to 'starting the clock' on an ADCIRC simulation. If the goal of the user is to produce time series of elevations and velocities, for the purposes of comparisons with data, these parameters must be calculated. Otherwise, the output, will not be properly synchronized in time.

Determination of Nodal Factors and Equilibrium Arguments

The author has found two different methods for calculating these parameters.

1. The first is a Fortran program, called tide_fac.f, and available from the ADCIRC webpage at http://www.adcirc.org. When compiled and executed, this program prompts the user for a date and time (GMT). For example, if a start at 11 p.m. on January 25th, 2006 is desired, the time is entered as:

   ```
   23 25 1 2006
   ```

   Execution of the program yields the following output:

   ```
   CONST    NODE      EQ ARG (ref GM)
   NAME    FACTOR     (DEG)


   K1     1.11206       19.09
   O1     1.18191       34.73
   ```

```
P1    1.00000     309.89
Q1    1.18191     101.74
N2    0.96350     120.42
M2    0.96350      53.40
S2    1.00000     330.00
K2    1.31448     218.05
```

2. The second is a Matlab program, called compute_modulation_v2.m, which is part of a Matlab package called t_tide, freely available online. When this program is executed, the user is, as with tide_fac, asked for the time (GMT) and date at which the nodal factor and equilibrium argument are desired. The output contains many more constituents than the tide_fac output. As just a single point of comparison it is found that:

   ```
   K1    1.1124      19.0543
   ```

   While there are some very slight differences, it appears that the two programs yield essentially equivalent results.

Determination of Amplitudes and Phases

Tidal constituents at the open boundaries may be extracted from the Eastern Pacific Database, found at http://www.unc.edu/ims/ccats/tides/tides.htm. In addition to the databases themselves, a fortran program for extracting information at requested points is provided. In brief, the fortran program requires an input file, entitled tides.in, whose first line is an integer specifying at how many points information is being requested. The following lines are simply the longitude and latitude coordinates of those points. The output file from the fortran program contains the amplitudes and phases of the M2, S2, N2, K2, O1, K1, P1, Q1, M4, and M6 constituents. Note that the amplitudes and phases for each constituent must be listed in the fort.15 file in the exact order in which the open boundary points are specified in the fort.14 file.

4.3 Output Specification

The last major portion of the fort.15 file has to do with user requests for output data. In general, the user may specify that data (including elevation, water velocity, and scalar concentration) be output either at specified nodes in the domain or at *all* nodes in the domain (global output). In addition, the user may specify at what times these data are output. Specifically, a start time, end time, and time step 'skip' may be specified. For example, consider an ADCIRC run that lasts for 14 days. The user may wish to specify that data are output beginning on the 10th day and ending on the 14th. Moreover he may wish to specify that the data be output at every 1000th model time step. Note that these 'global' output files (where data are written at every node) can become extremely large in their ASCII format. If needed, ADCIRC can be generate binary output files as well, which are more compact.

In addition to elevation and velocity time series data, it is possible to have ADCIRC perform harmonic analysis on model output. Harmonic analysis takes time series output and uses least-squares analysis to fit it to a specified number of constituents. As a result, the amplitudes and phases of the constituents can be determined. It is possible to request harmonic analysis output either at selected points or at every point in the domain.

Note that this is precisely how the Eastern Pacific (ENPAC) Database, as described above, was generated. In that case, tidal constituents at the open boundary of the ENPAC domain were extracted from global ocean models and were used to drive the ENPAC ADCIRC simulation. Subsequent harmonic analysis of the model output led to the tidal constituents in the ENPAC database. Now, the tidal constituents at the open boundaries of the (smaller) Glacier Bay domain are being extracted from the ENPAC database and used to drive an ADCIRC simulation of Glacier Bay. This 'nested model' approach is common and advantageous as it provides the desire resolution only in the regions where it is needed.

Chapter 5

fort.20 File - Freshwater Inflows

The inclusion of freshwater inflows is an important feature of the ADCIRC model. As discussed in Chapter 3, the fort.14 file contains information about the boundaries of the domain. To this point, we have considered only two types of boundaries:

1. No-flow boundaries, such as the main coastline or islands. For this type of boundary, water is not allowed to flow perpendicular, or normal, to the boundary.

2. Open boundaries, one in the Gulf of Alaska, the other in Lynn Canal. For this type of boundary, the elevation of the water surface is specified for all times.

There is another type of boundary, called a non-periodic normal-flow boundary. The main coastlines and islands are essentially non-periodic normal-flow boundaries where the normal flow is always zero. In other words, the land forms a solid boundary through which water can not flow.

A more general non-periodic normal flow boundary is one where the normal flow is prescribed to be some non-zero value. This, for example, is what occurs when a river discharges into the bay. Across a section of the boundary (the width of the river), the normal flow is set by the river flow.

Given the very large precipitation amounts in southeastern Alaska, it is very natural to question to what extent freshwater inflows will change the predictions of water surface elevation and velocity in Glacier Bay. Answering this question is one of the main objectives of the current project.

5.1 Inflow Data

The best case scenario would have numerous river gaging stations located in Glacier Bay so that the freshwater inflows could be measured directly and then input in the ADCIRC model. The reality is that very little data on streamflow exists within Glacier Bay. According to the Alaska Science Center (http://alaska.usgs.gov/science/water/index.php), data in the park are available only on the Kahtaheena River (1999 - 2004), near Gustavus. Within the model domain, the fact is that there are hundreds of streams contributing freshwater inflow to the bay. Further complicating matters is the presence of many glaciers, including several large tidewater glaciers. The traditional river gaging methods employed by the USGS do not allow for the measurement of the substantial submarine discharge coming from these tidewater glaciers.

5.2 Estimation / Modeling of Inflows

In order to run ADCIRC simulations to assess the relative significance of inflows, it was determined to try several strategies for estimating the discharges. Interested readers are directed to Ciavola (2007) for a complete discussion of this subject. Only an outline of the methodology will be provided here.

The 'output' of a hydrological study of Glacier Bay will consist of information about the magnitude and the timing of flows into the bay. Given the severe lack of requisite 'input' data, which will be elaborated upon below, it is unrealistic to expect a hydrological model that will accurately predict hourly and daily flows. Rather, the author is more interested in mean monthly flows, peak discharges, and annual flow statistics.

5.2.1 Obtaining Data

Precipitation and Temperature Data

Precipitation and temperature data were drawn from the National Climatic Data Center for numerous stations in the vicinity of Glacier Bay (Fig. 5.1). Data coverage over the past 50-60 years was found to be highly variable. Stations such as Yakutat and Juneau had reliable data every year while other stations had 10 to 20 years worth of data. The mean annual precipitation

(MAP) and mean minimum January temperatures (MMJT) for these stations are summarized in Table 5.1. Brief inspection of the precipitation data indicates that significant spatial gradients occur. Stations near the coast, such as Pelican and Yakutat receive around 12 feet of rain per year while inland stations such as Haines and Juneau receive around 4 feet per year.

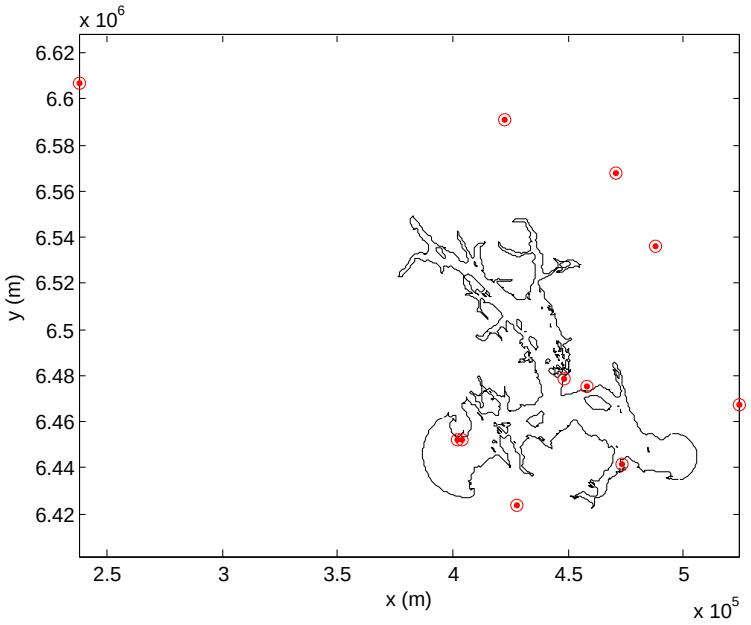

Figure 5.1: Locations of weather stations used in determining rainfall and temperature values.

Elevation Data

Digital elevation data are readily obtained from the USGS (http://seamless.usgs.gov/). Using their web-based interface, it is possible to zoom in on a general region of interest, draw a polygon around a specific region of interest, and then download data on a (roughly) 30 m grid. A grayscale raster image of this data is given in Fig. 5.2.

Station	Latitude	Longitude	MAP (in)	MMJT (°F)
Cape Spencer	58.2	-136.63	100.01	28.2
Eldred Rock	58.96	-135.21	46.56	21.32
Elfin Cover	58.2	-136.66	103.41	29.51
Glacier Bay	58.45	-136.66	70.34	22.96
Juneau	58.35	-134.58	56.89	19.25
Haines Airport	59.25	-135.51	49.21	17.78
Haines 40 NW	59.45	-136.36	49.68	10.02
Gustavus	58.41	-135.71	54.3	20.8
Hoonah	58.11	-135.45	64.46	25.45
Yakutat	59.51	-139.63	146.55	18.88
Pelican	57.95	-136.21	141.74	25.3

Table 5.1: Mean annual precipitation (MAP) and mean minimum January temperature (MMJT) values for weather stations in the vicinity of Glacier Bay.

Land Cover Data

One of the strategies employed for determining peak flows relies upon knowledge of land cover. Therefore, land cover data were downloaded from the Alaska Geospatial Data Clearinghouse (http://agdc.usgs.gov/data/usgs/erosafo/ak_lcc/ak_lcc.html). Separate files are provided for many different USGS quadrangles. These data files may immediately be loaded into ArcGIS. Note that a careful look at the metadata for each quadrant is warranted, as different land use codes are used for the different quads. With some care, the files from the quads making up Glacier Bay can be merged together into single layers for forests (Fig. 5.3), ice / snow (Fig. 5.4), etc.

Soils Data

Many traditional methods (curve number, etc.) of distributed modeling of runoff require detailed information about soil characteristics. The best location for this data is the NRCS Soil Data Mart, found at http://soildatamart.nrcs.usda.gov/. There, users can request data from the Soil Survey Geographic Database (ssurgo) and the State Soil Geographic Database (statsgo). However, it should be noted that the coverage of Glacier Bay in these databases is inadequate for this type of distributed modeling effort.

5.2.2 Delineating Watersheds

With data in hand, the next step in estimating runoff is the characterization of watersheds in the drainage basin. This analysis was performed using, among other tools, the spatial analyst toolbox in ArcGIS 9.2, and involved the following steps:

1. Filling the digital elevation model (DEM) to eliminate small 'sinks,' or cells of depression.

2. Calculating the flow direction raster, which simply indicates the direction of steepest descent for each cell.

3. Calculating the flow accumulation raster. Essentially, this operation calculates, for every cell in the DEM, the number of cells that flow into that cell.

4. Delineating watersheds. This operation is based upon 'pour points' (stream outlets) defined by the user. Note that, when delineating watersheds that feed into a long coastline, there will be hundreds or thousands, many of them extremely small. Therefore, it was decided to group watersheds into two classes, 'point-source' watersheds and 'line-source' watersheds. Classification as a point watershed is reserved for those watersheds exceeding an arbitrary minimum area. For the present analysis, this was set at approximately 7 km^2. As a result, some 40 point watersheds were identified Each of these represents a fairly major stream emptying into Glacier Bay. A line watershed simply represents the aggregate of all of the minor watersheds that lie between two adjacent major, or point, watersheds. For the purposes of the ADCIRC model, the water that falls on a line watershed will be modeled as running off uniformly distributed over the coastline of the line watershed. This strategy has been previously employed in the modeling of precipitation runoff in southeastern Alaska (Wang *et al.*, 2004). Fig. 5.5 shows, some 40-50 line watersheds are identified in addition to the 40 or so point watersheds for the Glacier Bay domain.

Figure 5.2: Digital elevation data for Glacier Bay National Park.

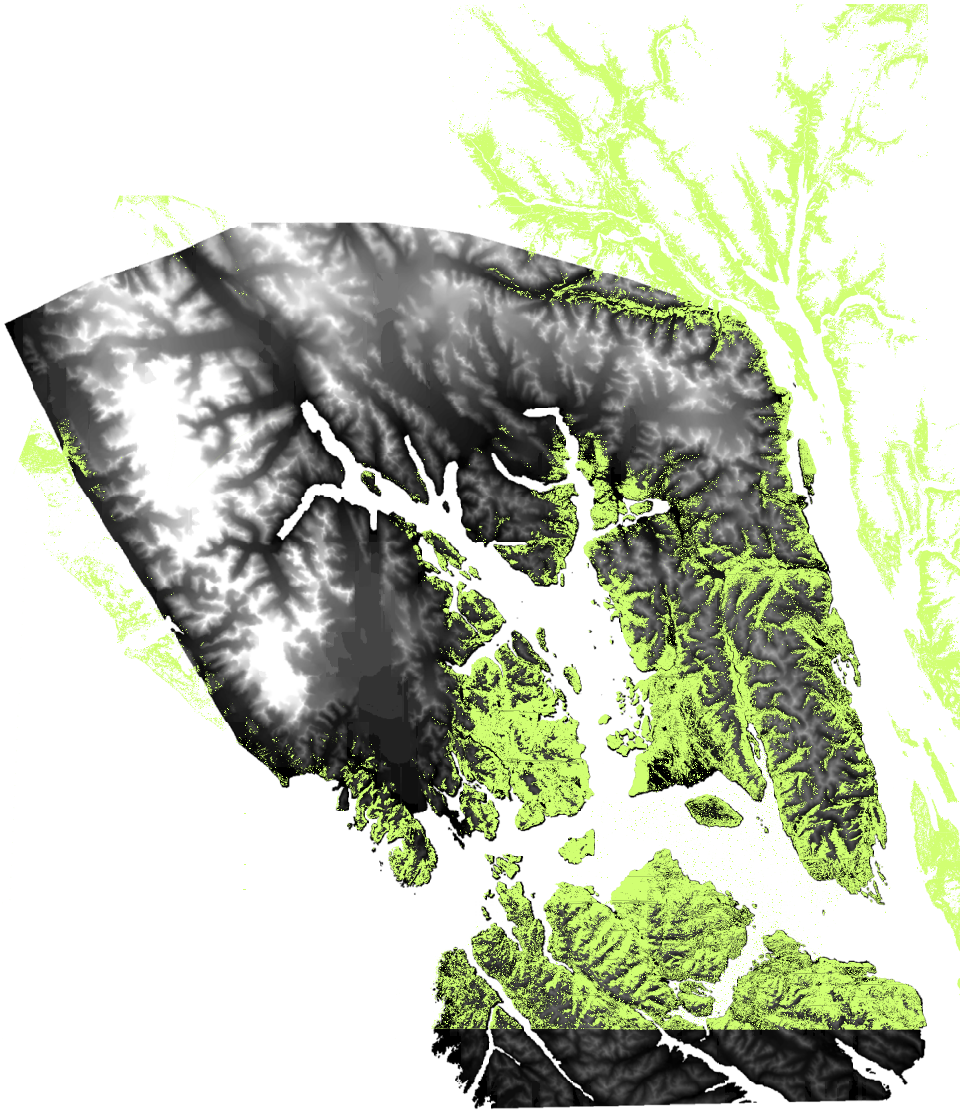

Figure 5.3: Forest cover, superimposed upon the elevation DEM.

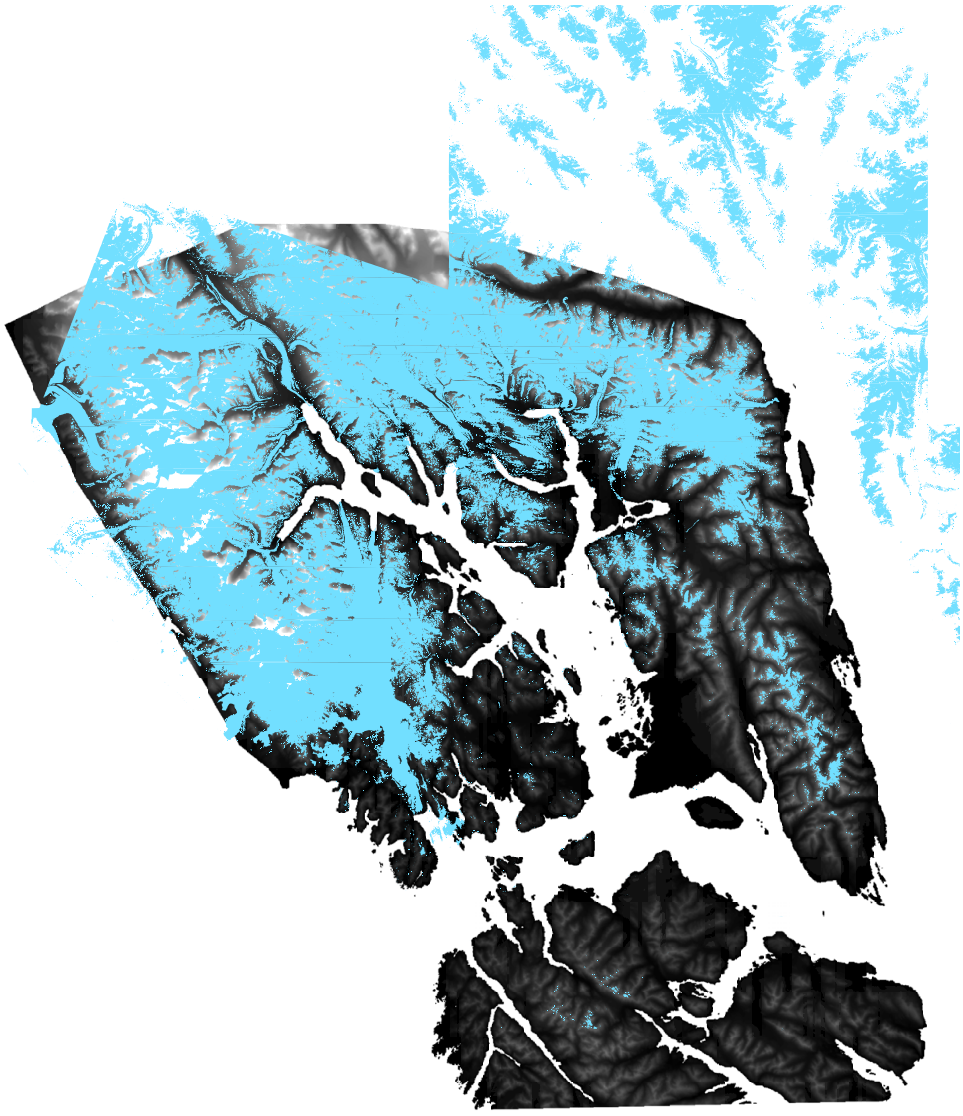

Figure 5.4: Snow / ice cover, superimposed upon the elevation DEM.

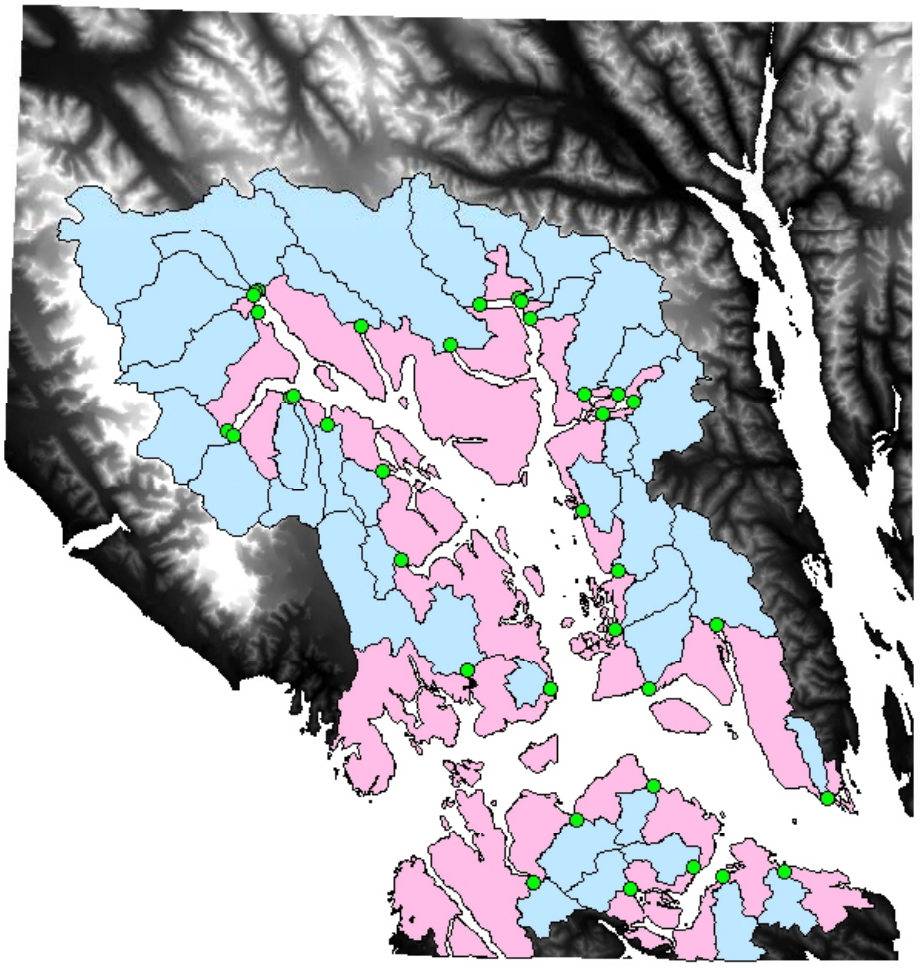

Figure 5.5: Point and line watersheds, ad delineated with GIS analysis, for the Glacier Bay domain.

5.2.3 Characterizing Watersheds

Once the watersheds have been defined, it is straightforward to interrogate them in ArcGIS in order to extract information of interest. Depending upon the type of runoff estimate that is being considered, this information will vary. Items of interest, as will be discussed below, include things such as the area and the centroid coordinates of the watershed, the mean elevation, and percent forest, snow, and water coverage. Specific details on how these data were determined are given in Ciavola (2007) and the interested reader is directed to that thesis.

5.2.4 Estimation of Peak Flows

As the present goal is to understand the extent to which inflows alter patterns of water elevation and velocity in Glacier Bay, it makes sense to initially consider high flow events, such as those following a substantial rainfall event. A report by Curran *et al.* (2003) discusses the development of regression equations for peak flows in Alaska. That report represents an intensive analysis of 361 streamflow-gaging stations in Alaska. In order to improve the accuracy of the derived estimation equations, the stations were grouped into 7 regions (Fig. 5.6). This grouping procedure was based upon hydrologic unit boundaries and regional boundaries developed by the USGS. Some refinement to this grouping scheme was made based upon basin characteristics.

For all of the watershed basins, Curran *et al.* (2003) determined a number of characteristics thought to be relevant to controlling the peak streamflows. In the end, the regression equations included, at most, drainage area, mean basin elevation, area (fractional) of forest, area (fractional) of lakes and ponds, mean annual precipitation, and mean minimum January temperature.

For regions 1 and 3 (Glacier Bay lies in region 1), which include 93 gaging stations, the regression equations for the 2, 5, 10, etc., year peak discharges are given by Table 5.2.

Based upon these equations, the corresponding peak discharges from all line and point watersheds were calculated. Detailed results are tabulated in Ciavola (2007). The summed discharges (total runoff into the Glacier Bay domain) are summarized in Table 5.3. Note that the 'runoff' from precipitation that falls directly onto the water surface is not included in these totals. Also note that these values, which are $O(10^5)$ cfs, are the same order of magnitude as typical flows in the Mississippi River.

Q_T	Error	Years
$Q_2 = 0.004119A^{0.8361}(ST+1)^{-0.3590}P^{0.9110}(J+32)^{1.635}$	38	0.88
$Q_5 = 0.009024A^{0.8322}(ST+1)^{-0.3670}P^{0.81280}(J+32)^{1.640}$	37	1.3
$Q_{10} = 0.01450A^{0.8306}(ST+1)^{-0.3691}P^{0.7655}(J+32)^{1.622}$	37	1.8
$Q_{25} = 0.02522A^{0.8292}(ST+1)^{-0.3697}P^{0.71650}(J+32)^{1.588}$	38	2.4
$Q_{50} = 0.03711A^{0.8286}(ST+1)^{-0.3693}P^{0.6847}(J+32)^{1.559}$	40	2.8
$Q_{100} = 0.05364A^{0.8281}(ST+1)^{-0.3683}P^{0.6556}(J+32)^{1.527}$	41	3.1
$Q_{200} = 0.07658A^{0.8276}(ST+1)^{-0.3669}P^{0.6284}(J+32)^{1.495}$	43	3.4
$Q_{500} = 0.1209A^{0.8272}(ST+1)^{-0.3646}P^{0.5948}(J+32)^{1.449}$	41	3.1

Table 5.2: Regression equations (for regions 1 and 3) for various recurrence intervals. Q_T is the discharge in cfs, A is drainage area in square miles, ST is the area of lakes and ponds in percent, P is the mean annual precipitation in inches, J is the mean minimum January temperature in degrees Fahrenheit. Equations are taken from Curran *et al.* (2003).

5.2.5 Annual Flow Statistics

A second set of useful regression equations has been developed by Wiley and Curran (2003). Whereas the peak flow statistics discussed in §5.2.4 were derived from annual peak flows, the statistics discussed in the current section pertain to annual flow statistics based upon daily streamflow data.

The report of Wiley and Curran (2003) shares many characteristics with that of Curran et al. (2003). Many of the same basins were analyzed and many of the same basin characteristics were used in the obtained regression equations. As summarized in Table 5.4, one set of equations is given for the 15, 10, 9,. . ., 1 percent duration flows. As an example, the 1 percent duration flow is exceeded one percent of the time. These equations therefore describe the high flow statistics.

Analysis of low flow statistics is complicated by the fact that, during the winter time, freezing leads to unreliable low flow data. Therefore, and as outlined in Table 5.5, a second set of equations is provided for low flow statistics. However, these equations are strictly valid only for the months of July, August, and September.

Based upon these two sets of equations, the flow statistics for each watershed were calculated and are tabulated in Ciavola (2007). The summed discharges for the entire Glacier Bay domain are plotted in Fig. 5.7 in the form of a flow duration curve. The results indicate that flows on the order

Recurrence Interval (years)	Peak Discharge (cfs)
2	198,000
5	282,000
10	340,000
25	414,000
50	471,000
100	528,000
200	589,000
500	668,000

Table 5.3: Peak discharge values, for various recurrence intervals, for the Glacier Bay domain.

of 10,000 to 100,000 cfs are expected.

5.2.6 Estimating Annual Hydrograph

Finally, in addition to estimating peak flows and annual flow statistics, it is of interest to consider the annual variation of discharge over a given year. There are many strategies that may be taken towards this goal. As with the previous sections, readers are directed to Ciavola (2007) for a more complete discussion; only a brief review is provided here.

Observed Characteristics of Annual Hydrograph

Royer (1979) gave consideration to runoff, particularly as it impacts circulation patterns in the Gulf of Alaska. He noted the difference between the annual cycles observed in temperature and precipitation. Regarding the former, a peak is observed in the summer months, and regarding the latter, a strong peak is observed in October. He then proposed a simple 'box model' wherein precipitation that fell during winter months (November to April) would be largely locked up as snow and precipitation that fell during the rest of the year would run off immediately. Stored snow was then forced to run off under a hydrograph increasing linearly from May to a maximum in September, before dropping off again to zero in November. The result of this model is a hydrograph with a single peak (snowmelt runoff plus immediate runoff) typically in September.

OSn (cfs)	Coefficient of Determination	Standard error of estimate, in percent
$OS15 = 0.1358A^{0.9960}P^{1.016}$	0.97	22
$OS10 = 0.2145A^{0.9472}P^{0.9740}$	0.97	21
$OS9 = 0.2372A^{0.9422}P^{0.9652}$	0.97	22
$OS8 = 0.2670A^{0.9374}P^{0.9550}$	0.97	22
$OS7 = 0.3033A^{0.9307}P^{0.9443}$	0.97	22
$OS6 = 0.3486A^{0.9234}P^{0.9329}$	0.96	22
$OS5 = 0.4120A^{0.9162}P^{0.9179}$	0.96	23
$OS4 = 0.4875A^{0.9074}P^{0.9057}$	0.96	23
$OS3 = 0.6039A^{0.8963}P^{0.8892}$	0.96	24
$OS2 = 0.7960A^{0.8829}P^{0.8697}$	0.95	25
$OS1 = 1.279A^{0.8637}P^{0.8293}$	0.94	27

Table 5.4: Regression equations (for regions 1 and 3) for annual high duration flows. OSn is the discharge, having an n percent exceedence probability, in cfs, A is drainage area in square miles and P is the mean annual precipitation in inches. Equations are taken from (Wiley & Curran, 2003, Table 2)

Wang *et al.* (2004), building upon Simmons (1996), developed a distributed model for estimating runoff into the Gulf of Alaska. This effort delineated point-source and line-source watersheds using a DEM. Forced with daily temperature and precipitation data, their work attempted to reproduce observed runoff patterns by modeling snow storage and melt directly, rather than assuming a snowmelt hydrograph. Empirical parameters for baseflow, routing velocity, and infiltration coefficients were necessary and were used to calibrate the output to observed data.

These approaches are summarized in Fig. 5.8. The hydrograph of Wang *et al.* (2004) closely approximates the annual cycle in temperature (not shown) and not precipitation, suggesting that runoff into the Gulf of Alaska is dominated by snow and glacial melt. The hydrograph of Royer (1979) is best viewed as a balance, or average, between low-lying watersheds dominated by precipitation (immediate runoff) and higher-elevation watersheds dominated by snow storage and melt.

This idea can be explored further by considering runoff data from gaging

J-Sn (cfs)	Coefficient of Determination	Standard error of estimate, in percent
$J - S98 = 2.532 \times 10^{-9} A^{1.142} P^{1.521} E^{1.674}$	0.93	66
$J - S95 = 7.423 \times 10^{-9} A^{1.104} P^{1.485} E^{1.612}$	0.94	55
$J - S90 = 2.479 \times 10^{-8} A^{1.080} P^{1.451} E^{1.520}$	0.95	49
$J - S85 = 5.016 \times 10^{-8} A^{1.058} P^{1.380} E^{1.506}$	0.95	45
$J - S80 = 8.813 \times 10^{-8} A^{1.044} P^{1.347} E^{1.477}$	0.96	43
$J - S70 = 2.456 \times 10^{-7} A^{1.028} P^{1.300} E^{1.407}$	0.96	39
$J - S60 = 6.997 \times 10^{-7} A^{1.013} P^{1.264} E^{1.323}$	0.97	35
$J - S50 = 2.089 \times 10^{-6} A^{0.9961} P^{1.226} E^{1.232}$	0.97	32

Table 5.5: Regression equations (for region 1) for annual low duration flows. J-Sn is the discharge, having an n percent exceedence probability, in cfs, A is drainage area in square miles, P is the mean annual precipitation in inches, and E is the mean basin elevation in feet. Equations are taken from (Wiley & Curran, 2003, Table 2)

stations in southeast Alaska. Table 5.6 presents a summary of mean monthly flows for a number of gaged watersheds. The flows have been normalized by the mean annual total for the purposes of comparison. A quick perusal of the data in the table indeed reveal a nearly 'bi-modal' distribution of hydrographs. Many of the watersheds have their peak flows in the summer months; these hydrographs are plotted together in Fig. 5.9a. The remaining watersheds have their peak flows in October, and these hydrographs are plotted in Fig. 5.9b. For the watersheds where mean elevation data were available, these elevations are plotted against the peak-flow-month in Fig. 5.9c. It is clear that watersheds with a mean elevation above roughly 2000 feet are dominated by the snowmelt contribution. Watersheds with a lower mean elevation have a hydrograph dominated by precipitation. Indeed, Fig. 5.9b looks very much like the normalized precipitation curve in Fig. 5.8.

Modeled Glacier Bay Hydrograph

Having demonstrated some attributes of the annual cycle, attention is finally turned to the problem of quantifying discharges. The easiest way to estimate discharge into Glacier Bay, as a function of calendar month is as follows. Note

		Month											
Station Name	Station ID	1	2	3	4	5	6	7	8	9	10	11	12
ALSEK R NR YAKUTAT AK	15129000	0.01	0.01	0.01	0.02	0.07	0.19	0.24	0.21	0.13	0.07	0.03	0.02
ANTLER R BL ANTLER LK NR AUKE BAY AK	15055500	0.03	0.02	0.02	0.03	0.11	0.2	0.17	0.14	0.14	0.1	0.04	0.05
FISH C NR KETCHIKAN AK	15072000	0.08	0.07	0.06	0.08	0.11	0.1	0.07	0.07	0.1	0.15	0.12	0.09
KADASHAN R AB HOOK C NR TENAKEE AK	15106920	0.07	0.07	0.06	0.1	0.14	0.09	0.04	0.05	0.11	0.16	0.11	0.09
KAKUHAN C NR HAINES AK	15056030	0.01	0.01	0.01	0.02	0.08	0.18	0.23	0.22	0.13	0.08	0.03	0.02
MENDENHALL R NR AUKE BAY AK	15052500	0.01	0.01	0.01	0.01	0.05	0.14	0.22	0.24	0.19	0.1	0.02	0.01
MONTANA C NR AUKE BAY AK	15052800	0.04	0.04	0.04	0.05	0.11	0.13	0.12	0.13	0.15	0.13	0.07	0.05
SITUK R NR YAKUTAT AK	15129500	0.08	0.08	0.07	0.07	0.08	0.07	0.05	0.08	0.14	0.16	0.1	0.12
STANEY C NR KLAWOCK AK	15081497	0.12	0.1	0.09	0.08	0.05	0.03	0.03	0.05	0.13	0.17	0.15	0.16
TAIYA R NR SKAGWAY AK	15056210	0.01	0.01	0.01	0.01	0.07	0.17	0.25	0.25	0.15	0.06	0.03	0.01
TAKU R NR JUNEAU AK	15041200	0.01	0.01	0.02	0.03	0.13	0.22	0.2	0.16	0.12	0.07	0.03	0.02

Table 5.6: Normalized mean monthly flows for several USGS gaging stations in southeast Alaska

that this approach assumes static glaciers, no evaporation, and no infiltration losses.

1. Select an annual precipitation amount for Yakutat, which has served as the reference station.

2. Based upon the network of weather stations at which annual data is available, spatially interpolate this rainfall amount to the centroids of all the watersheds.

3. Depending upon whether the mean elevation of each watershed is less than or greater than 2000 ft, adopt one of the two idealized annual hydrographs as discussed in the previous section.

4. Release this precipitation over the 12 months of the year, allowing for an overall hydrograph for the Glacier Bay domain to be determined. As has been convention, we continue to neglect the rainfall landing on the surface of the water itself.

Sample results, using the mean annual precipitation, are given in Fig. 5.10. The hydrographs for the point and line watersheds are given separately in addition to the overall hydrograph. Several points are worth noting. First of all, the summed hydrograph for the point watersheds is clearly dominated by snow melt. This is because the point watersheds are the larger ones with large mean basin elevations. The summed hydrograph for the line watersheds, on the other hand, is clearly dominated by precipitation. This is due to the fact that these watersheds are close to the coastline and therefore have low mean basin elevations. Third, the division of total discharge between point and line watersheds is found to be fairly close, with about 55% coming from the former and 45% from the latter. Finally, the overall hydrograph is dominated by snow melt (point watersheds), exhibiting a single peak in the summer, but is noticeably 'broadened' by the contribution from the precipitation (line watersheds).

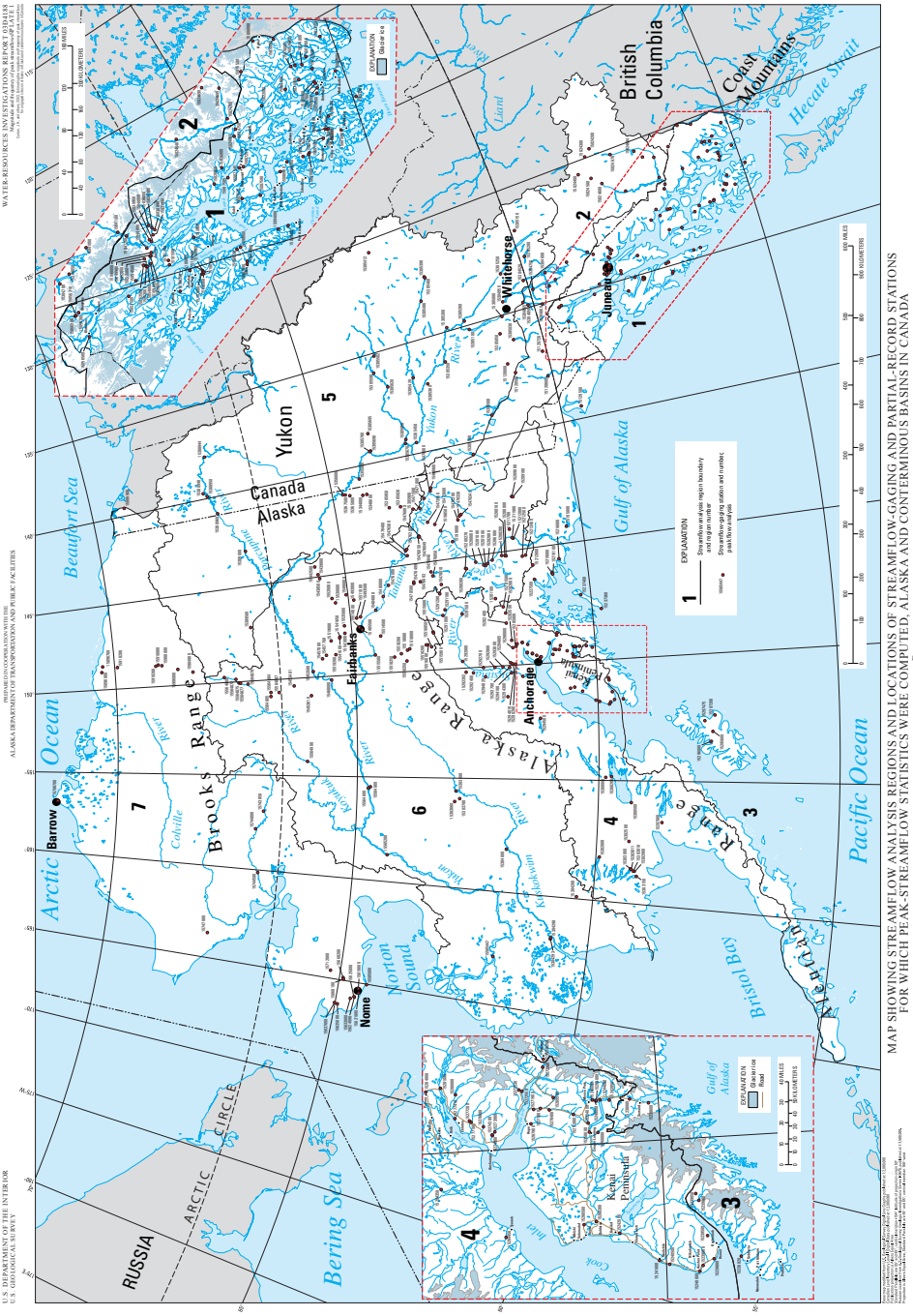

Figure 5.6: Streamflow analysis regions for Alaska. Figure reproduced from Curran *et al.* (2003).

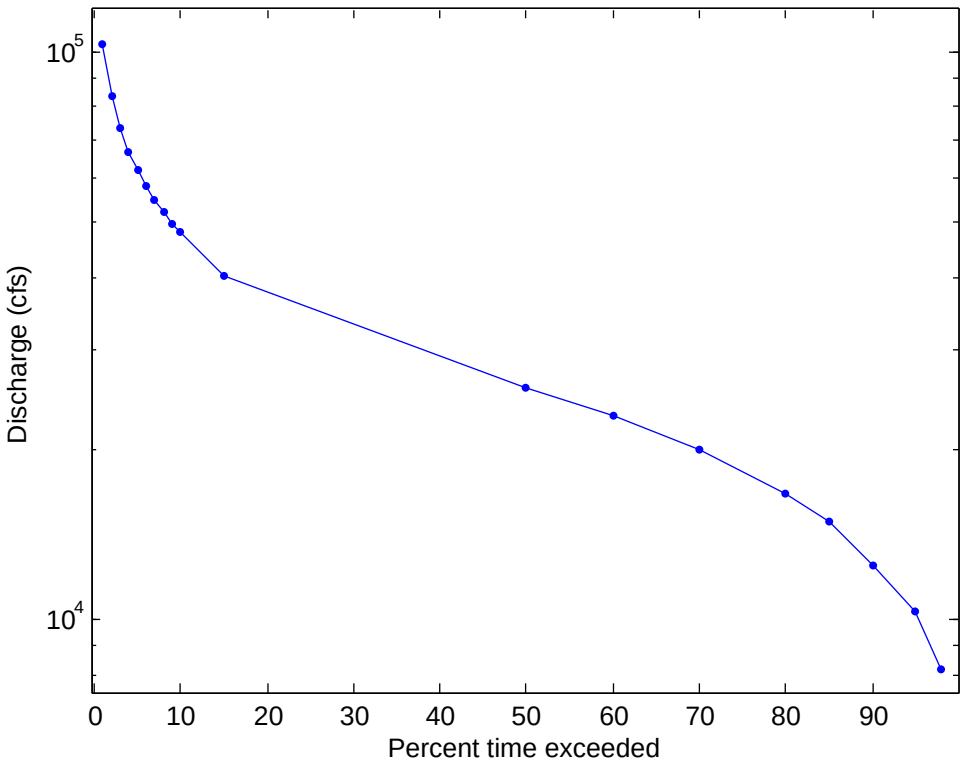

Figure 5.7: Flow duration curve for the Glacier Bay domain.

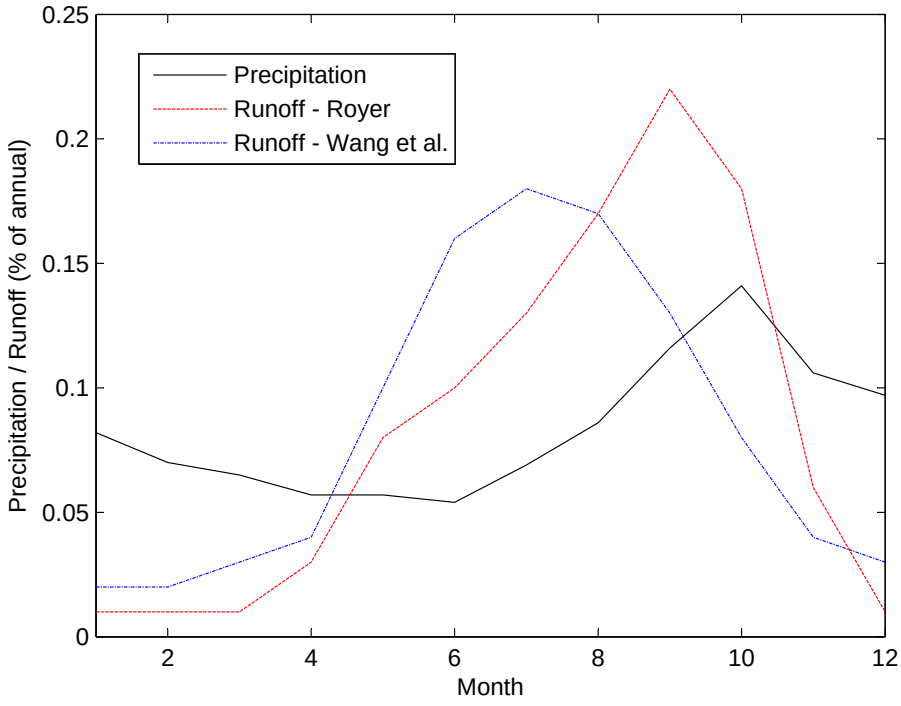

Figure 5.8: Normalized annual precipitation and runoff for the Gulf of Alaska from Wang *et al.* (2004). The hydrograph of Royer (1979), as determined from the meteorological data in Wang *et al.* (2004) is also shown.

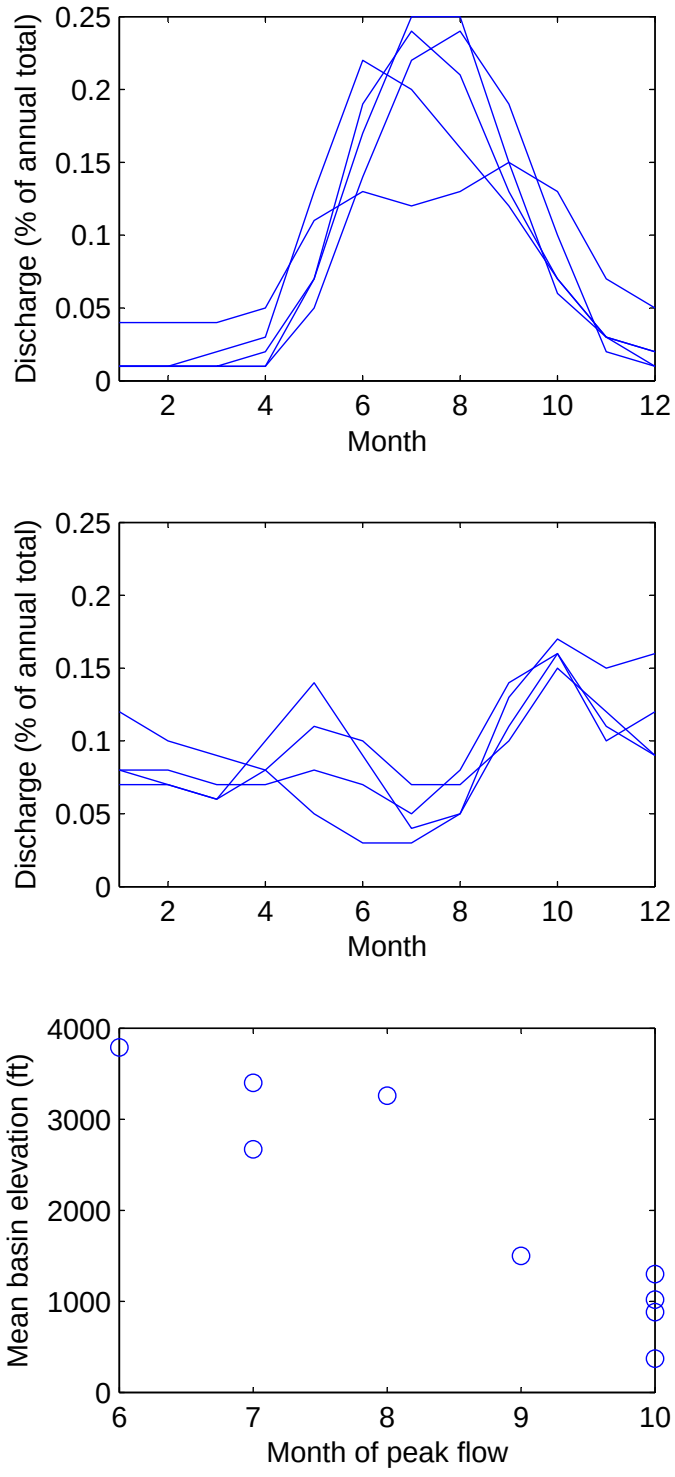
Discharge (% of annual total)
0.25
0.2
0.15
0.1
0.05
0
2
4
6
8
10
12
Month
Discharge (% of annual total)
0.25
0.2
0.15
0.1
0.05
0
2
4
6
8
10
12
Month
Mean basin elevation (ft)
4000
3000
2000
1000
0
6
7
8
9
10
Month of peak flow

Figure 5.9: .

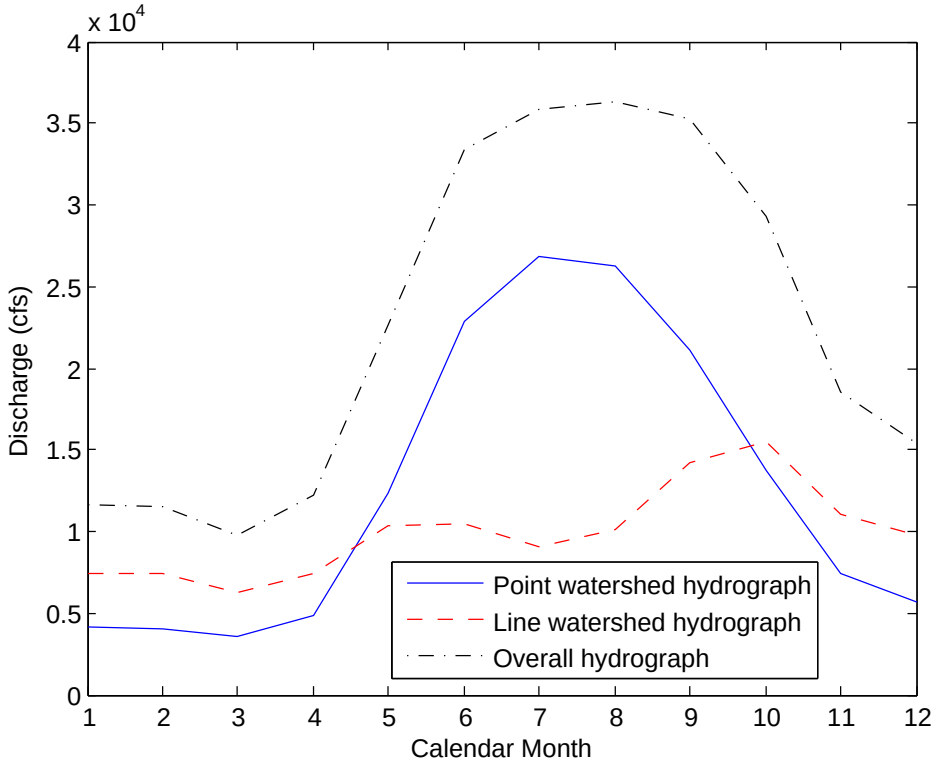

Figure 5.10: Modeled annual hydrograph for Glacier Bay Domain.

Chapter 6

fort.22 File - Meteorological Conditions

The ability of ADCIRC to incorporate meteorological forcing is extremely sophisticated. As ADCIRC was developed, in part, to facilitate hurricane simulations, this flexibility is no surprise. As just a few examples, meteorological data can be specified either at all grid points in the domain, or on a regular grid, such as the National Weather Service's ETA 29 km grid. Additionally, data can be input at time steps corresponding to the model, or at any user-specified time step.

The use of meteorological forcing in the Glacier Bay domain warrants some discussion. First of all, predictions of storm surges due to storms / hurricanes is not an objective of this project, so the need to rely upon and incorporate NWS forecast data does not exist. That said, however, it is of interest to this project to assess the extent to which winds and pressure might influence the circulation patterns and tidal heights predicted to occur. A significant obstacle to this goal is the severe lack of meteorological data that exists in the vicinity of Glacier Bay. Thus, this chapter discusses what limited data exist and how they might be incorporated, in a simplistic way, into the present simulations.

6.1 Data Availability

Figure 6.1 illustrates the availability of historical and present data in the vicinity of Glacier Bay, as taken from the National Climatic Data Center

(NCDC). Note that, while many stations are shown, several of these prove to be of little use. For example, the availability of data at a station may be limited to only a short period. As another example, a station may have wind data, but not pressure data.

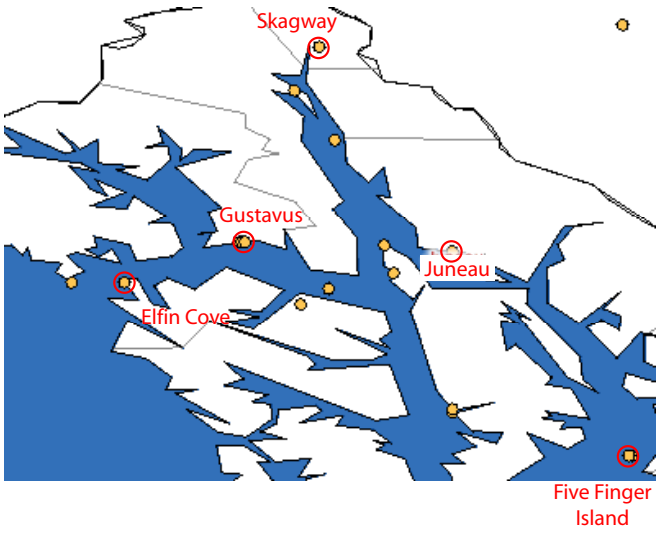

Figure 6.1: Select climate data stations in the vicinity of Glacier Bay.

6.2 Preparation of Data

Given these constraints, the following approach was taken. The goal is to have a climatic database, with values of wind speed, wind direction, and surface pressure available on an (roughly) hourly basis. When an ADCIRC user then desires to conduct a run with meteorological forcing, a fort.22 data file can be prepared based upon this database. To that end, wind data were extracted from the Gustavus station from the period of January 1988 to April 2006. Note that, during the extraction process from the NCDC website, the user has the ability to select options such as what parameters to output and what time reference to use. For the present study, all data were output relative to GMT time.

In the extracted file, there are columns corresponding to the date / time, the wind direction, and the wind speed, among others. These data are generally available on the top of the hour, but, in some instances, data are reported

at other times within the hour. During some lengthy intervals, no data are available, perhaps due to a sensor malfunction. These 'missing' data points were filled in by averaging the data values from the most closely available bracketing times.

With regards to surface pressure, the Gustavus station has no values available. Therefore, pressure values were obtained, for the same time period, from three stations in the vicinity: Skagway Airport, Juneau International Airport, and Five Finger Island. These data were then binned and averaged on an hourly basis. For example, all existing data values between 00:00:00 (GMT) and 01:00:00 (GMT) on 1 January, 2000 were collected and averaged in order to determine a regionally-averaged value of surface pressure for that hour long period. These average pressure values were then added to the Gustavaus data file.

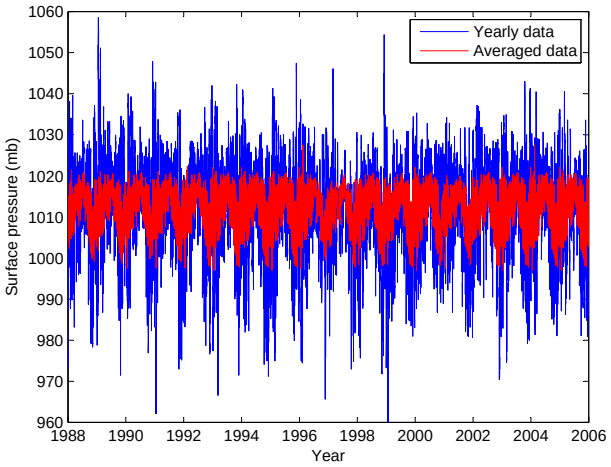

Figure 6.2: Plot of surface pressure over an 18 year period. Also shown is the data, binned hourly and averaged over the 18 year period of the record.

Also included in the final data file, glba_climate.txt, are columns giving the direction, speed, and pressure, in hourly bins, averaged over the 18 year period of the record. These data are helpful in revealing longer-term trends in the climatic records. For example, Fig. 6.2 shows the 18 year record of surface pressure, averaged over the three stations given above. It also shows the pressure data when averaged on an annual basis. This latter curve shows a clear annual cycle, with relatively low pressures in winter and high

pressures in summer. These annually-averaged values could, in principle, be of use in terms of estimating the climatic conditions for a time period that lies outside the range (1988-2006) of the generated climate data file. However, this extrapolation must be viewed with considerable caution, given the wide variation (shown in Fig. 6.2) that can exist between the conditions of a given year and the long-term average.

6.3 fort.22 Creation

With the existence of the Glacier Bay climatic data base, stored in the glba_climate.txt data file, a fort.22 file can easily be created. It should be reiterated that the approach adopted here is assuming that meteorological parameters, while functions of time, are constant in both horizontal directions. Of the many choices for input format, the author is using the case where NWS = 5. In this case, wind speed in the x direction, wind speed in the y direction, and surface pressure are input, for every grid point, at a specified time interval. Given that climatic data are available on an hourly basis, the obvious choice is to include climatic data in the fort.22 file on the same time interval.

Upon execution, the Matlab script write_fort22.m prompts the user (i) for the start time of the simulation (GMT) and (ii) the duration of the simulation. Based upon these selections, the script interpolates the data in the climatic database to the times required for the fort.22 file. As an example, assume that the ADCIRC user wished to conduct a run that began at 11:34:50 (GMT) on August 2nd, 2002 and was to run for 6 hours. The script would then go in to the climate database on that date and linearly interpolate between 11:00:00 and 12:00:00 in order to determine the conditions at 11:34:50. These values would be used for the first hour of the model run, and then new values would be obtained.

Chapter 7

Post Processing, Visualization, and Sample Output

Upon successful execution of an ADCIRC run, a number of output files will be created. Specifically which files are created depends upon how the fort.15 file was structured, i.e. what type of output was requested.

ADCIRC output can be written either in ASCII (simple text) or binary format. The former has the advantage of being easily read in by a wide variety of applications (text editors, spreadsheets, etc.) while the latter has the advantage of being far more compact. As ADCIRC output is very dense, both spatially (large finite-element grids) and temporally (output is available at as many time steps as the user desires), output data files can quickly become extremely large.

Finding efficient and attractive ways to visualize this output is crucial to the end user. The intent of the current chapter is to outline several Matlab scripts written by the author with the goal of visualizing and / or animating the model output. Sample results will be provided to help illustrate the capability of these scripts. Specific and more detailed results, pertaining to issues of interest in Glacier Bay, are reserved for later chapters.

7.1 Water Surface Elevation

Water surface elevation data can be written in one of two ways. First, data can be written at only specified points (fort.61 files). Second, data can be written at *all* nodal points in the mesh (fort.63 files). The former is useful

if the user wants to inspect a highly-resolved time series of elevation (much like a tide gage) while the latter is useful if the user wishes to plot a contour map of elevation over the entire (or a portion) domain.

With regards to temporal resolution, note that, since fort.61 only outputs data at (presumably limited) requested points, data may be requested at a very small time interval while still yielding an output file of modest size. As a point of comparison, NOAA frequently provides water elevation data at 6 minute intervals. For the purposes of comparison (model output to data), therefore, there is no need to request time series output at a smaller time step than this.

In principle, one can extract time series of elevation from the global fort.63 file, but the temporal resolution of global output is generally limited (say, one half hour to one hour) by file size. Therefore, it is recommended that the fort.61 output option be used when time series at limited points are desired.

7.1.1 Time Series of Elevation

The Matlab script read_fort61.m is used to load and plot the time series data written to fort.61. When executed, the user first loads the specified files and is then presented with a graphical rendering of the domain (Fig. 7.1. Symbols indicate the locations (as was specified in the fort.15 file for that run) where time series elevation data was requested. The user can then click on any number of these stations in order to select a subset for plotting. Upon completion of this selection, time series from the selected stations are plotted in a second figure (Fig. 7.2. The horizontal axis is in days and is referenced to 12:00 a.m. (GMT) of the first day of the simulation period.

7.1.2 Contour Plots / Animations of Elevation

While the time series are helpful in understanding the tides at a give point or points, it is also useful to visualize the tides as a 'field variable.' In other words, it is helpful to make a two-dimensional plot or 'snapshot' of the water surface elevation at a given time.

The Matlab script view_elevation.m allows the user to view such a snapshot at any of the times that were written to the fort.63 file. Additionally, the program allows the user to create an animation of the elevation fields over the entire duration of the simulation. This animation can then be written out to an .avi file, which is readily viewed by a number of graphics applications.

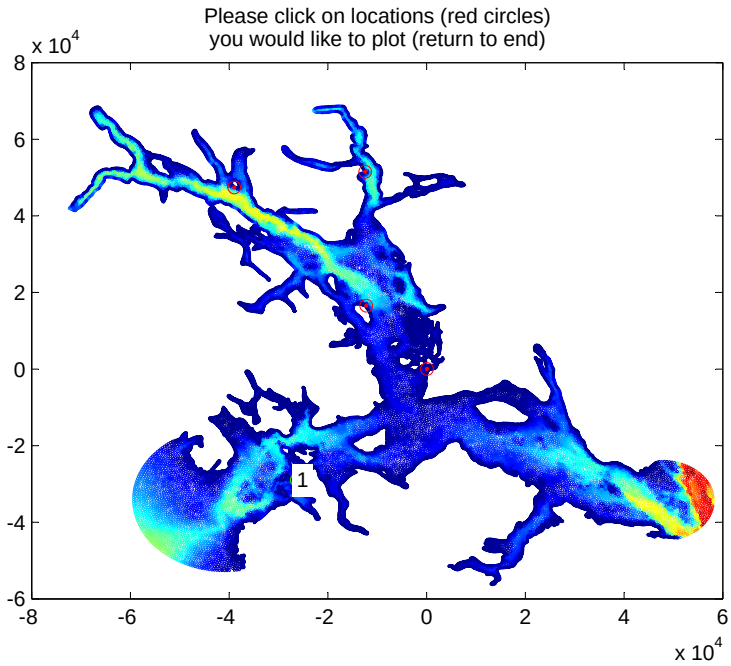

Figure 7.1: User selection of the fort.61 stations to plot as time series.

Upon execution of this script, the user is prompted to load the related data files and then is asked to choose between making a single contour plot of the elevation at a given time or an animation. In the case of the animation, the user will need to (if desired) zoom in on the region of interest before proceeding. Additionally, it is necessary for the user to specify expected minimum and maximum elevation, as these values set the range of the 'colorbar' used for visualizing the results. Values on the order of -3 m and 3 m work well in most cases for the Glacier Bay domain. Finally, if an animation is selected, the user is prompted to specify the file name (.avi format) to which the animation should be saved. A sample 'snapshot' of elevation is given in Fig. 7.3. Note that, in the case of the animation, the script is fairly slow as a tremendous amount of data has to be read and then rendered to the screen as graphical output.

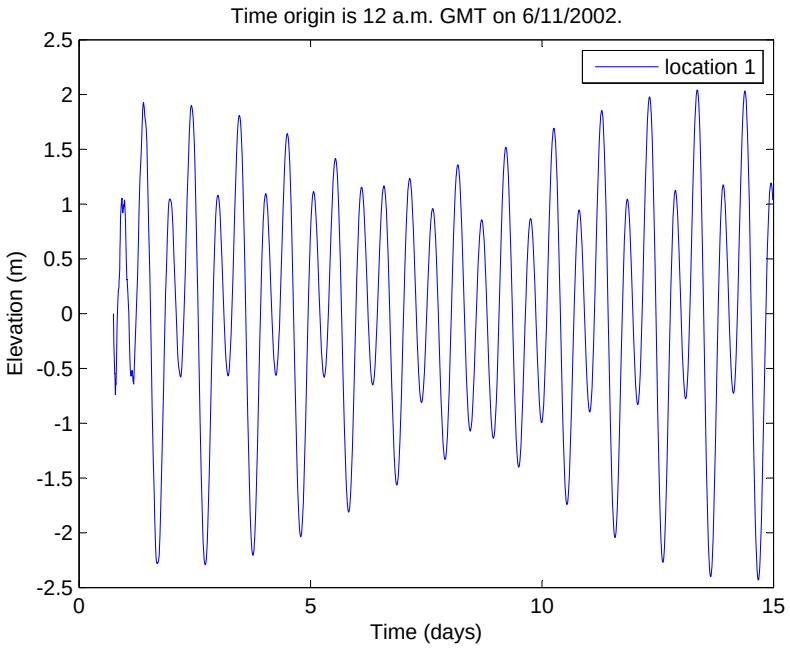

Figure 7.2: Time series of water surface elevation for the selected station(s).

7.2 Two Dimensional Velocity Fields

The work described in this report comes from ADCIRC runs in 'two-dimensional' mode. This means that, at each grid point, a two-dimensional horizontal velocity vector is output. This velocity vector represents the vertical average over the water column. For a system, such as Glacier Bay, where significant salinity gradients exist, a fully three-dimensional approach would be ideal and this is the subject of ongoing work.

As was the case with elevation, velocity information can be reported in one of two ways. The first, contained in the fort.62 file, reports velocity at specified locations only. This would be useful, for example, for comparing calculations to data obtained from a moored velocity meter, such as an acoustic doppler current profiler. The second, contained in the fort.64 file, reports velocity in the 'global' sense, i.e. at all grid elements. In this latter case, it is very useful to make a plot where the two-dimensional velocity *vectors* are displayed. This provides the user with a good grasp of the flow field at the given time.

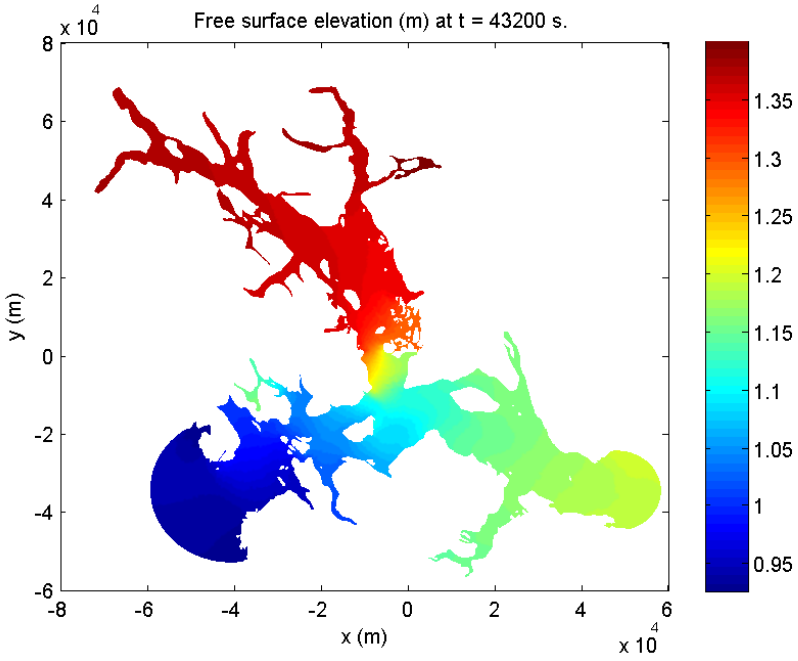

Figure 7.3: Sample contour plot of free surface elevation at a given simulation time.

The Matlab script view_global_velocity.m has many of the same features as the view_global_elevation.m script described above. Upon execution, it will prompt the user to load the fort.14, fort.15, and fort.64 files. The user can then select between a plot at a single time step, or an animation of all of the results available in the fort.64 file. In the case of a static plot, the entire domain is plotted and the user can subsequently go in and zoom in / out and pan around the domain, in order to explore the results more closely.

In both cases (static plot and animation), the user has the choice of plotting, along with the velocity vectors, contours of either the bathymetry, the water speed, or the vorticity. Vorticity is a measure of the 'rotation' of a fluid and regions of high vorticity are indicative of swirling motions and possibly eddies. For the case of a static plot, the minimum and maximum limits of the contour plot are set by the global minimum and maximum from the entire domain. For an animation, the user will have to specify expected minimum and maximum values. While this may take a bit of practice and experience, it is necessary to ensure that all contour plots throughout the

animation are on an identical scale. Figures 7.4-7.5 illustrate sample results in the area of Sitakady Narrows.

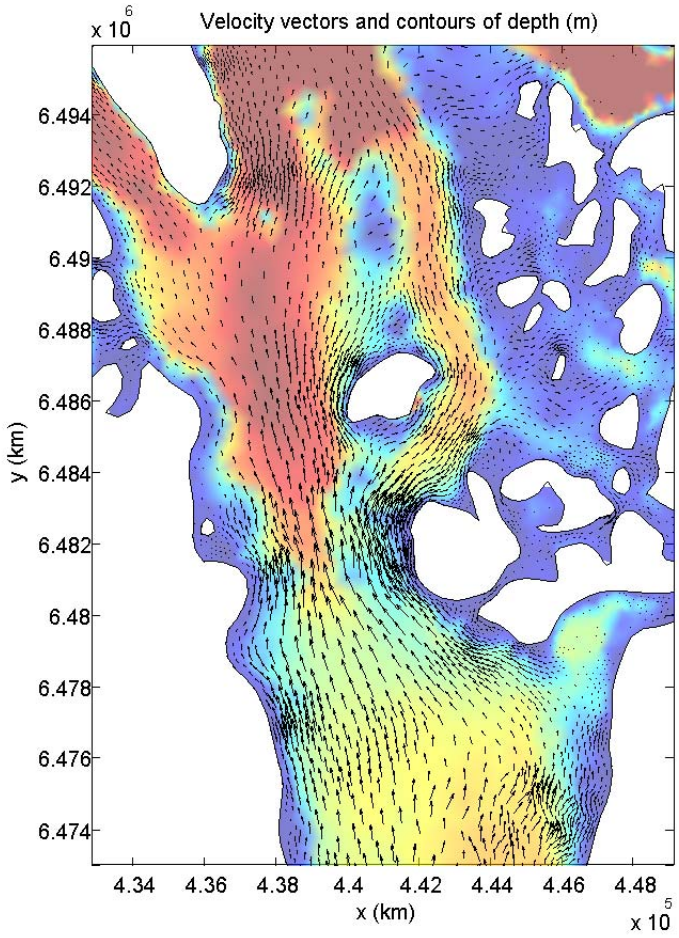

Figure 7.4: Sample velocity vectors showing the two-dimensional flow field and contours of bathymetric depth in the Sitakady Narrows area.

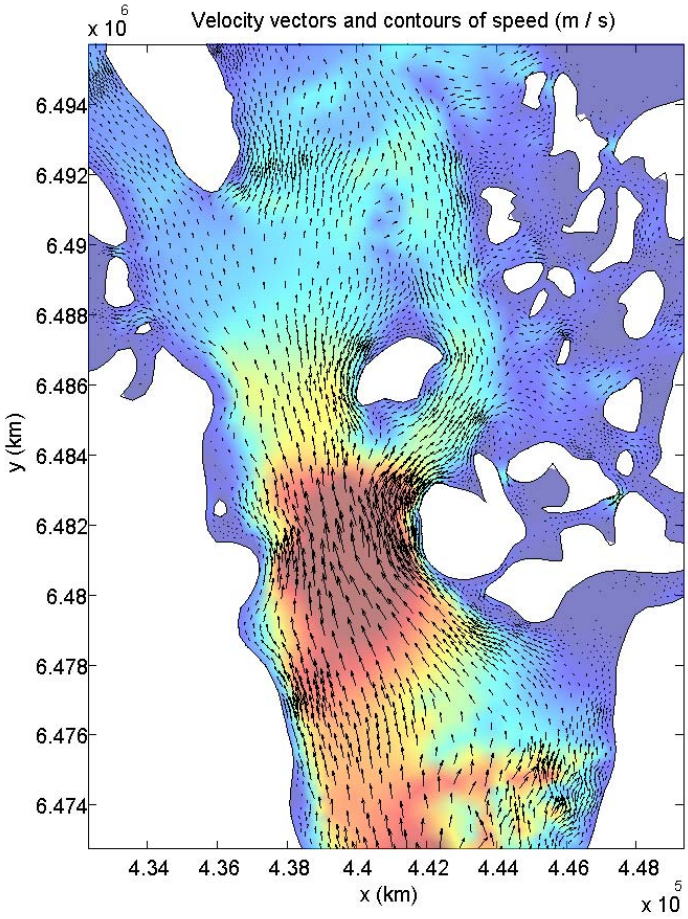

Figure 7.5: Sample velocity vectors showing the two-dimensional flow field and contours of water speed in the Sitakady Narrows area.

7.3 Particle Trajectories

Finally, it is of great interest to be able to predict that path, or trajectory, taken by an identified parcel of water over time. This concept brings into focus the difference between Eulerian and Lagrangian approaches to mechanics. An Eulerian approach calculates output variables as 'field variables.' In other words, velocity or elevation information gets reported at fixed points in space. In this framework, a flow variable is a function of both space and time.

A Lagrangian approach, on the other hand, identifies what are called 'material elements' and tracks them as they move. In this case, which is precisely the case of a released drifter or drogue, velocity information is solely a function of time and of the initial position of the material element.

For an environmental hydraulics application, there are a number of reasons why it would be of interest to calculate trajectories taken by marked particles. One might be interested in the transport of a spilled contaminant, or of a passive biological species. In any case, provided that the assumption that the tracer of interest follows the flow is a suitable one, the velocity fields output by ADCIRC may be used to calculate trajectories over time.

Before illustrating this, there are a few practical considerations to take into account. ADCIRC generally utilizes a very small time step in making its calculations. However, and as has been discussed previously, results are not written out at each of these time steps. If that were the case, then output files would be excessively large. Instead, the model outputs data at a user-specified interval. Given the large mesh for the present application, a fort.64 file containing ASCII output at 100 times results in a file of approximately 150 MB. If these times span a single day, then the time resolution of the output is on the order of 15 minutes.

The issue of consequence here has to do with the calculation of Lagrangian particle paths based upon Eulerian data at relatively coarse temporal resolution. Recall first that the semi-diurnal tide repeats every 12 hours. If velocity data were only available every hour, calculated trajectories would demonstrate significant error. There is, therefore, a balance to be struck between managable file size and requirements for accuracy.

7.3.1 Numerical Integration

Next, consider a very brief introduction on exactly how particle paths may be calculated from the velocity fields in the fort.64 file. The two horizontal velocity components are defined by

$$\frac{dx}{dt} = u \equiv f_1(\underline{x}, t) \tag{7.1}$$

$$\frac{dy}{dt} = v \equiv f_2(\underline{x}, t). \tag{7.2}$$

The functions f_1 and f_2 are called 'derivative functions.' These differential equations are continuous and smoothly varying in time. However, since we have information only at *discrete* points in time (separated by the user-specified interval), we choose to replace the differential equations with equivalent difference equations.

Euler Method

The simplest way of doing this is to replace, for example,

$$\frac{dx}{dt} \rightarrow \frac{x_{n+1} - x_n}{\Delta t}, \tag{7.3}$$

where Δt is the time interval and the subscripts refer to the time step. Thus, the equation is rearranged to obtain

$$x_{n+1} = u_n \Delta t + x_n. \tag{7.4}$$

This so-called 'explicit Euler method' states that the position of a particle at the 'next' time step can be computed from the position and velocity of the particle at the present time step. While this method is extremely easy to implement, it is relatively low-order and can lead to large errors accumulated over time, especially if Δt is too large.

Consider as a simple example the case of 'stagnation flow.' This steady, two-dimensional flow field is given by the velocity components $u = y$ and $v = -x$. Based upon an initial location of x_0, y_0, it is straightforward to show that the exact answer for the trajectory taken by a particle upon its release is given by the equation $xy = x_0 y_0$. This exact answer, along with two approximate trajectories, as calculated by the Euler method, is shown in Fig. 7.6. Note that the flow comes in from the top and exits to the right. Note also the significant variation of the trajectory with time step.

Runge Kutta Method

A far more accurate method than the first-order Euler method is the fourth order Runge-Kutta method. With this method, we have (using, as above, the x component of velocity as an example)

$$x_{n+1} = x_n + \frac{1}{6}(\Delta x_1 + 2\Delta x_2 + 2\Delta x_3 + \Delta x_4), \tag{7.5}$$

where

$$\Delta x_1 = \Delta t f_1(x_n, t_n) \tag{7.6}$$

$$\Delta x_2 = \Delta t f_1\left(x_n + \frac{\Delta x_1}{2}, t_n + \frac{\Delta t}{2}\right) \tag{7.7}$$

$$\Delta x_3 = \Delta t f_1\left(x_n + \frac{\Delta x_2}{2}, t_n + \frac{\Delta t}{2}\right) \tag{7.8}$$

$$\Delta x_4 = \Delta t(x_n + \Delta x_4, t_n + \Delta t). \tag{7.9}$$

Similar equations exist for y. As is evident from this formulation, calculation of x_{n+1} now requires more than just x_n and $u_n = f_1|_n$. Sample results, for the same time steps used in Fig. 7.6, are given in Fig. 7.7. Note that, even for the very coarse time step, the approximate results are in excellent agreement with the exact results.

7.3.2 Application to ADCIRC Output

The Matlab script trajectory.m was written in order to allow the user to visualize the paths taken by identified material elements. Presently, there are a number of ways in which the initial locations of the elements may be set. When the script is executed, and the grid and model run files (fort.14 and fort.15) are loaded, the user is presented with the option of placing individual particles, a 'cloud' of particles, or a 'rake' (evenly distributed along a line) of particles. Note that it is possible to combine multiple instances of all of these release methods.

When the user is finished, the velocity data is loaded and the Lagrangian paths taken by the particles are computed via the Runge-Kutta method. Figure 7.8 illustrates the consequences of relying on the less-accurate Euler method. For this example, the global velocity output is at 5 minute intervals. Many of the trajectories show a steadily accumulating discrepancy

between the Euler and Runge-Kutta methods. One, in particular, shows how these small errors can, depending on the bathymetric details, lead to wildly different ending locations for the particles.

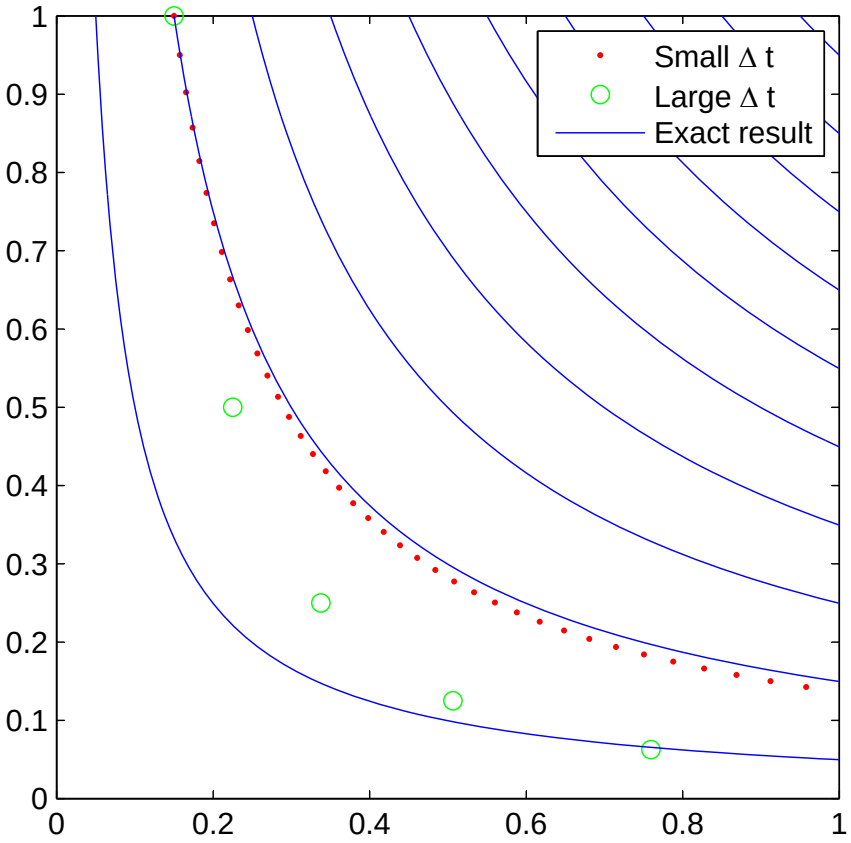

Figure 7.6: Sample particle trajectories, based upon the Euler method, using small and large time steps. Also shown are the exact trajectories.

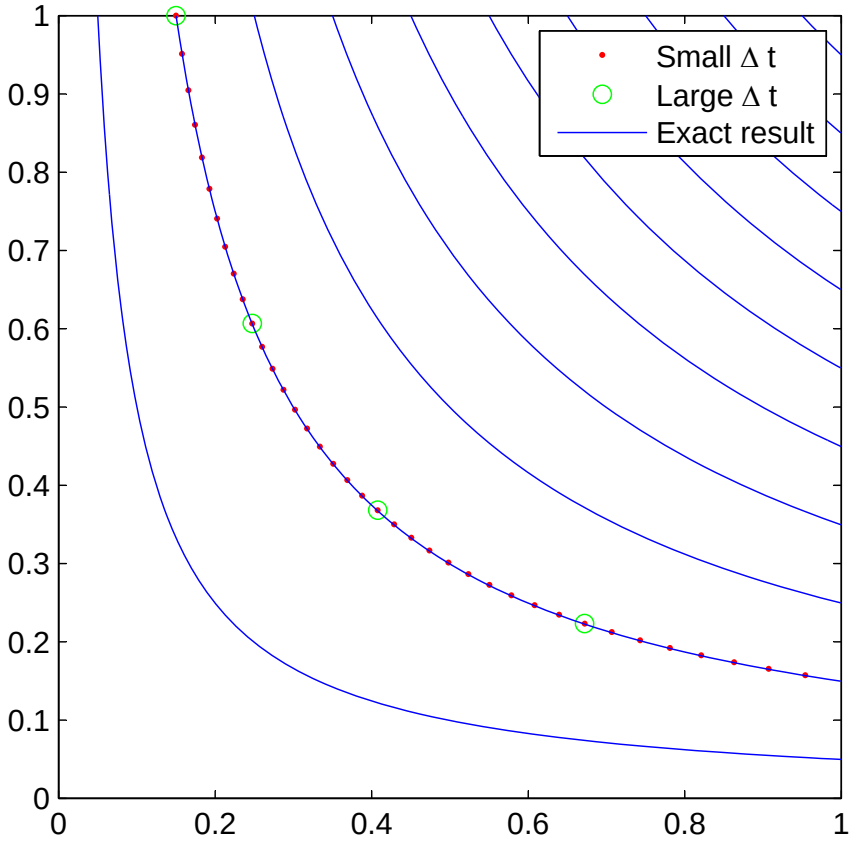

Figure 7.7: Sample particle trajectories, based upon the Runge-Kutta method, using small and large time steps. Also shown are the exact trajectories. Note that the time steps used are the same as in Fig. 7.6.

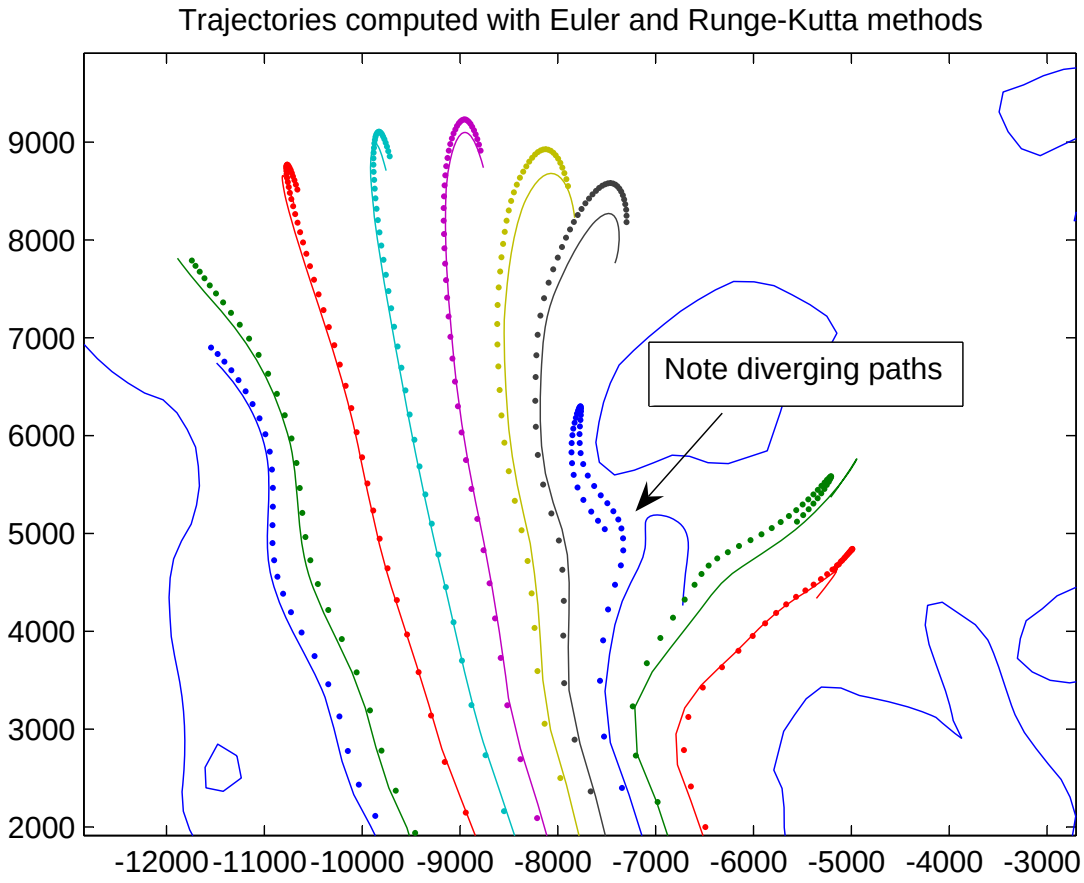

Figure 7.8: Particle trajectories, in the Beardslee Islands area, calculated with both the Euler (solid lines) and the Runge-Kutta methods (dots).

Chapter 8

Model Testing and Validation

Before turning to specific simulations of interest, a number of initial tests were carried out in order to assess the accuracy of the simulations and to help determine the appropriate parameters for the fort.15 file.

8.1 Spin up Time

There are many different objectives in carrying out an ADCIRC run. For example, some users use it to determine the tidal constituents at a given location. In this case, a long simulation is carried out and then a harmonic analysis is performed on the time series of predicted elevation at that point. In this case, the origin of the 'time axis' is relatively unimportant.

Other users are interested in performing an ADCIRC simulation for a very specific time period. In this way, the model output can be compared against data from an ADCP or a tidal gage for a specific date and time. Properly setting the origin of the time coordinate for the simulation is therefore of paramount importance.

Related to this is the issue of how much time is required for the model to 'spin up.' When ADCIRC begins a simulation, the initial shape of the water surface must be known. However, it is generally unknown. So, it is common to perform a 'cold start' by simply assuming the water surface in the entire domain to be flat. If this is the case, then it is intuitive to expect that some time will be required for the domain to fully adjust to its boundary forcing. If the model was spun up only one hour before output was to be compared to field data, it seems unlikely that a meaningful comparison would be obtained.

The question, therefore, is how long the model must be run before one can assume that the transients from the cold start have dissipated. Conversations with other researchers suggested that the answer to this question was highly domain-specific, but initial suggestions of one to two weeks were made.

To test this hypothesis, it was decided to perform a simulation for the 0.25 day period beginning at 17:38:51 (GMT) on June 25, 2002. Two ADCIRC runs were performed, the first beginning 7 days before this (total run duration of 7.25 days), the second beginning 14 days before this (total run duration of 14.25 days). If the output from the two simulations differed significantly for the 0.25 day target period desribed above, the conclusion would be that a seven day spin up was not sufficient.

Time series of elevation at a given point for the two runs are given in Fig. 8.1. Note that the time axes of the two simulations are synchronized and that the origin is taken to be 12:00:00 GMT on June 11, 2002. For the first seven days or so, only one time series is observed, since the second trial had not yet begun. Seven days after the commencement of the 14 day run, the 7 day run begins. The lower portion of the figure plots the absolute value of the difference between the two results from this time onward.

First of all, note that, by the end of the simulation periods, the discrepancy between the two results is on the order of 5×10^{-4} m, whic is 0.01% of the tidal wave height of ~ 5 m. The lack of significant discrepancy between a 7 day and a 14 day run suggests that 7 days is more than adequate in terms of initializing the model from an initially flat water surface.

Next, note that, within two days of the 7 day simulation starting up, the discrepancy between it and the 14 day simulation is only 0.1% of the tidal wave height. This suggests that the very modest period of only a few days is an adequate spinup time. The fact that this result is so much shorter than the two week suggestion from other researchers likely has to do with the relatively small physical size of the domain, compared to oceanic scales.

8.2 Validation of Water Surface Elevation Calculations

There are two ways of validating the values of water surface elevation calculated by ADCIRC. First, they may be compared to actual data from a tidal gage. Second, they may be compared to calculations / predictions at a station

with accepted tidal constituents. Extensive repositories of both data and predictions are available from NOAA at http://tidesandcurrents.noaa.gov/. At that site, an interactive map (see Fig. 8.2) will allow the user to select a station from which historical data and / or tidal predictions may be extracted and downloaded. Note that the available information will vary depending upon the selected station.

As a test, predictions were extracted, for the time period corresponding to the 14 day simulation described above. Predictions were obtained for Elfin Cove, Port Althop (Station ID 9452634), which lies near the southwestern portion of the ADCIRC model domain. These predictions are plotted together with the ADCIRC output in Fig. 8.3. As the figure illustrates, the agreement is extremely good, both in terms of phase and amplitude. At lower tidal amplitudes, e.g. near days 8 and 9, some minor discrepancies appear in the predicted crest and trough elevations. Overall, however, Fig. 8.3 is convincing confimation of ADCIRC's ability to predict water surface elevations.

The Elfin Cove station also has historical observtaional data archived for various periods. Therefore, a second test was performed, in order to see how the ADCIRC output, and the NOAA predictions, compared against actual observations. Fourteen days of data were extracted, beginning on 1 January, 2006, 00:00:00 GMT. The ADCIRC run was begun at this same time and a 14 day simulation was carried. out. The results of this comparison are shown in Fig. 8.4. As with the previous comparison, the agreement between the NOAA predictions and the ADCIRC out is exceptional. Both of these sets of predictions are also in good agreement with the observational data. There is a clear systematic offset, with the data being consistently higher than the predictions. Other comparisons for different time periods yielded different results, with the data being consistently lower than the predictions. Recalling that tidal constituents capture only gravitational influences, it is not surprising that there are modest differences between predicted and observed tides. For example, strong meteorological forcing in the form of winds and surface pressure can lead to slight differences between observation and prediction. With this caveat, it is clear that ADCIRC successfully predicts water surface elevations in the Glacier Bay domain.

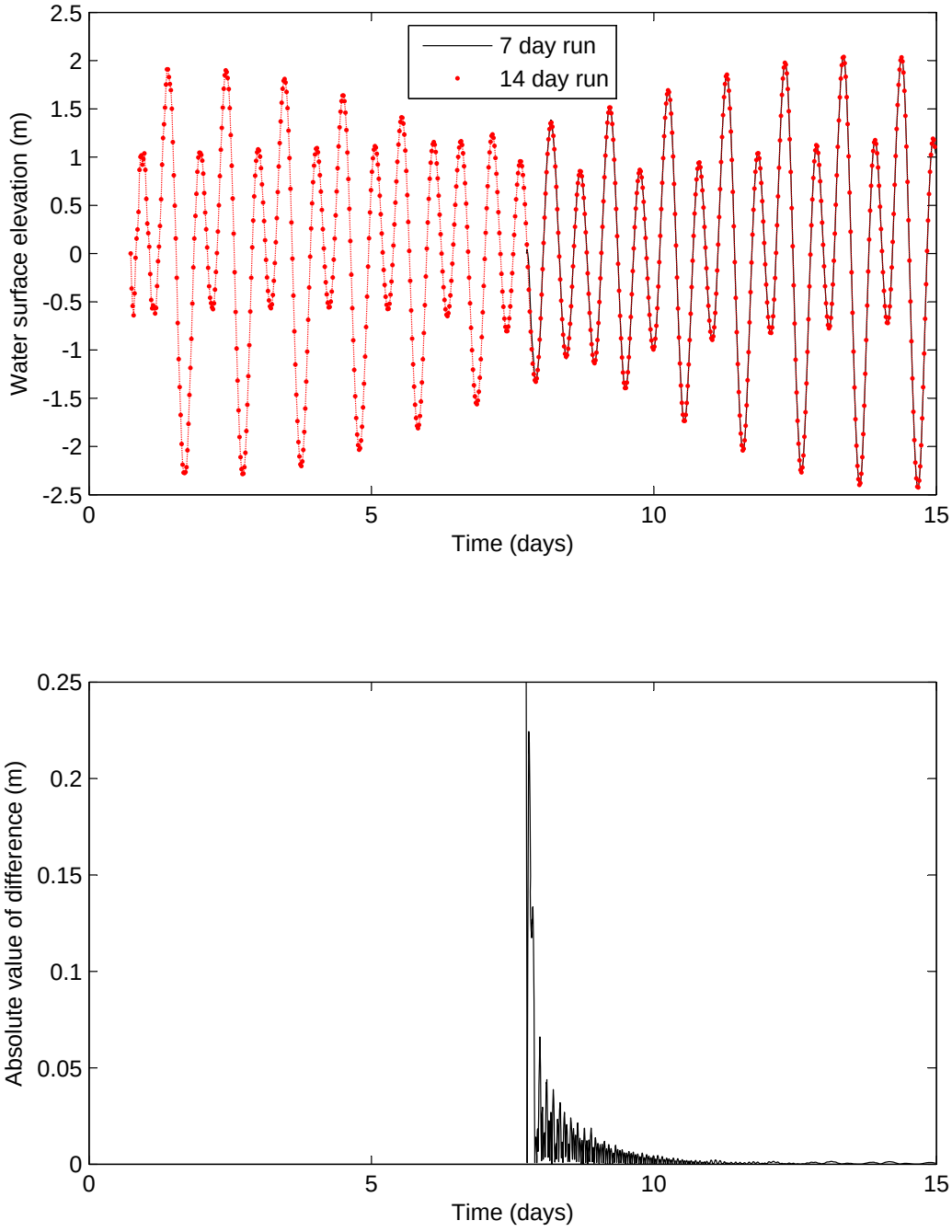

Figure 8.1: Comparison of output from a 7 day and a 14 day simulation. Also shows is the absolute value of the difference between the two runs.

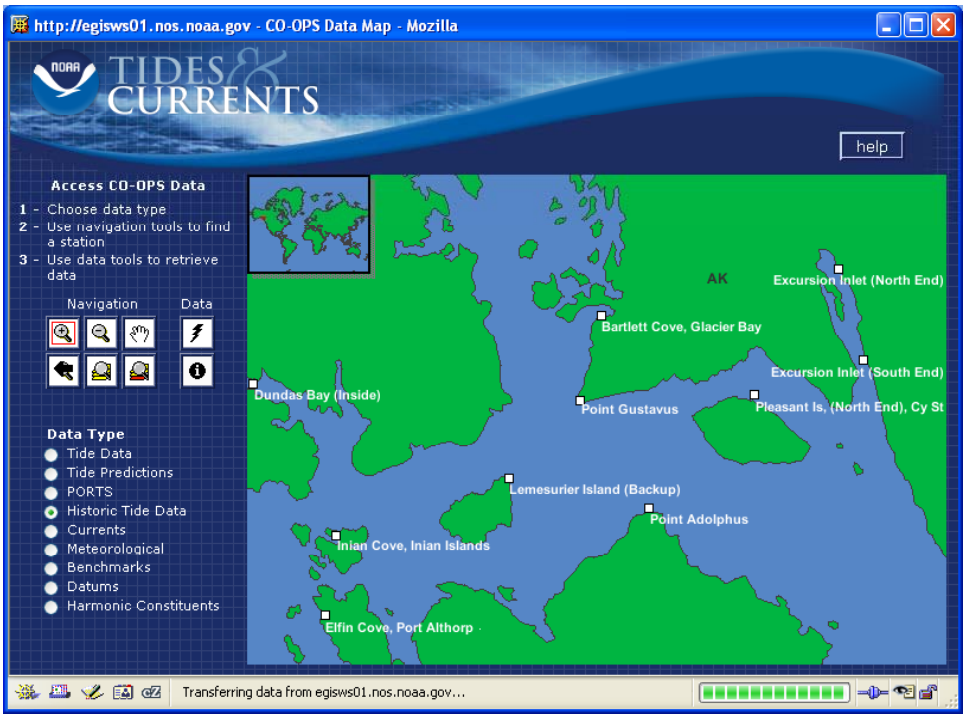

Figure 8.2: Interactive map allowing for the extraction of historic tidal data and tidal predictions.

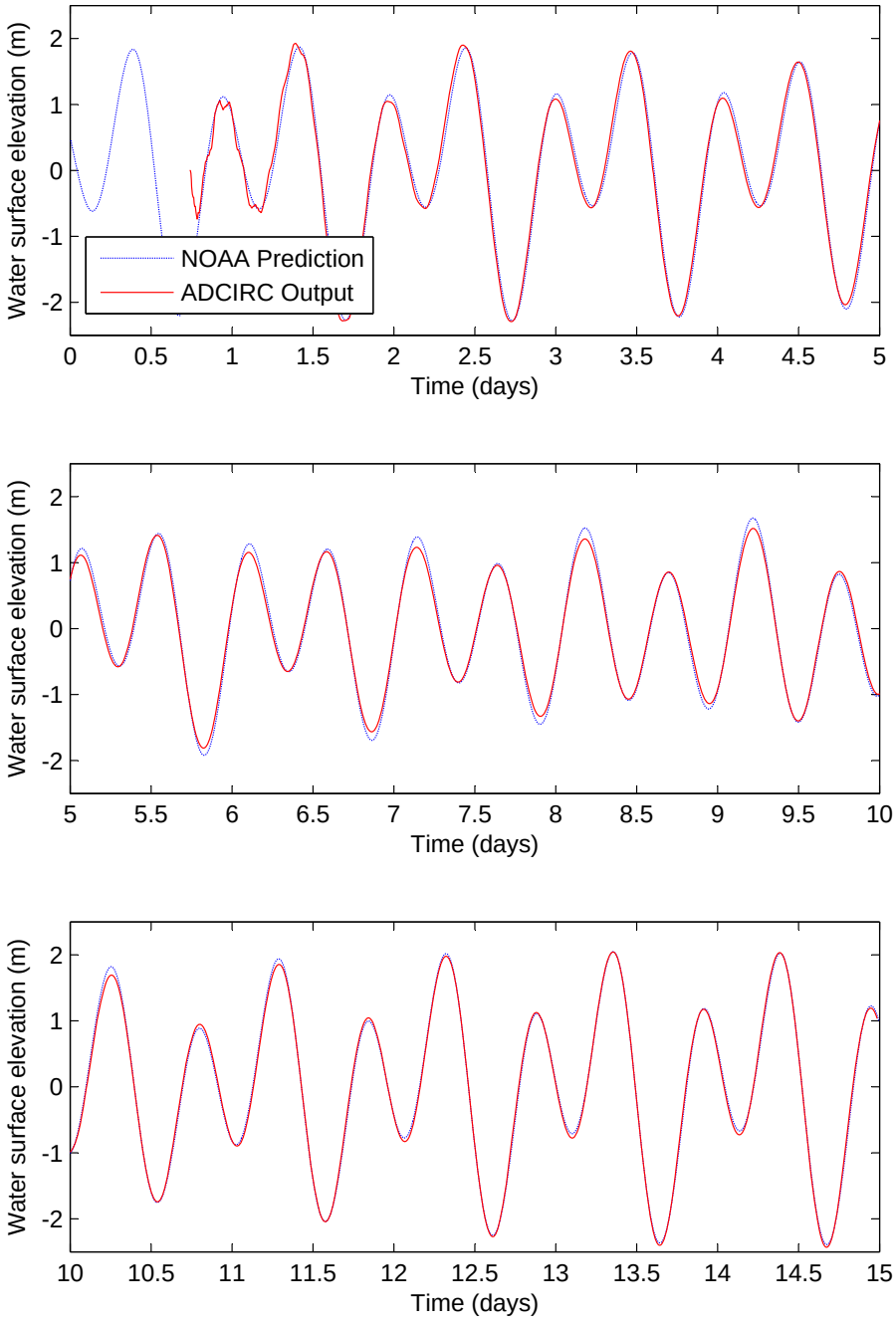

Figure 8.3: Comparison of NOAA predictions and ADCIRC calculations at the Elfin Cove Station for the 14 day period beginning 6/25/2002.

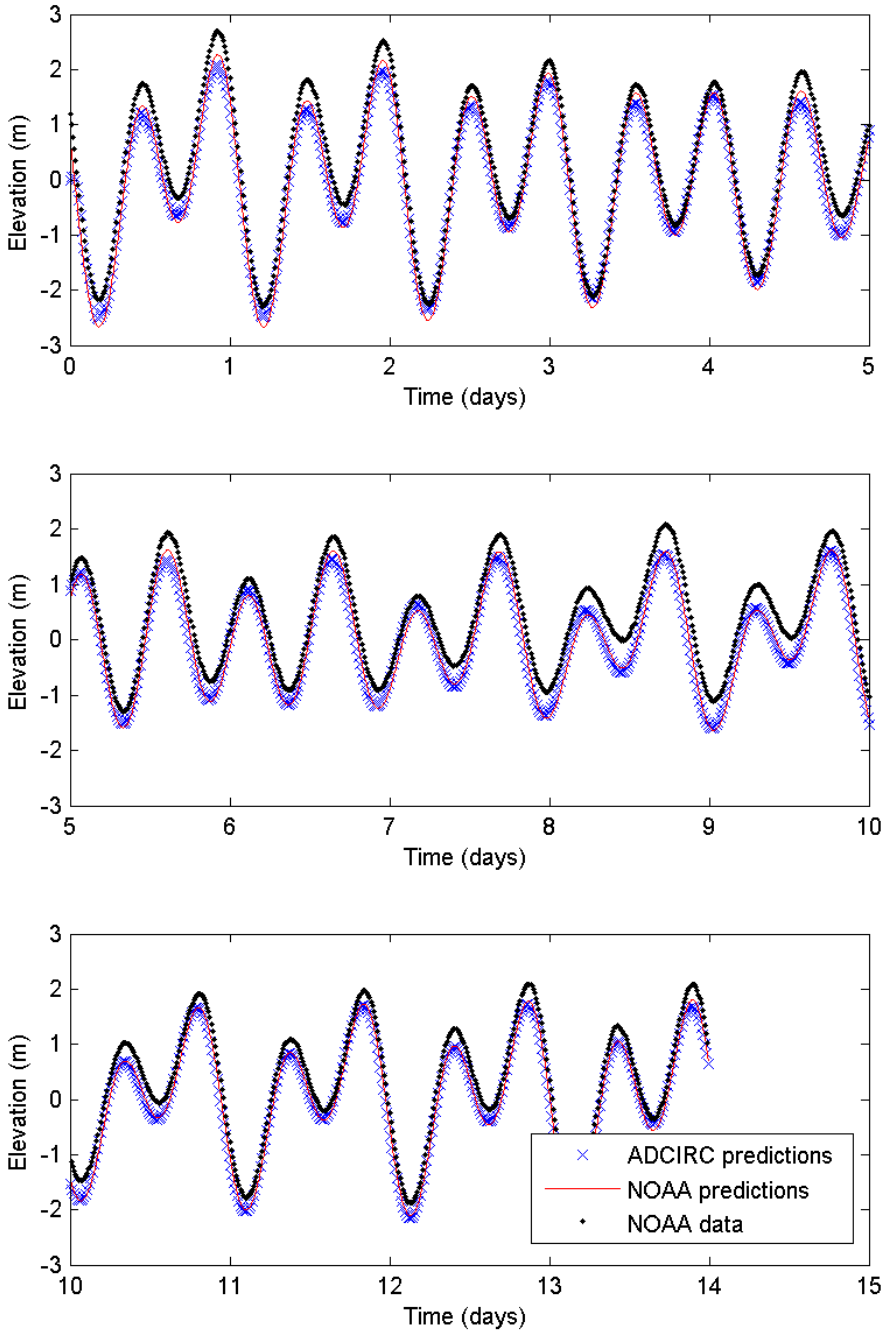

Figure 8.4: Comparison of NOAA predictions, ADCIRC calculations, and observational data at the Elfin Cove Station for the 14 day period beginning 1/1/2006.

Chapter 9

Modeling Results for Glacier Bay

Finally, attention is now turned to a number of specific results of interest for the Glacier Bay domain.

9.1 Water Surface Elevation

In the previous chapter, some preliminary results on water surface elevation were shown in order to 'validate' the model output. This was done by comparing model output to NOAA predictions and observations at a single station. There are a number of ways that we can now look at the spatial variation of the tides, in terms of magnitude and timing.

9.1.1 Tidal Amplification and Phase Lag

By requesting time series output at a number of stations, the amplification or attenuation of the tidal wave as it propagates up-fjord is readily studied. As shown in Fig. 9.1, time series output was requested at five stations dispersed throughout the domain.

Figure 9.2 shows the model output at these five stations. First, it is clear that the tidal wave amplifies as it propagates up-fjord. This is primarily due to the narrowing of the fjord which produces a shoaling effect on the wave. Second, the 'phase lag' between stations is clearly evident. Station 2 roughly corresponds to Bartlett Cove, station 3 to Willoughby Island, and stations

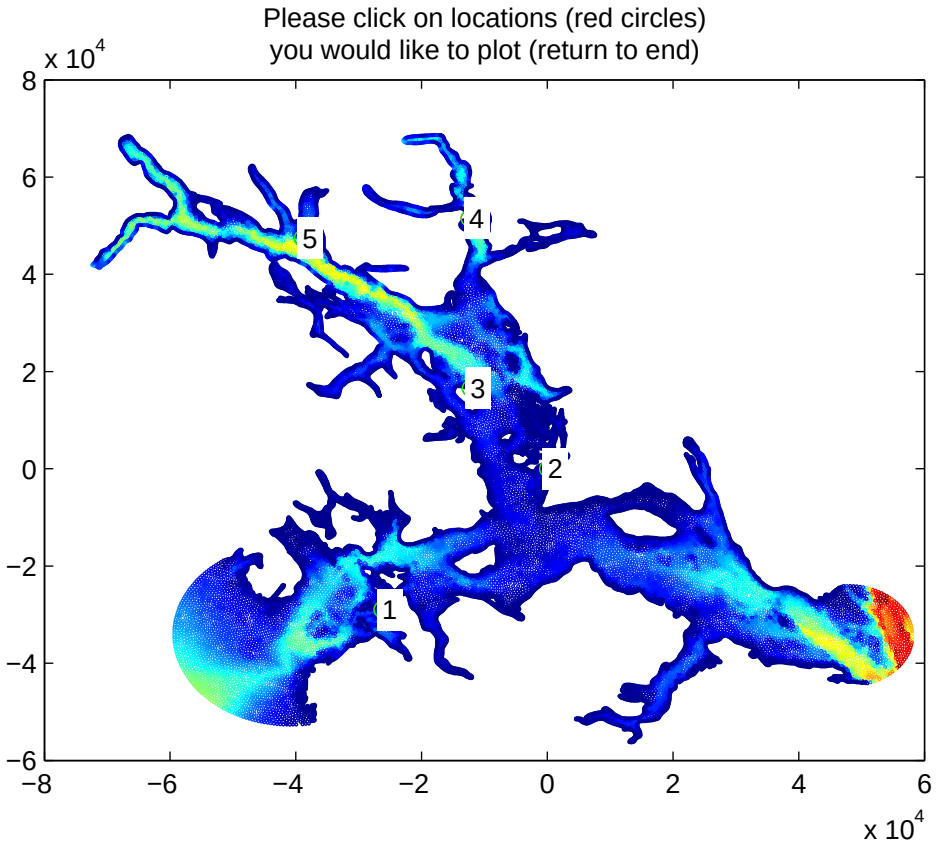

Figure 9.1: Domain map indicating five stations specified for time series output.

5 and 4 to the middle of the East and West Arms respectively. The results indicate a phase lag of approximately 15 to 20 minutes between stations 2 and 3. From station 3 to stations 4 and 5, the lag is only a few minutes. These results are consistent to the corrections published by NOAA.

Additional insight is gained by considering the contours of water surface elevation over the entire domain. Figure 9.3 shows a snapshot of the water surface at the commencement of an ebb tide during spring tide conditions. The tides are relatively low out in the Gulf, somewhat higher in Icy Strait and Cross sound, and higher still in Glacier Bay proper. Within the Bay proper, the variation in tidal amplitude becomes fairly weak.

If the limits on the color contours are changed and a zoomed in view

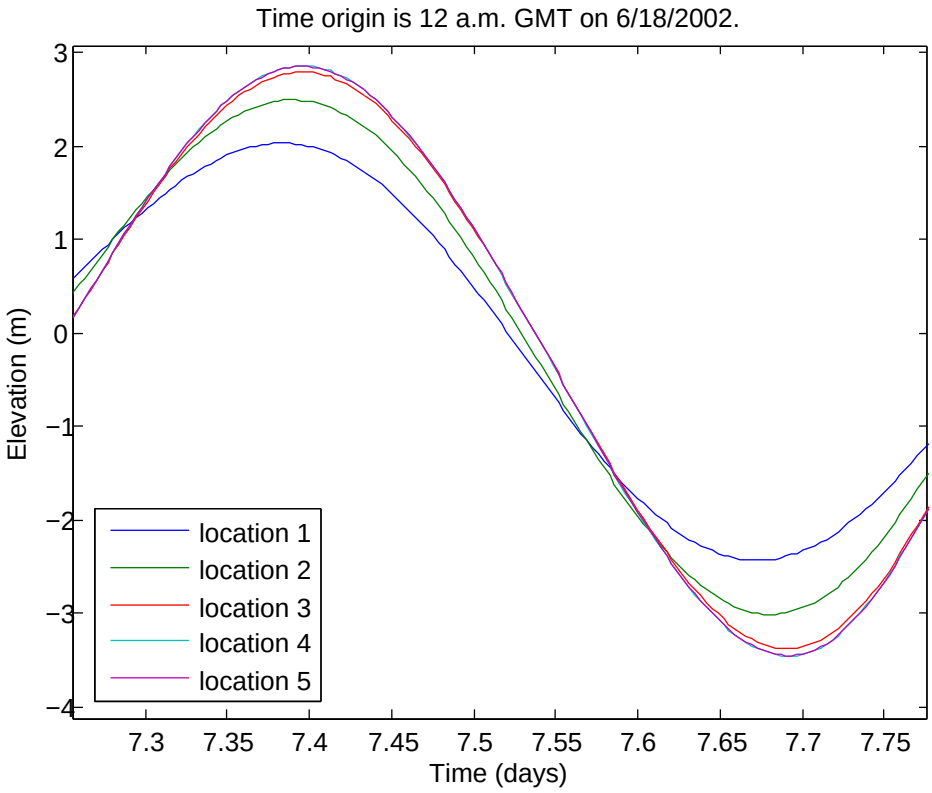

Figure 9.2: Domain map indicating five stations specified for time series output.

is taken (Fig. 9.4), the variation in tidal amplitude with up-fjord distance becomes more apparent. It is found that the highest tides in the bay occur in Adams Inlet in the East Arm.

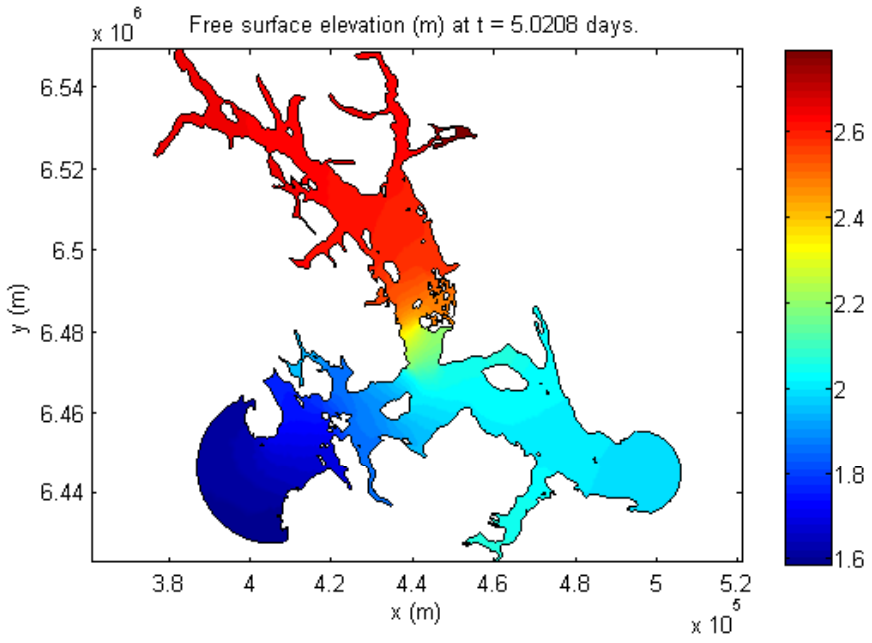

Figure 9.3: Color contours of water surface elevation.

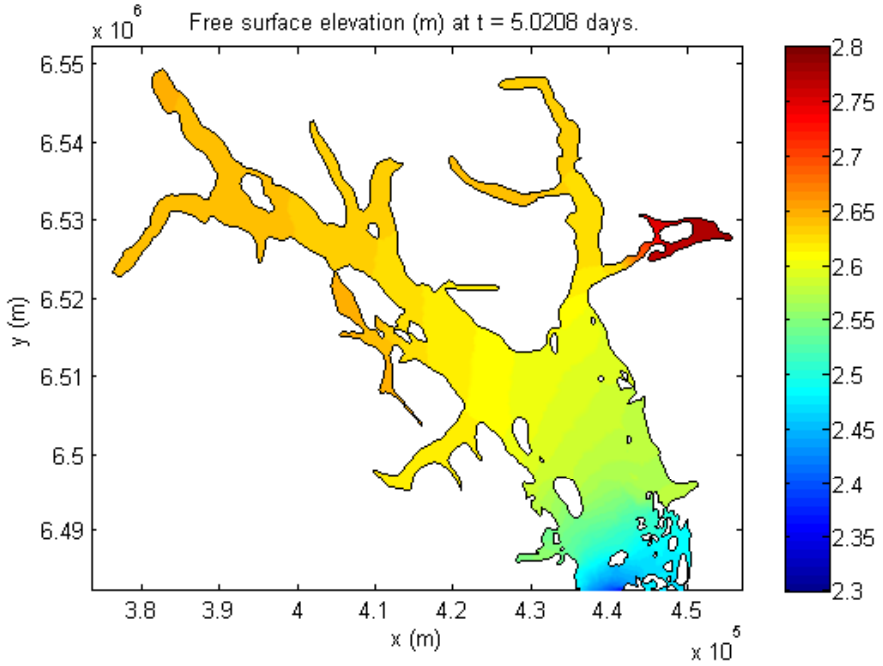

Figure 9.4: Color contours of water surface elevation in Glacier Bay proper.

9.1.2 Spatial Variation of Tidal Datums

As discussed in previous chapters, ADCIRC has the powerful ability to perform harmonic analysis of model output. This is essentially a least-squares analysis that fits model output to a user-specified number of tidal constituents. For each tidal constituent, the amplitude and phase is computed by the analysis. This information can then be used to compute tidal datums, such as mean higher high water (MHHW), mean lower low water (MLLW), and so on. These tidal datums are useful long-term indicators of the tidal conditions at a given location.

For the present application, a harmonic analysis was performed by conducting a 90 day simulation with a 20 day ramp. The last 45 days of the simulation period were used for the harmonic analysis. The results of the harmonic analysis, in terms of constituent amplitudes and phases, were then analyzed using the harmonic constant datum method (Mofjeld *et al.*, 2004). The results for MHHW, MLLW, and tidal range, here defined as the different between MHHW and MLLW, are shown in Figs. 9.5-9.7.

Note first of all the presence of numerous locations that seem discontinuous. For example, the region to the southeast of Point Gustavus. This has to do with the presence of very shallow regions that 'dry' during the simulation. The dry periods significantly affect the calculation of tidal constituents and, in turn, the tidal datums.

Second, the tidal datums show the same sort of behavior that was observed in the instantaneous 'snapshot' of the water surface (Fig. 9.3). The tides are lowest out in the Gulf, higher in Icy Strait and Cross Sound, and higher still inside Glacier Bay proper. Tidal ranges in excess of 4.5 meters are observed in most of Glacier Bay.

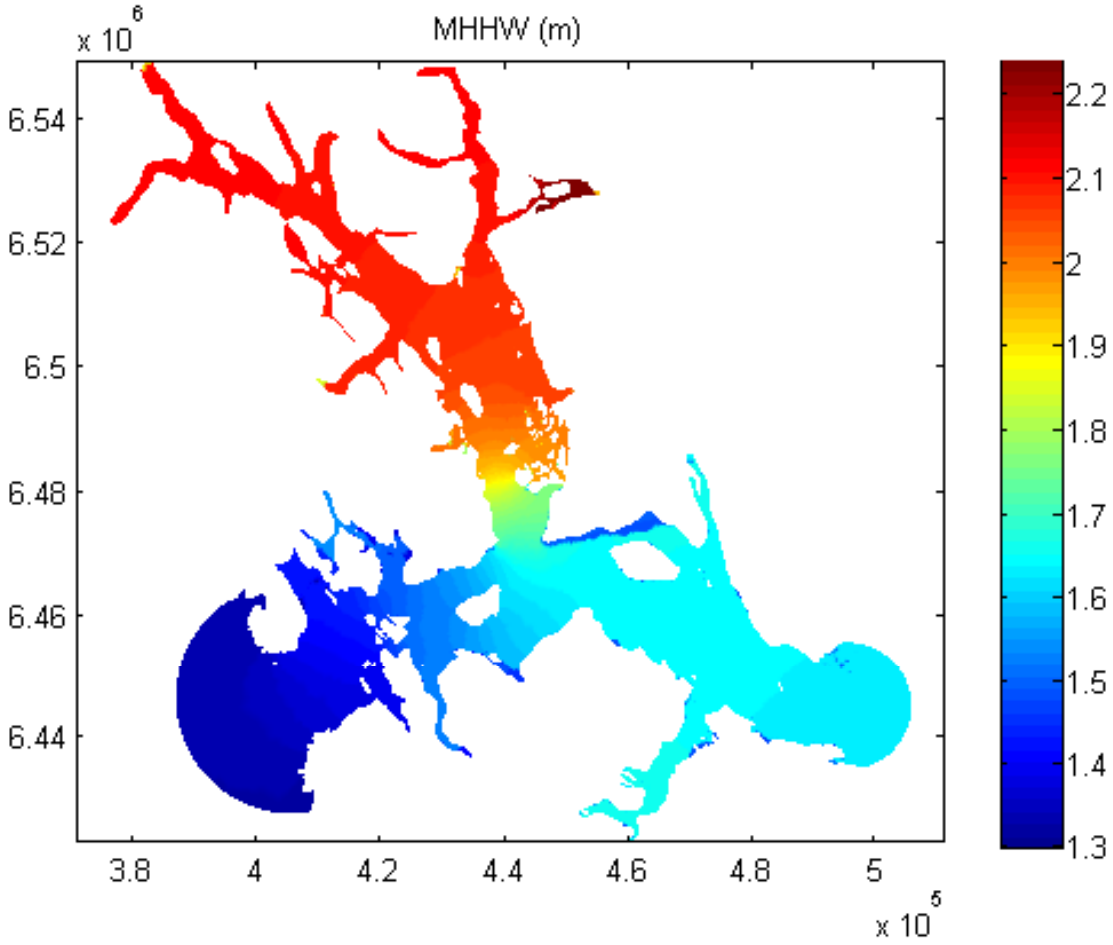

Figure 9.5: Color contours of MHHW in meters.

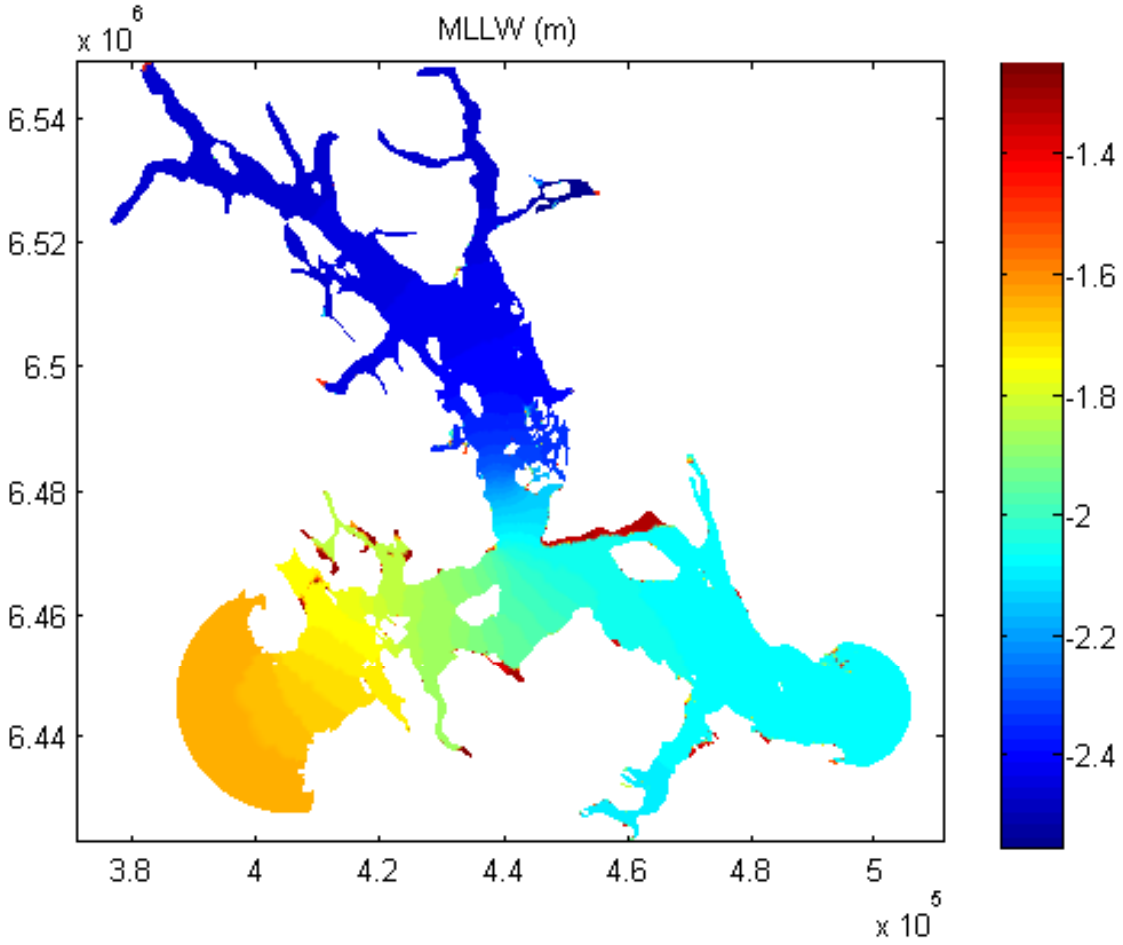

Figure 9.6: Color contours of MLLW in meters.

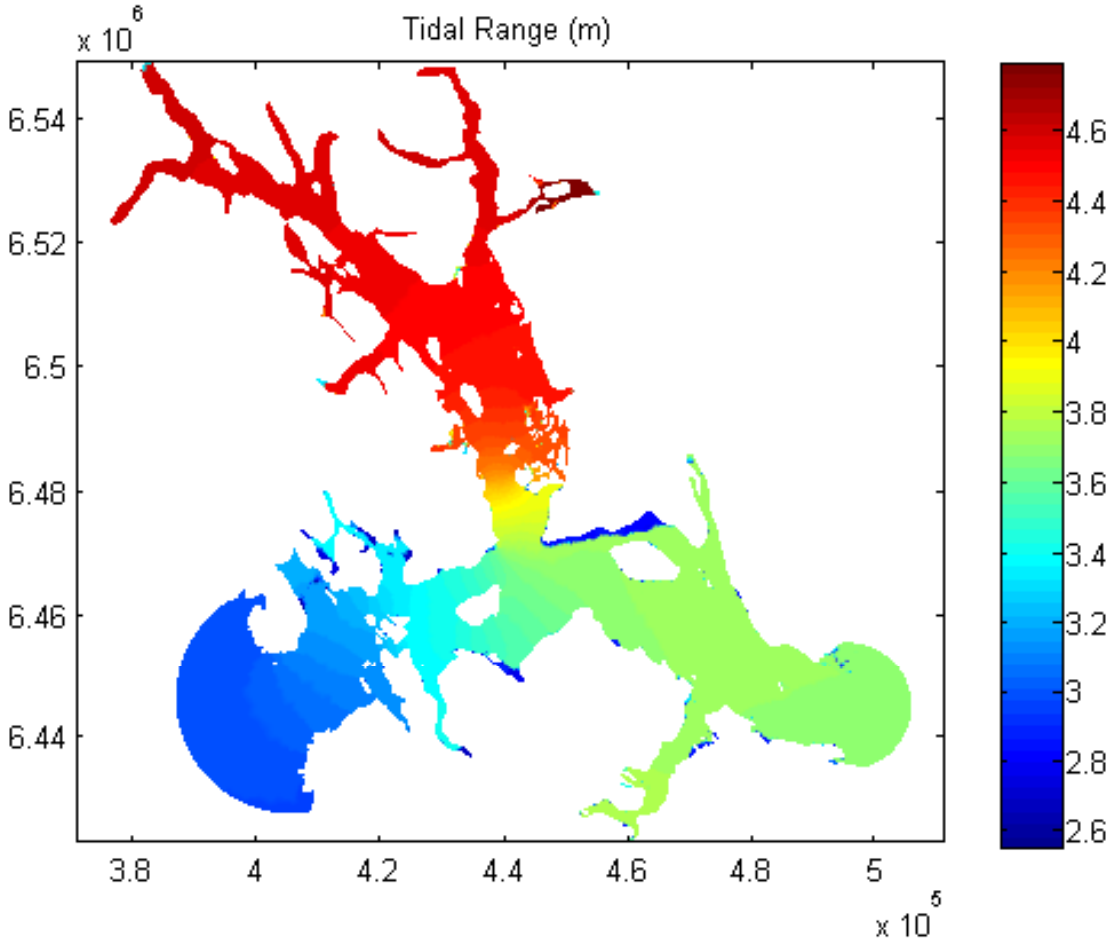

Figure 9.7: Color contours of tidal range in meters.

9.2 Tidal Velocity

The previous section demonstrated that the water surface elevation varies across the domain, but only weakly. The results for tidal velocity, in contrast, are completely different. This is due primarily to the extreme gradients in bathymetry and in channel width that exist in Glacier Bay.

An instantaneous snapshot of tidal velocity, such as given in Fig. 9.8, clearly reveals the very strong variability in tidal speed. Given that tidal speed is a good proxy for tidal mixing and vertical stratification, an understanding of the spatial variation in the velocity results is of great importance.

Additionally, many interesting features can be observed through a careful analysis of the velocity results. For example, Fig. 9.9 illustrates a very complex series of eddies that form in the Sitakaday Narrows area (between Rush Point and Young Island) when the tide changes from ebb to flood and vice versa. This computationally confirms the abundant anecdotal accounts of strong tide riffs in this area. This eddying behavior can be found at numerous other locations within the domain.

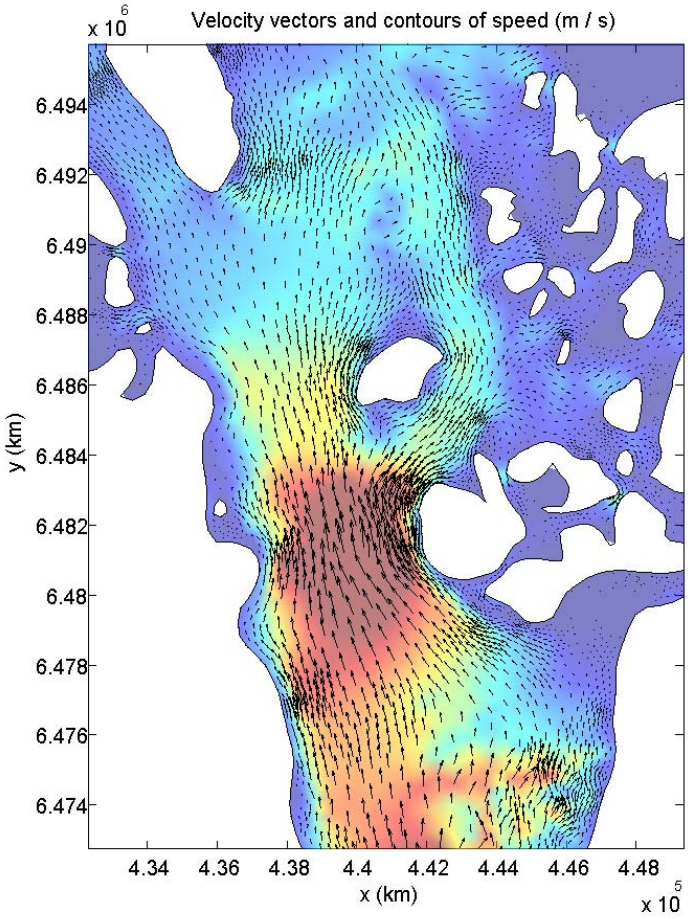

Figure 9.8: Sample velocity vectors showing the two-dimensional flow field and contours of water speed in the Sitakady Narrows area.

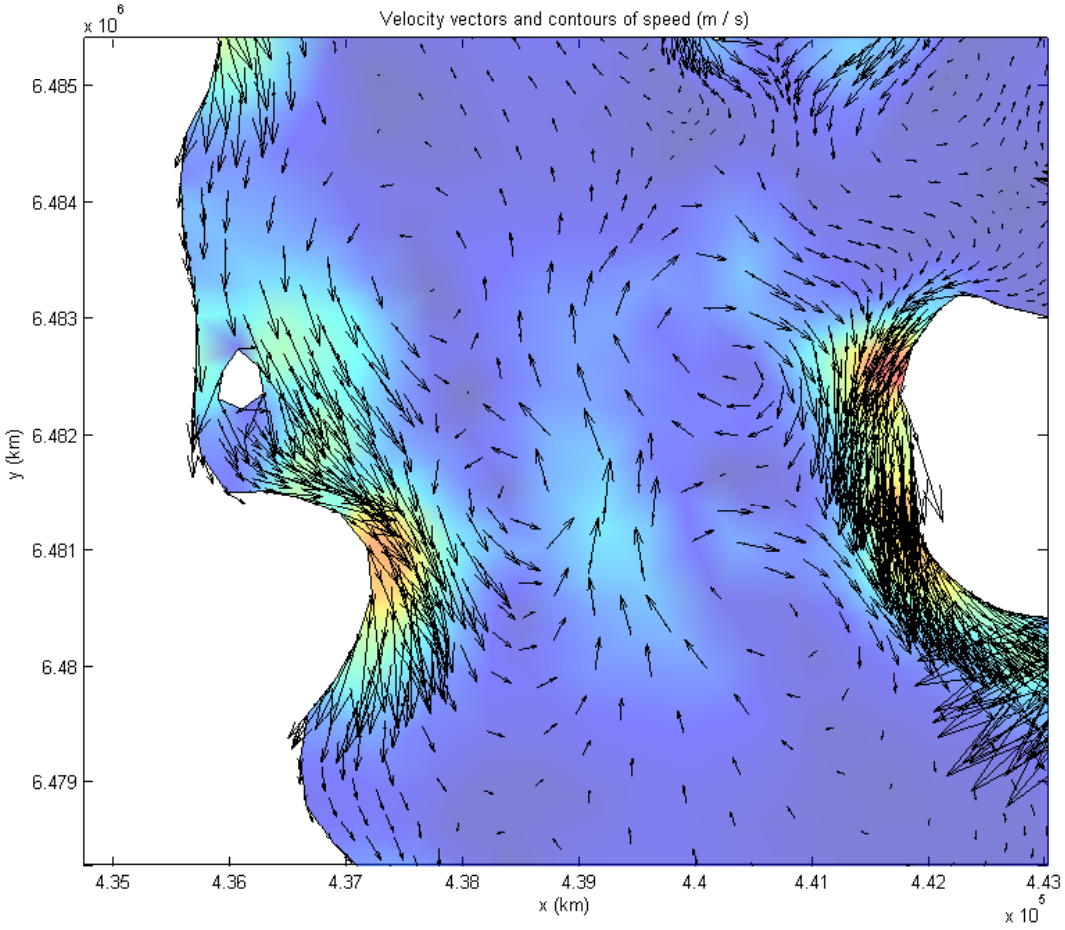

Figure 9.9: Illustration of complex eddying in Sitakaday Narrows, between Young Island and Rush Point.

9.2.1 Root Mean Square Tidal Speeds

It is perhaps most illuminating to, much as was done with the computation of tidal datums, consider some sort of long term average value for tidal velocity. To that end, it was decided to calculate the room mean square tidal speed throughout the domain. Briefly, the root mean square value of a variable $x(t)$ is given by

$$x_{\text{rms}} = \sqrt{\frac{1}{T}\int_0^T x^2\, dt}, \tag{9.1}$$

where T is some suitable averaging time. So, if velocity data (specifically the east-west (U) and the north-south (V) velocity components) were available from a current meter, it is straightforward to first calculate the tidal speed

$$q = \sqrt{U^2 + V^2} \tag{9.2}$$

and then compute the root mean square speed from the time series.

Here, the capabilities of ADCIRC can again be exploited. ADCIRC will perform harmonic analysis of the velocity results, yielding, at every point in the domain, a set of constituent amplitudes and phases for both velocity components. This means that both velocity components are easily expressed as the sum of Fourier (sinusoidal) terms

$$U(t) = a_1 \cos(\sigma_1 t + \phi_1) + a_2 \cos(\sigma_2 t + \phi_2) + \ldots \tag{9.3}$$

$$V(t) = b_1 \cos(\sigma_1 t + \psi_1) + b_2 \cos(\sigma_2 t + \psi_2) + \ldots. \tag{9.4}$$

From this, it is straightforward to show that the root mean square speed is given by

$$q_{\text{rms}} = \frac{1}{\sqrt{2}}\sqrt{\sum a_i^2 + \sum b_i^2}. \tag{9.5}$$

The root mean square speeds for the Glacier Bay domain were calculated and are presented in Fig. 9.10. Unlike the case of elevation, the results show massive variation across the domain. In particular, note the very high speeds observed in the Sitakaday Narrows area, around Point Carolus, and in Adams Inlet. A zoomed-in view of the Sitakaday area is shown in Fig. 9.11. These results all agree with anecdotal observations of tidal currents in these areas. The maximum rms speed is found to be about 1.5 m s^{-1}. Recall, of course, that this is an average of sorts and that maximum instantaneous speeds will be considerably larger than this. For example, calculations of spring tide

conditions have shown that speeds in the Sitakaday Narrows area can be in excess of 2.5 to 3 m s^{-1}.

In contrast to these high velocities, the tidal speeds in the upper reaches of Glacier Bay are found to be extremely small. This is due to the fact that, near the head of a steep sided fjord, the tidal wave is essentially a standing wave, or anti-node. At these locations, the horizontal motion asymptotically disappears and the motion becomes purely vertical.

To help quantify this, Fig. 9.12 (Etherington *et al.*, 2004) shows 24 locations where the United States Geological Survey collected oceanographic data during the period of 1993 - 2002. The root mean square tidal speeds at these stations are summarized in Table 9.1. The results show a distinct steady decrease in speed with up-fjord distance. For example, stations 5 - 12 run from (roughly) the mouth to the head of the West Arm. and the tidal speeds steadily decrease from 5 to 1 cm s^{-1}. Stations 13 - 18 run up the East Arm and show a very similar decrease in speeds.

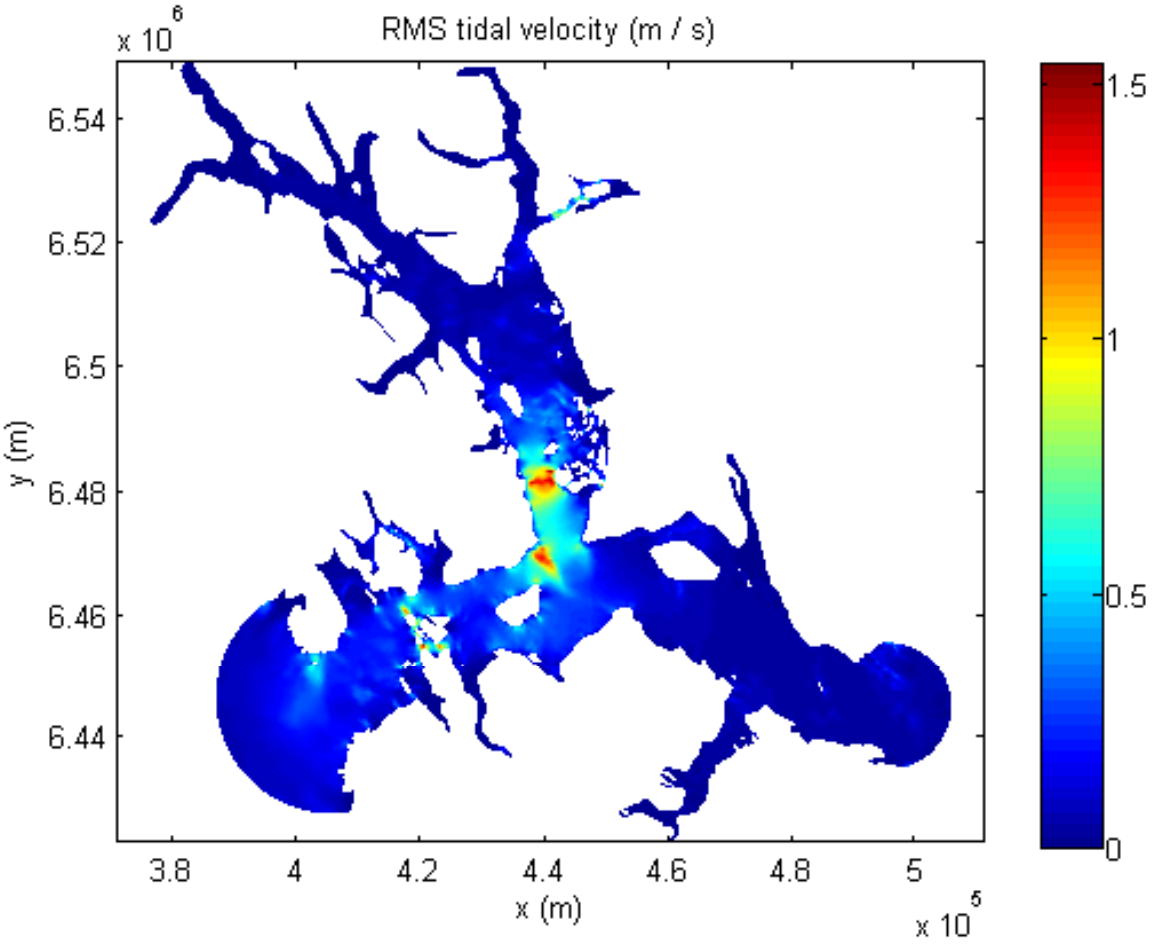

Figure 9.10: Color contours of root mean square tidal speed.

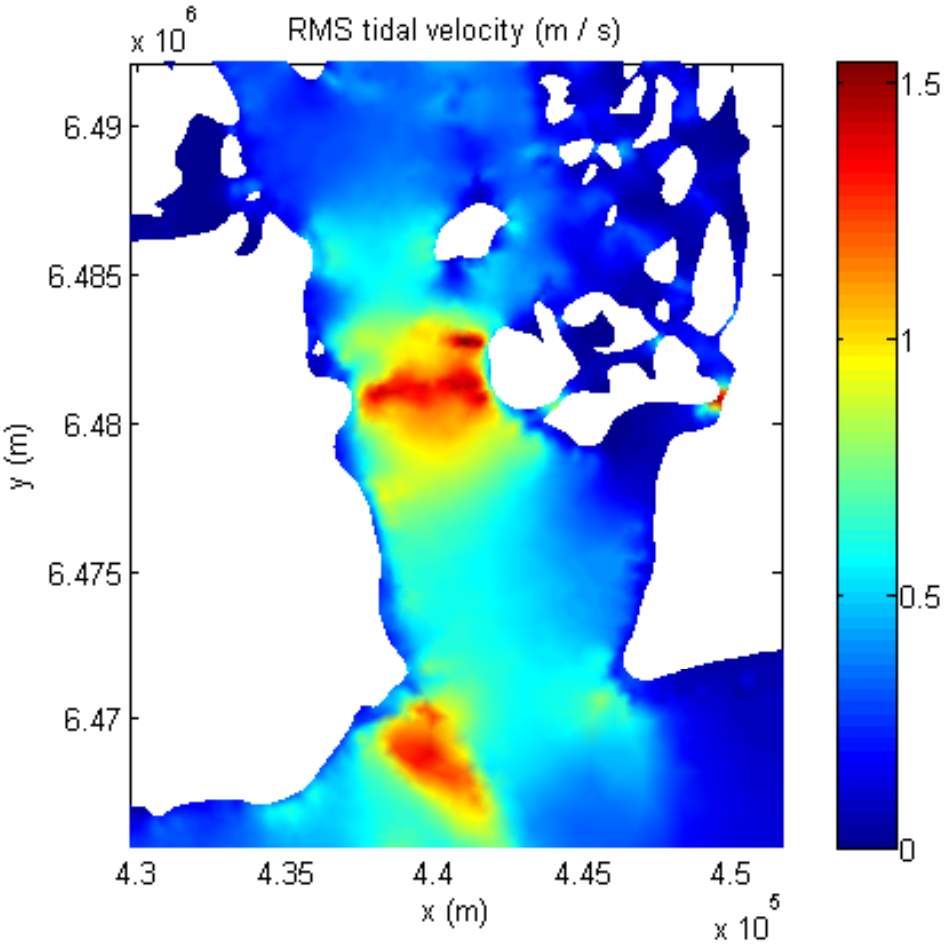

Figure 9.11: Color contours of root mean square tidal speed in the Sitakaday Narrows area.

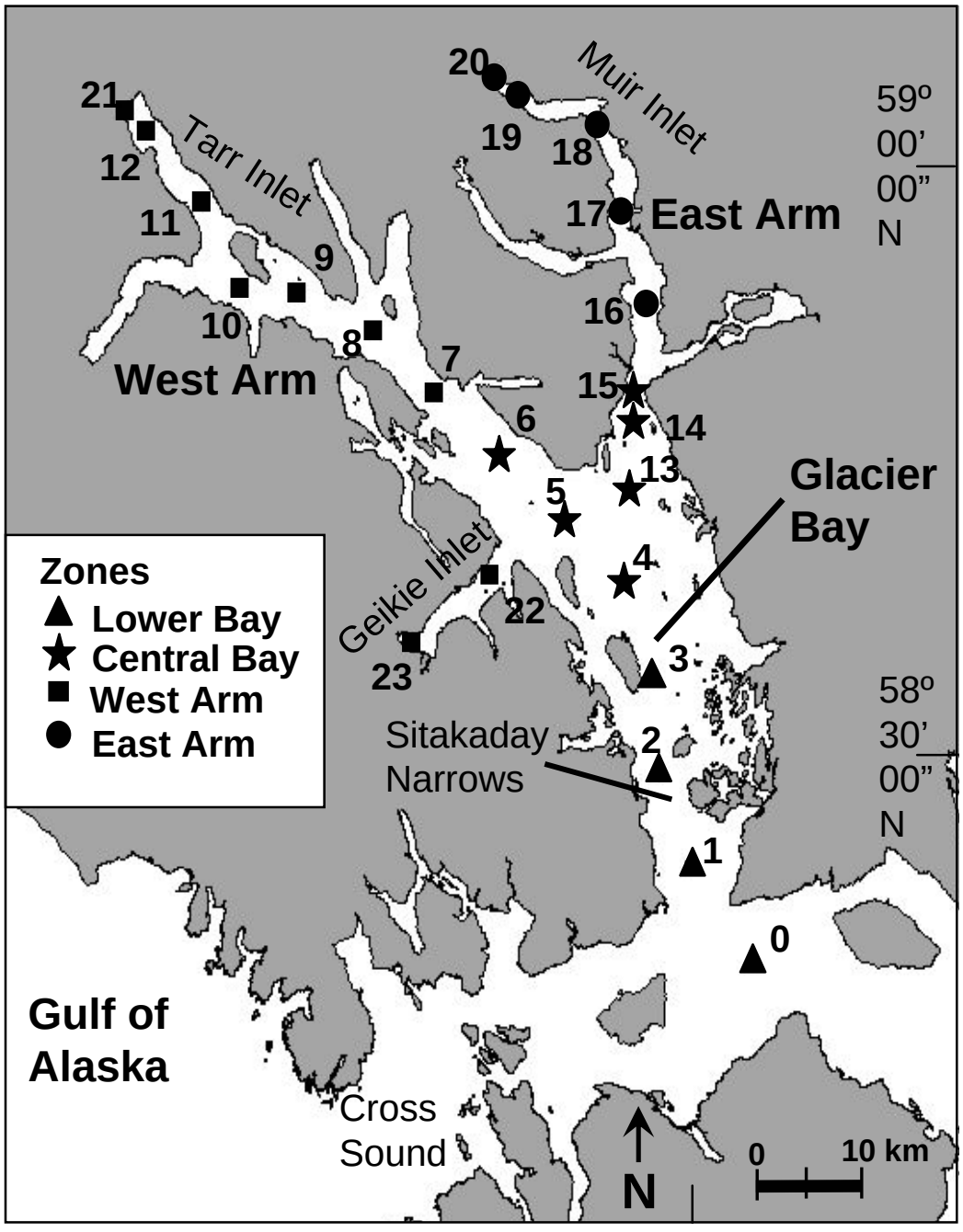

Figure 9.12: Location of oceanographic data collection stations. Figure reproduced from Etherington *et al.* (2004).

Station	RMS Speed (m s^{-1})
0	0.18
1	0.56
2	0.72
3	0.33
4	0.074
5	0.051
6	0.043
7	0.043
8	0.028
9	0.027
10	0.024
11	0.010
12	0.004
13	0.049
14	0.122
15	0.139
16	0.020
17	0.024
18	0.010
19	n/a
20	n/a
21	0.001
22	0.023
23	0.007

Table 9.1: Root mean square tidal speeds at USGS oceanographic station locations.

9.3 Particle Trajectories

The plotting of particle trajectories is an extremely helpful tool, in terms of visualizing the currents in Glacier Bay. To help illustrate this, simulations were carried out both for typical spring and typical neap tide conditions. Specifically, four trials were conducted, each reporting output for a two day period. The beginning times of these simulations (and corresponding Bartlett Cove stage) are given below:

1. March 21, 2007, 11:22 GMT, 18.2 ft H
2. March 21, 2007, 17:42 GMT, -3.5 ft L
3. March 12, 2007, 3:11 GMT, 8.7 ft H
4. March 12, 2007, 8:32 GMT, 7.1 ft L

Thus, trial 1 represents spring tides, beginning with an ebb, trial 2 spring tides beginning with a flood, trial 3 neap tides beginning with an ebb, and trial 4 nea tides beginning with a flood.

Figure 9.13 gives a quick overview of how these particle trajectories vary over the Glacier Bay domain for the case of trial 2. The red dots indicating the starting points and note that the two day simulation period corresponds to about four complete tidal cycles. It is immediately clear that vast spatial gradients in tidal excursions exist within the bay. In the upper reaches of the east and west arms, the tidal motion is quite weak. Tidal excursions (maximum distance between flood and ebb points) are found to be on the order of 0.5 to 1.5 km. In the lower bay, however, the strong tidal currents produce tidal excursions on the order of 20 km.

A closer look at the lower bay region for trial 2 is presented in Fig. 9.14. One item of great interest, in terms of the exchange of bay waters with outlying waters in Icy Strait, is that there seems to exist a near 'barrier' of sorts between eastern Icy Strait and the mouth of Glacier Bay. During the flood phase, it is observed that several particles from western Icy Strait are swept into Glacier Bay and travel significant distances up-bay. The particles in eastern Icy Strait are more or less held in place.

The results for trial 1, which begins with an ebb phase, are shown in Fig. 9.15. The phenomenon referred to above again appears. Looking specifically at the particles that start at the bay mouth, all but one are swept to the west during the initial ebb. Additionally, it is observed that most of the

particles starting at the bay mouth are carried out and do not return to the bay proper.

Moving on to neap conditions, Fig. 9.16 and Fig. 9.17 show calculated trajectories for trials 4 and 3, which begin with flood and ebb phases respectively. The clear differences in these figures, when compared to Figs. 9.14-9.15, has to do with the much shorter tidal excursions. It is found that the excursions for the neap tides are roughly half those for the spring tides. In the upper bay, neap tide excursions are on the order of 0.25 - 0.75 km and in the lower bay, they are limited to about 10 km.

Finally, the complexity of tidal flows in Glacier Bay is further illustrated in Fig. 9.18, which shows trajectories for spring tide conditions in the vicinity of the Beardslee Islands. While the figure is quite visually busy, it is clear that the fate of a particle is very strongly dependent upon its initial position. Some trajectories do not stray far from their initial positions. Others find their way into 'conveyer belts' of very high tidal velocity and are therefore able to travel very far. In particular, particles that are able to make it out of the channel between Lester and Young Islands find themselves in a region of very high velocity. Additionally particles that make it into the channel separating Young and Strawberry islands experience similarly high velocities and lengthy tidal excursions.

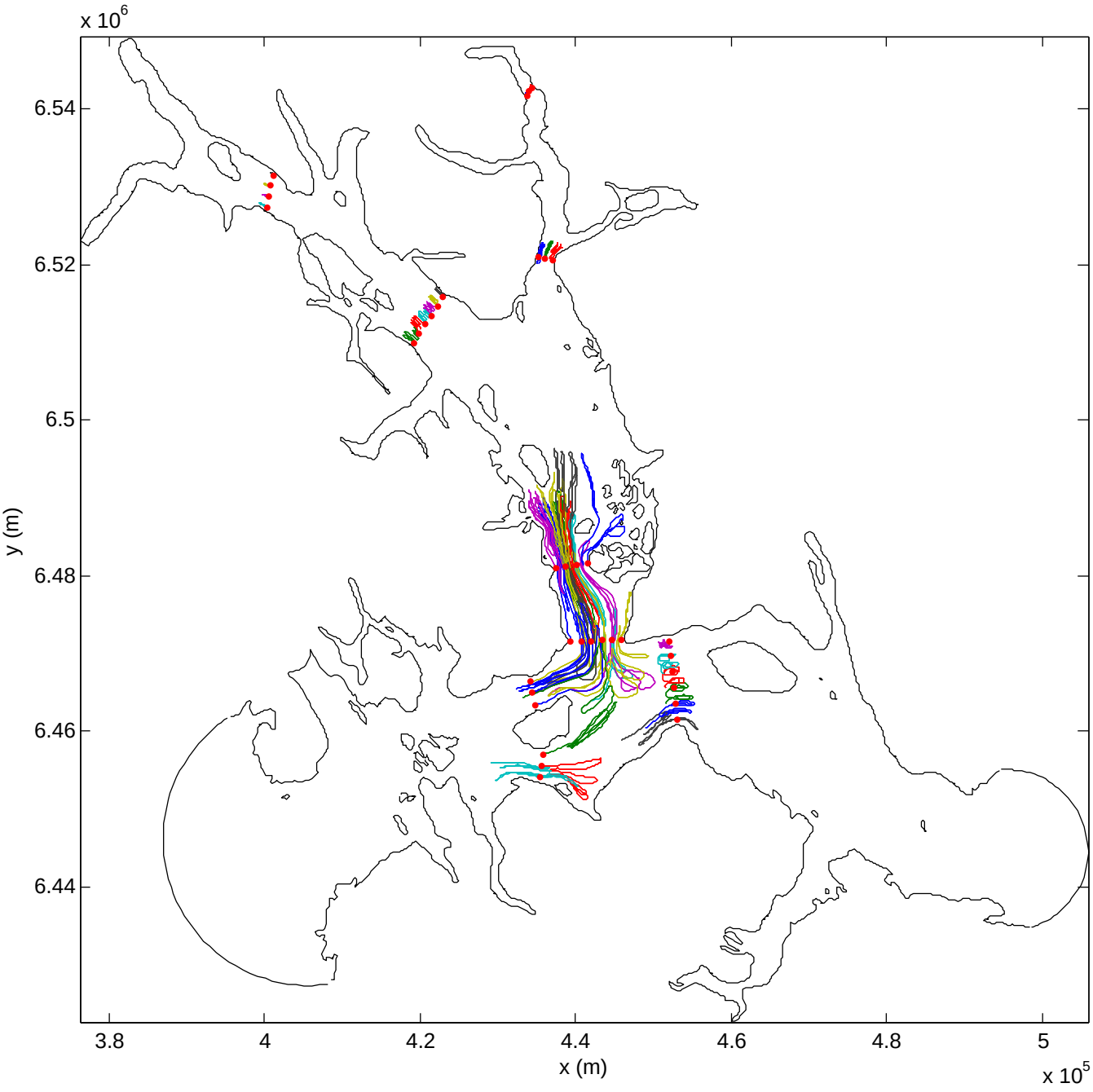

Figure 9.13: Particle trajectories for trial 2 for the entire domain.

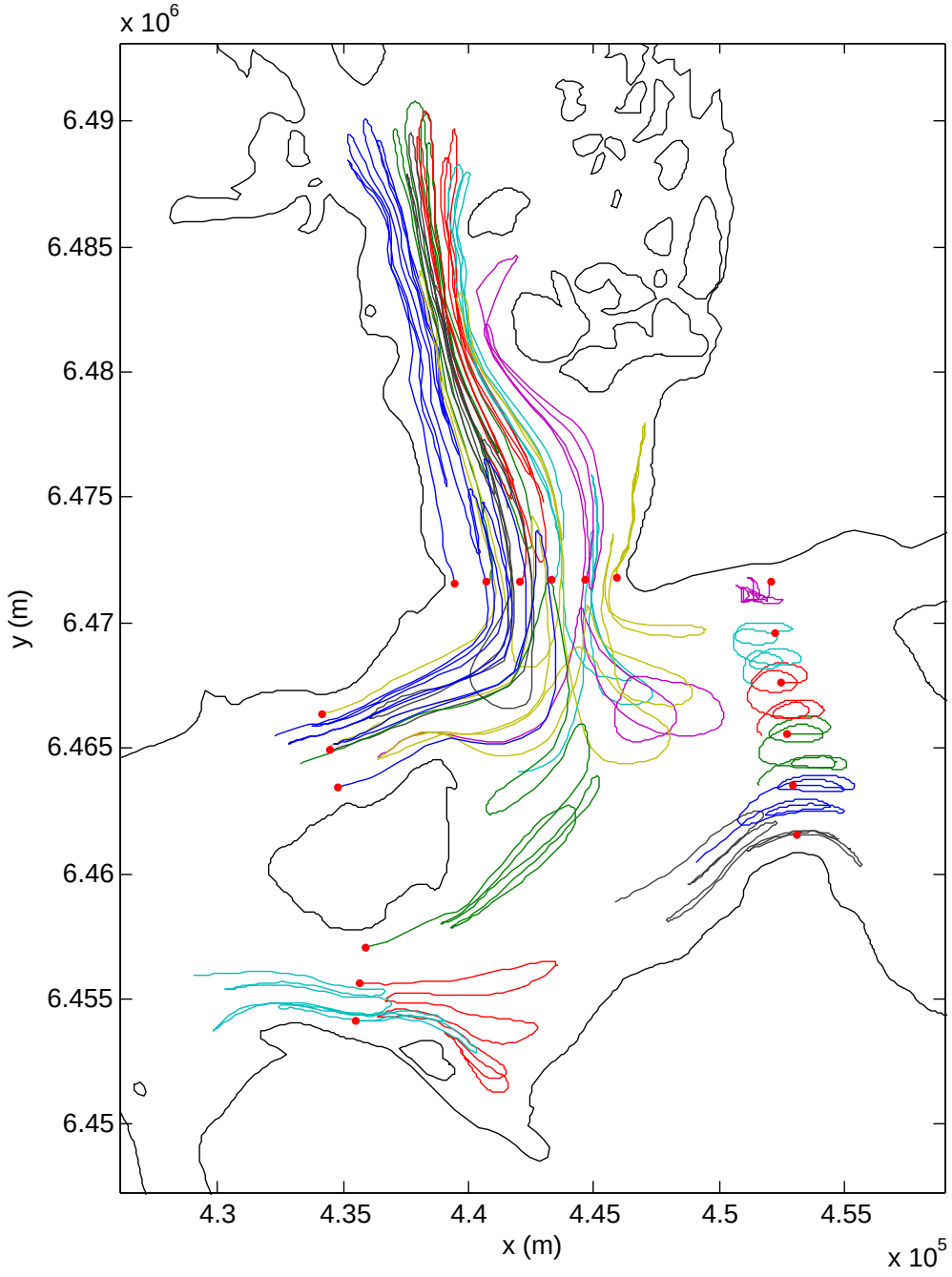

Figure 9.14: Particle trajectories for trial 2 for the lower bay region.

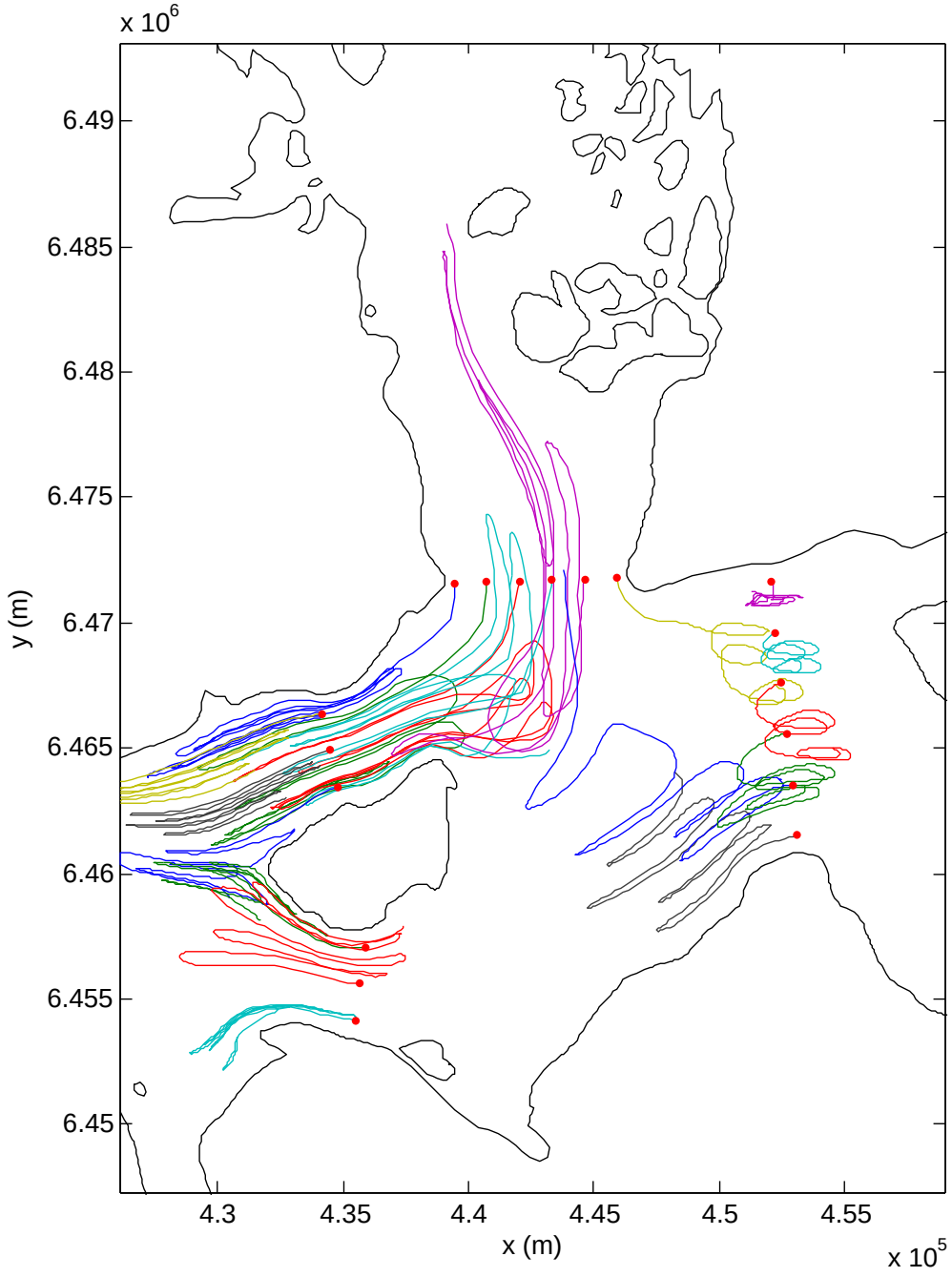

Figure 9.15: Particle trajectories for trial 1 for the lower bay region.

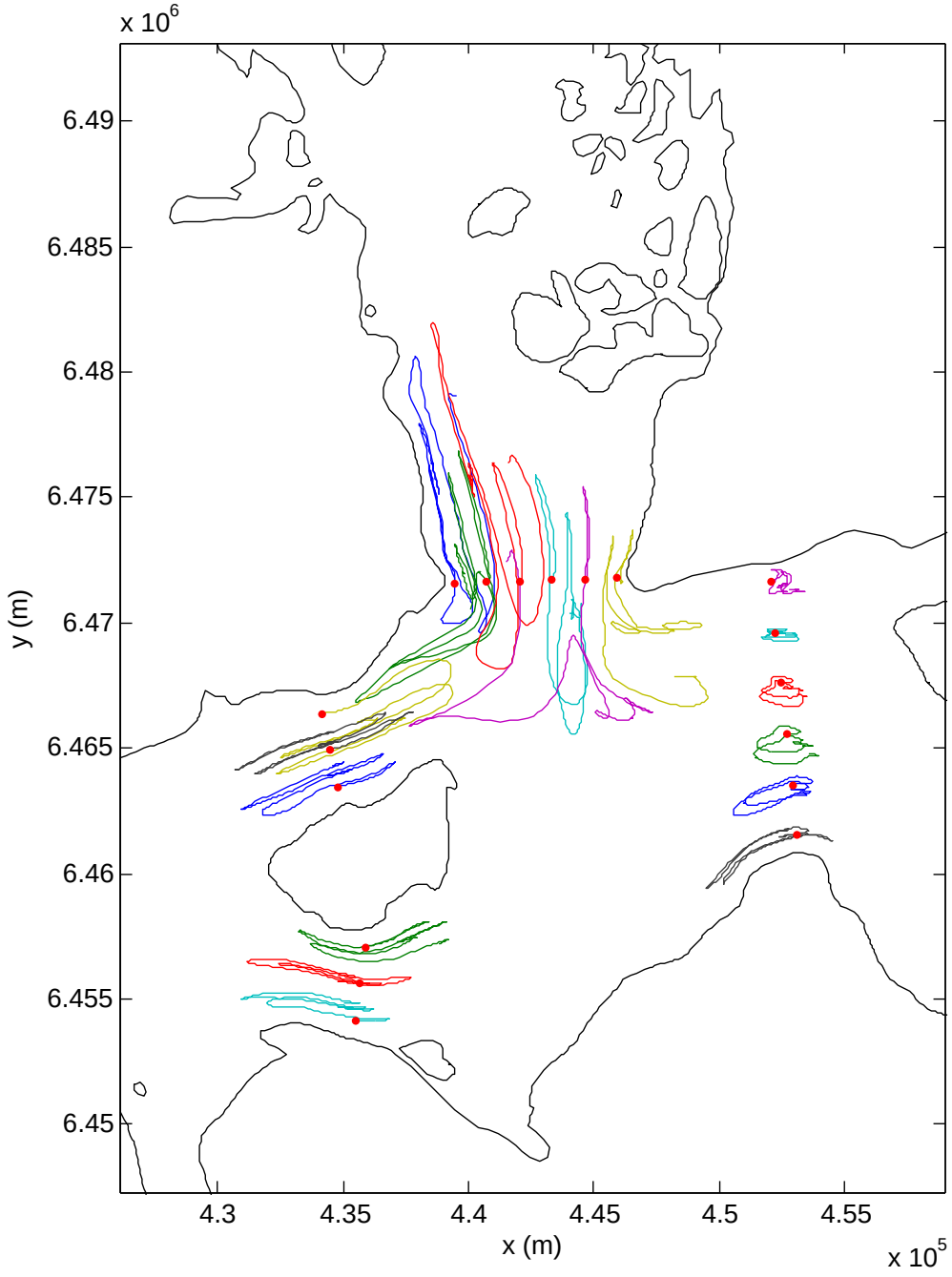

Figure 9.16: Particle trajectories for trial 4 for the lower bay region.

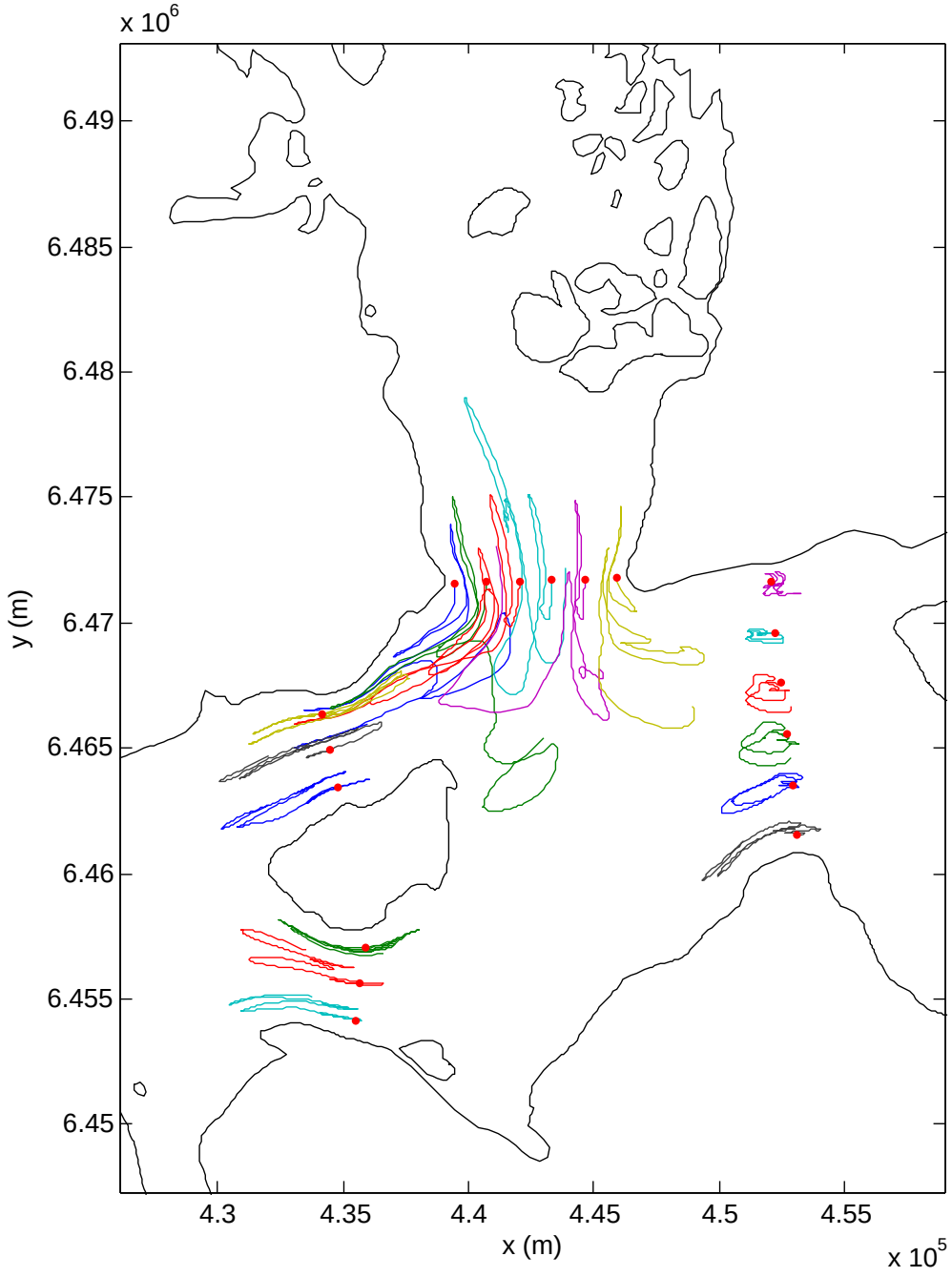

Figure 9.17: Particle trajectories for trial 3 for the lower bay region.

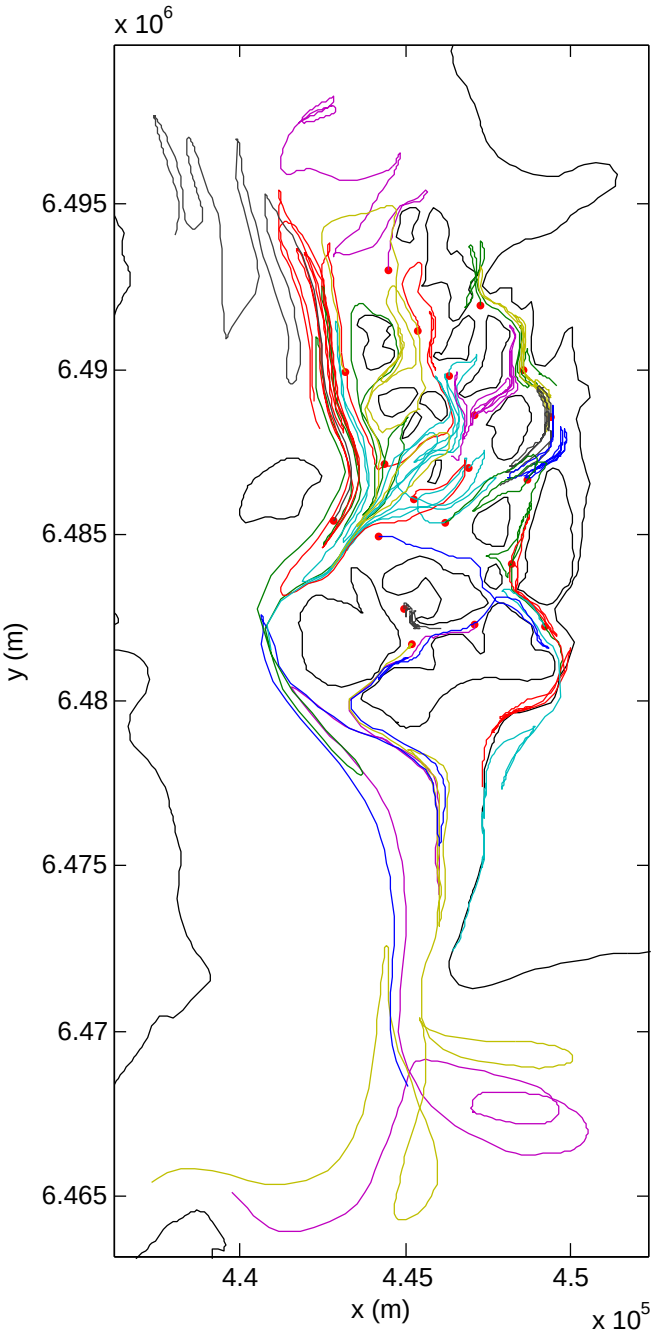

Figure 9.18: Particle trajectories for spring tides in the Beardslee Islands area.

9.4 Influence of Meteorological Forcing

As discussed in Chapter 6, a database of meteorological conditions was prepared for the Glacier Bay region. This database covers the period from 1988 to 2006 and describes hourly wind speed and direction and surface pressure. Based upon this database, fort.22 files are easily prepared by the user if a run with meteorological forcing is desired.

To test the significance of the wind, two simulations were carried out. Both lasted for 7.25 days, beginning at 17:38:51 (GMT) on 18 June, 2002. For the first simulation, meteorological forcing was suppressed while, for the second, it was included. The relevant wind data are presented in Fig. 9.19. Time series of elevation and velocity data were requested at five recording stations for the entire simulation period files. These stations are at (roughly) Elfin Cove, Bartlet Cove, Willoughby Island, Muir Inlet, and Composite Island (Fig. 9.20). Additionally, global velocity output was requested, on a five minute time step, for the last 0.25 days of the simulation period.

9.4.1 Velocity Data

Figure 9.21 summarizes the effects of the wind and pressure forcing on the x and y components of tidal velocity. Specifically, the absolute value of the difference between the 'wind' and the 'no wind' calculations is shown for each of the five locations. Note that the results are normalized by the maximum value of (no wind) tidal velocity at each of the recording stations. In this way, the data give a *relative* measure of the meteorological influence.

The results for the two velocity components are fairly similar, with a maximum difference of about 35%. This fairly large difference suggests that the wind and pressure fields are quite capable of influencing the velocity fields in Bay. If Fig. 9.21 is compared to Fig. 9.19, the observed wind speeds appear to correlate fairly well with the observed differences in the calculations. For example, the peaks in wind speed observed (roughly) at days 1, 2, 5, 6, and 8 match up with similar peaks in the difference curves. Additionally, the relatively quiet period (in the wind record) between days 2.5 and 4.5 is matched by a period of good agreement between the wind and no wind calculations.

9.4.2 Elevation Data

Figure 9.22 illustrates, in a similar fashion to the previous figure, the effect of the wind / pressure forcing on the predictions of water surface elevation. Again, the differences in the data are normalied by the maximum values of elevation recorded at each station. Unlike the velocity results, where differences of up to 35% were observed, Fig. 9.22 suggests that meteorological forcing has a negligible effect on the water surface elevation. Indeed, the maximum observed difference is less than one half of one percent. Given some consideration, this is not a surprising result. The wind stress is applied tangential to the water surface. So, while it is able to 'drag' the water column horizontally and influence the velocity field, it has only a limited ability to raise or depress the water surface. It must be noted that, for the simulation period considered here, the observed wind speeds were relatively low. More extreme wind conditions will result in increased differences between the 'wind' and 'no wind' cases.

9.4.3 Calculated Trajectories

Given that particle trajectories (see §7.3) are determined through the integration of the velocity fields, the large differences observed in Fig. 9.21 suggest that similarly large differences may be found in the trajectories. Note that this is dependent upon location; Fig. 9.21 revealed a wide range of degree of agreement, depending upon location within the bay. Also, note that the relative directions of the wind and the tides can serve to mitigate or exacerbate trajectory differences. For example, if the wind opposes the tide on flood and then changes direction to oppose the tide on ebb, the net effect on a particle trajectory may well average out to zero over the diurnal cycle. It is furthermore anticipated that trajectory differences will be cumulative in time, leading to larger and larger errors as the simulation period increases.

The two simulations described above can be used to investigate the effects of climate on particle trajectories, although they are limited (0.25 day) in duration. At $t = 7$ days, particles were released at the five stations considered above. For the next 0.25 days (running to the end of the simulation period), trajectories were compared for the 'wind' and 'no wind' cases.

Table 9.2 summarizes the total distances traveled by the particles. Note that the total distance traveled is computed by integrating along the path taken; it does *not* simply reflect the linear distance between starting and

ending points. The table also gives the distance (Δs_e) between the endpoints of the 'wind' and 'no wind' runs. Finally, this difference is normalized by the 'no wind' distance traveled in order to give a non-dimensional measure, (Δs_e^*), of the error in neglecting the wind.

For regions characterized by relatively strong tidal velocity, say locations 1 - 3, the error is fairly slight. However, in regions characterized by weak tidal velocity, locations 4 and 5, the error can be very significant. In these locations, the drift velocity induced by the wind is comparable to the tidal velocity, leading to large errors. As these results show, if the goal is to accurately predict the paths taken by material elements, the effects of even modest winds are non-negligible and should be included in the ADCIRC simulations.

Location	Total (no wind) distance (km)	Total (wind) distance (km)	Δs_e (m)	Δs_e^*
1	7.62	7.75	107	0.014
2	4.01	4.06	1	0.0003
3	1.79	1.78	121	0.067
4	0.72	0.71	283	0.39
5	0.94	1.09	269	0.29

Table 9.2: Summary of trajectory information for particles released at 5 stations within the domain.

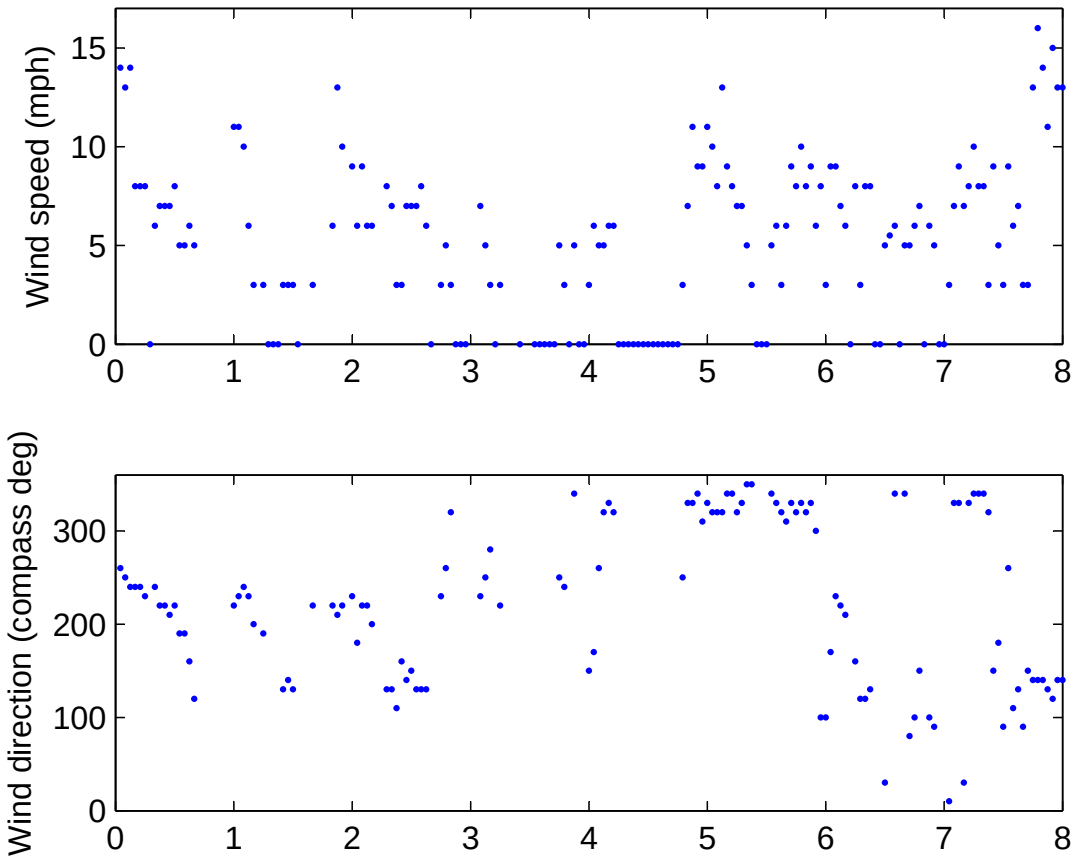

Figure 9.19: Wind speed and direction data for the period in question.

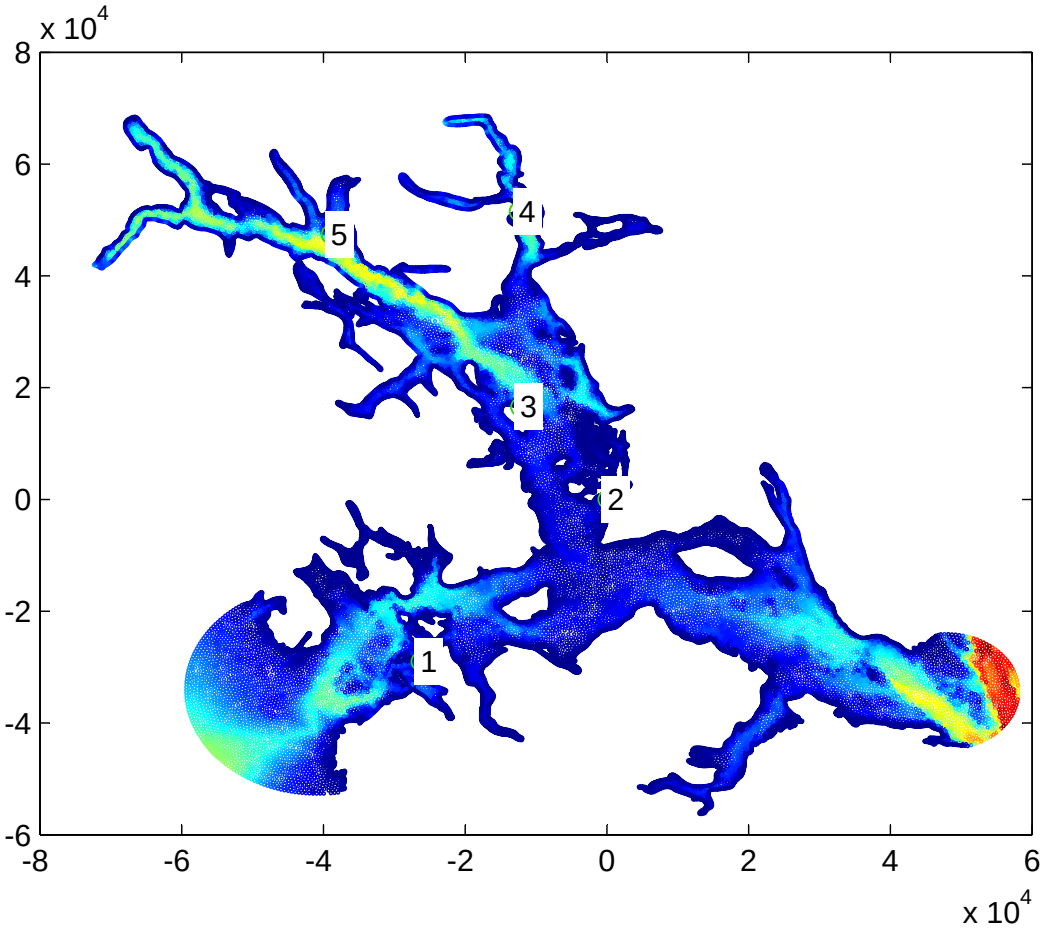

Figure 9.20: Model domain, with the five recording stations identified.

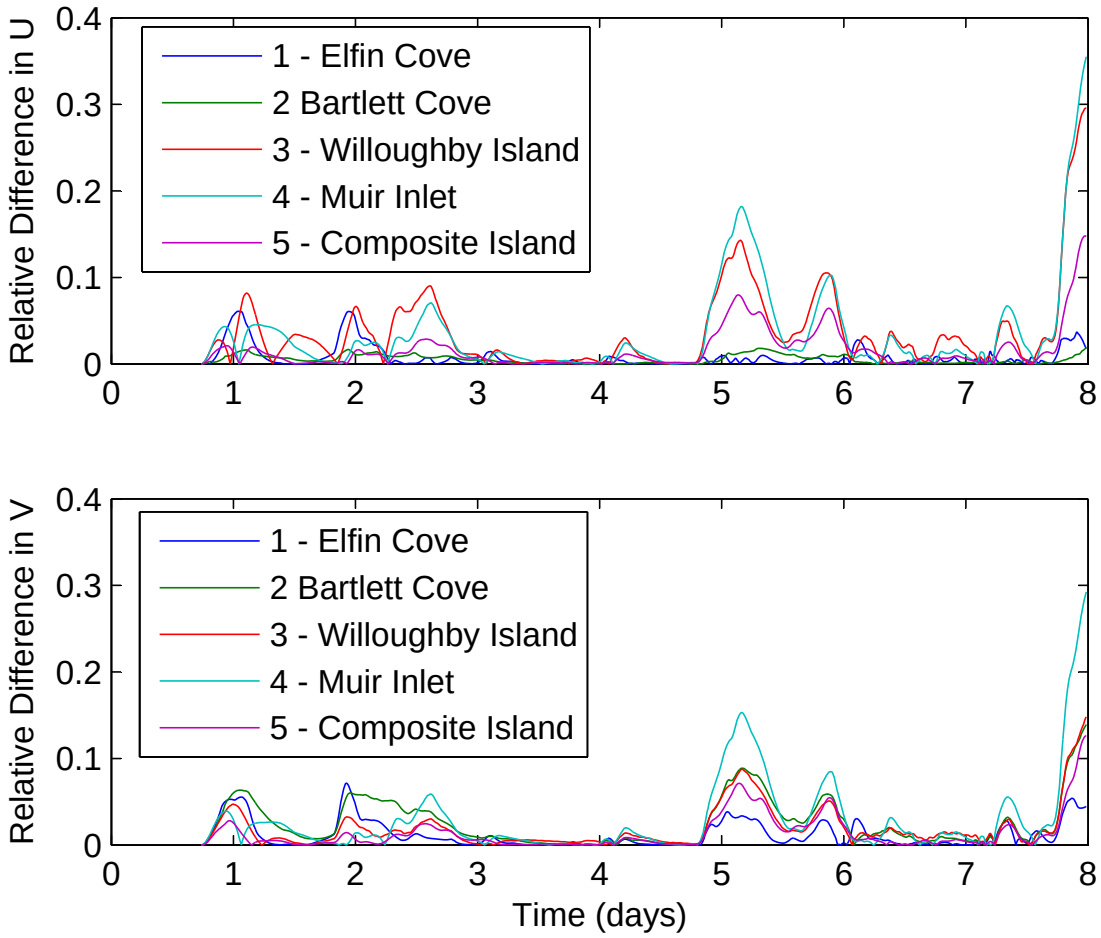

Figure 9.21: Normalized absolute value of the difference between the 'wind' and 'no wind' x and y components of velocity.

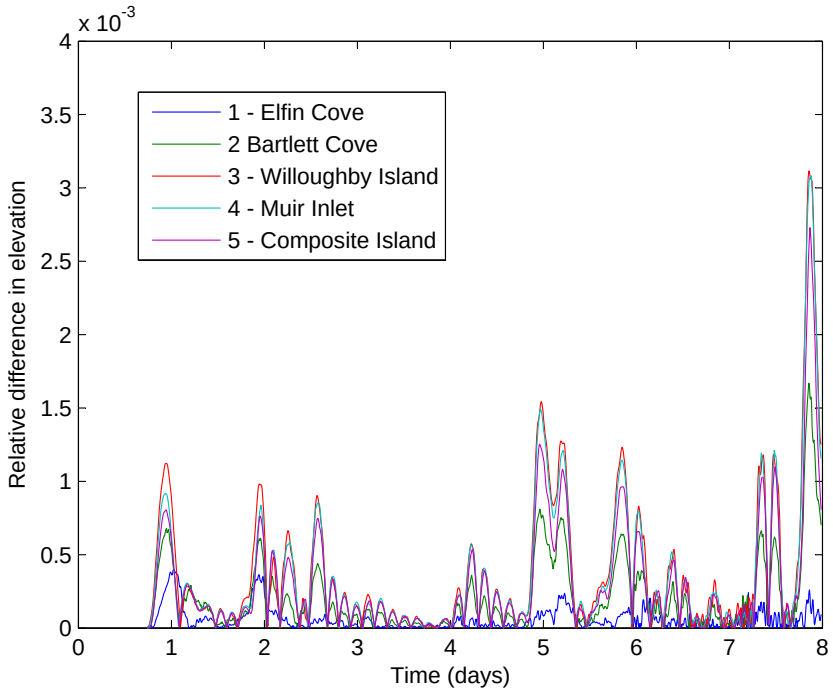

Figure 9.22: Normalized absolute value of the difference between the 'wind' and 'no wind' calculations of water surface elevation.

9.5 Influence of Inflows

Finally, it is of considerable interest to consider the significance of freshwater input to the bay. As Chapter 5 revealed, the discharges into the bay were estimated to be very considerable. These inflows will have several effects. First of all, the momentum that they impart to the bay waters will alter tidal circulation patterns. Secondly, they will result in a net seaward drift. Finally, in the context of three-dimensional modeling, the freshwater input will be a primary control on the observed vertical stratification of the water column.

As the present modeling effort is two-dimensional, the results stemming from the inclusion of freshwater inflows are of limited use. This is because, by virtue of the depth-integrated approach, the freshwater drift will be computationally distributed evenly over the entire water column. Given the large depths observed in most of the bay, this will result in quite small drift velocities. In reality, due to the stratified nature of most of the bay, the freshwater flows will be concentrated in the extreme upper layers. The net effect of this is that the present computational results substantially underpredict the expected drift. Extension of the modeling effort to three-dimensions will allow for the full utilization of the inflow estimates outlined in Chapter 5.

It *is* of value to consider the effects of freshwater inflow in the vicinity of the Sitakaday Narrows area and the bay mouth. As has been demonstrated by Etherington *et al.* (2007), this lower bay region remains unstratified to weakly-stratified throughout the year. This vigorous tidal mixing is due to the large tidal velocities in this area (Fig. 9.11) and the observed uniformity of the water column suggests that the depth-averaged approach of the ADCIRC model is adequate for handling the freshwater discharge in this area.

Figure 9.23 illustrates the influence of freshwater inputs for one simple test case. Here, a line of drifters was placed along the bay mouth at the start of a flood tide (spring conditions). The figure shows the location of the drifters at the subsequent slack water (3 hours later). The blue markers represent the absence of freshwater inputs, and the red markers represent the case where freshwater inflows (2 year peak discharge values) have been included. It is clear that the freshwater flow seaward has the effect of reducing the intrusion of the drifters into the bay.

Figure 9.24 shows the same comparison, but this time carried out for 48 hours. Here, the trajectories are shown as faint lines, for purposes of visual clarity. The key point is that, with freshwater inflows (red markers) included,

all but one of the drifters has been flushed out of the bay.

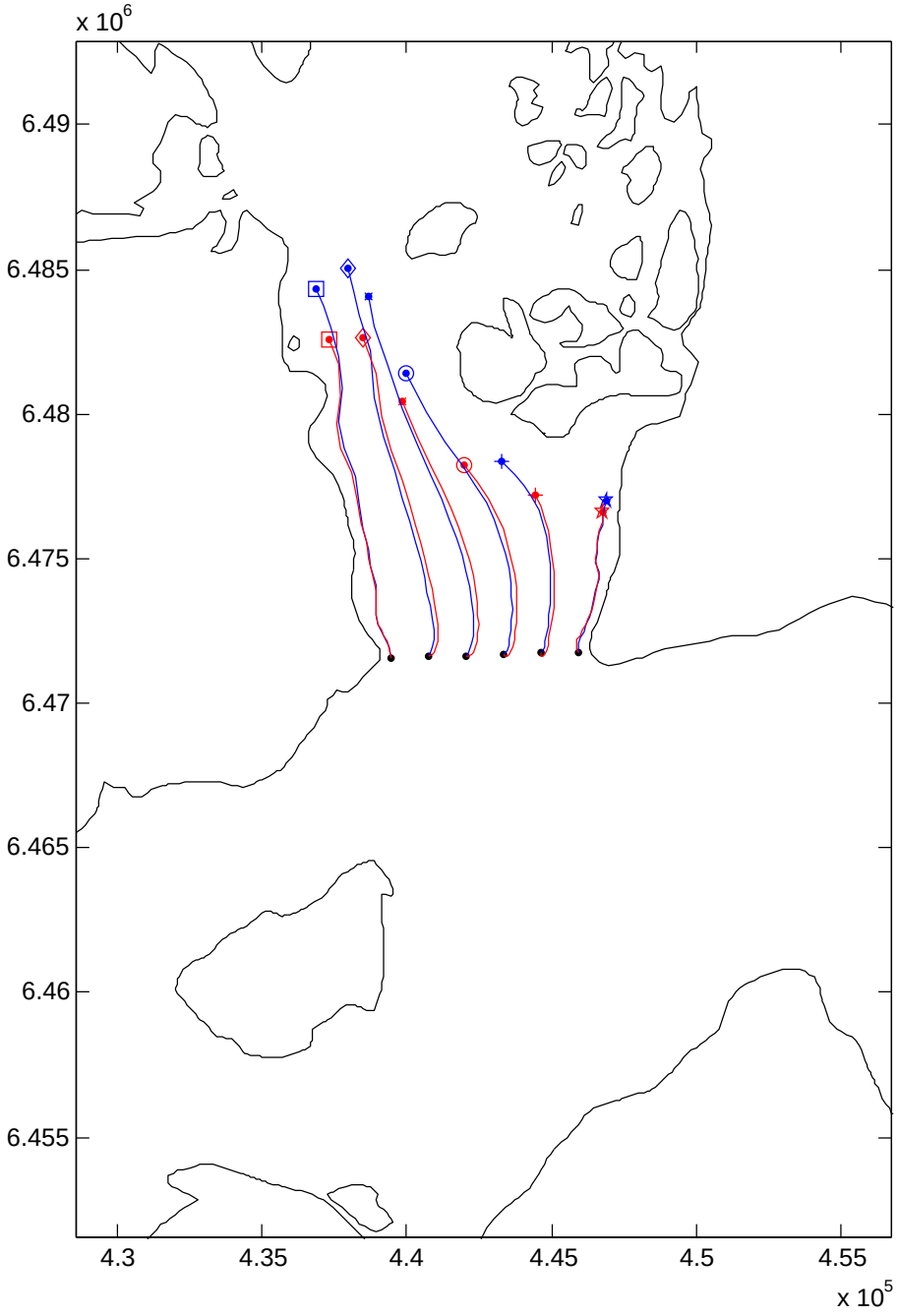

Figure 9.23: Particle trajectories, for spring tide conditions, as calculated in the presence (red markers) and absence (blue markers) of freshwater input. Tracks correspond to three hours of simulation time.

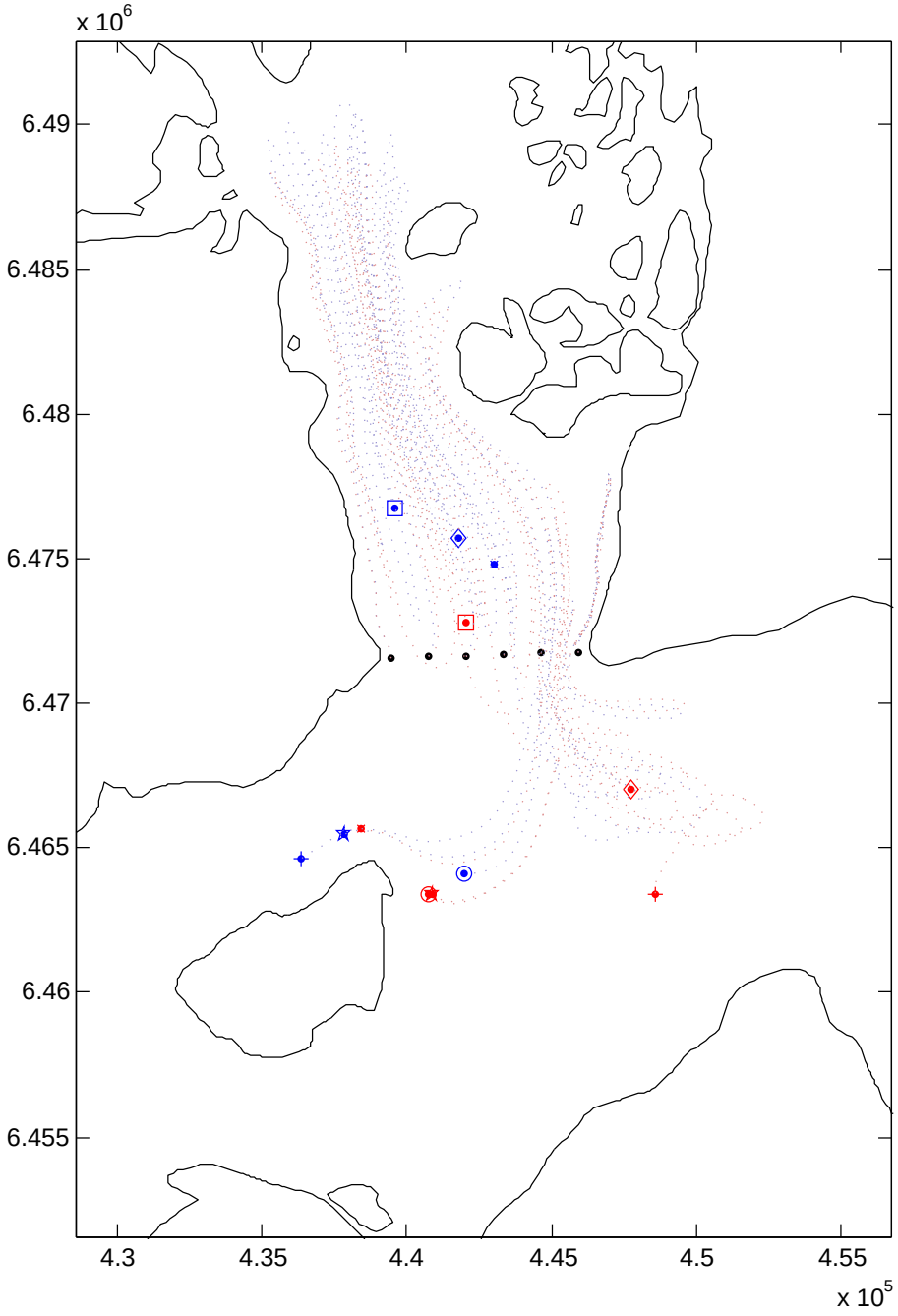

Figure 9.24: Particle trajectories, for spring tide conditions, as calculated in the presence (red markers) and absence (blue markers) of freshwater input. Tracks correspond to two days of simulation time.

Chapter 10

Conclusions and Recommendations

The present report represents the first comprehensive effort to model the tidal circulations found in Glacier Bay, Alaska. As was put forth in the introductory chapters, Glacier Bay is a location of great interest and importance and it is my hope that this report is a substantial contribution to the physical understanding of this area.

The open-source model ADCIRC was adopted due to its relative ease of use and reasonable level of online and user-community support. The flexibility of ADCIRC, in particular with regards to model output, means that a great number of questions can be asked and answered with the model. As was shown, information on elevation, water velocity, and particle paths can be easily obtained.

To sum up key results, it was found that tidal elevations steadily increase with up-bay distance. Regarding velocity, contour maps of root-mean-square tidal speed revealed very strong spatial gradients. In the lower bay regions, speeds on the order of 2 - 3 m s^{-1} were observed while, in up-bay regions, speeds fully two orders of magnitude less were observed. Computed particle paths showed a similar behavior. In up bay regions, the observed tidal excursions were very slight, on the order of 1 km. In the vicinity of Sitakaday Narrows, on the other hand, it was found that particles would move in excess of 20 km during spring tide conditions.

Numerous localized features of interest were found through careful study of the numerical results. For example, complex clusters of eddies were found in Sitakaday Narrows and in other locations throughout the bay. Addition-

ally, an interesting 'barrier' connecting Points Gustavus and Adolphus was found by considering numerical drifter experiments in the vicinity of the bay mouth.

It was found that the effects of freshwater input were substantial in the vicinity of the bay mouth. Upon inclusion of freshwater input, computed drifter tracks were altered substantially, and drifters were flushed out of the bay.

10.1 Future Work

There are several important extensions to this work that should be carried out in the future. These include:

1. First of all, the study of the effects of freshwater input on the barotropic tide should be refined. Regression equations based upon watershed classification by flow regime, and not geographic proximity, should be pursued. Additionally, analysis of glacial volumetric change should be carried out, as this will be a significant addition to the freshwater budget.

2. Second, studies of contaminant / tracer transport can easily be carried out. This is a current feature of the ADCIRC model. These studies will show how an initial distribution of some material of interest is advected and dispersed due to the tidal motion.

3. Third, and most importantly, the modeling effort needs to be extended to three dimensions. This will allow for the resolution of vertical stratification and the quantification of vertical mixing. This comes at the penalty of increased computational cost, however. Therefore, it will be necessary to reduce the horizontal resolution of the domain. Nevertheless, this is by far the most important step to be taken to further advance our understanding of present and future conditions in the bay.

Bibliography

Ciavola, S. 2007 A gis-based study of the freshwater discharge into glacier bay, alaska. *Tech. Rep.*. The Pennsylvania State University, b.S. Honors Thesis.

Curran, J., Meyer, D. & Tasker, D. 2003 Estimating the magnitude and frequency of peak streamflows for ungaged sites on streams in Alaska and conterminous basins in Canada. *Tech. Rep.*. United States Geological Survey, uSGS Water Resources Investigations Report 03-4188.

Edwards, K. & Werner, F. 2002 A simple guide (with examples) to generating a finite element mesh of linear triangular elements using battri. *Tech. Rep.* NML-02-07. Numerical Methods Lab, Dartmouth College.

Etherington, L., Hooge, P. & Hooge, E. 2004 Factors affecting seasonal and regional patterns of surface water oceanographic properties within a fjord estuarine system, Glacier Bay, Alaska. *Tech. Rep.*. United States Geological Survey, prepared for Glacier Bay National Park.

Etherington, L., Hooge, P., Hooge, E. & Hill, D. 2007 Oceanography of Glacier Bay, Alaska: implications for biological patterns and productivity in a glacial fjord estuary. *Estuaries and Coasts* **submitted**.

Hooge, P. & Hooge, E. 2002 Fjord oceanographic processes in glacier bay, alaska. *Tech. Rep.*. USGS Alaska Science Center, prepared for the National Park Service, Glacier Bay National Park.

Luettich, R. & Westerink, J. 1991 A solution for the vertical variation of stress, rather than velocity, in a three-dimensional circulation model. *International Journal for Numerical Methods in Fluids* **12**, 911–928.

Mofjeld, H., Venturato, A., Gonzales, F., Titov, V. & Newman, J. 2004 The harmonic constant datum method: options for overcoming datum discontinuities at mixed-diurnal tidal transitions. *Journal of Atmospheric and Oceanic Technology* **21**, 95–104.

Royer, T. 1979 On the effect of precipitation and runoff on coastal circulation in the Gulf of Alaska. *Journal of Physical Oceanography* **9**, 555–563.

Simmons, H. 1996 Estimation of freshwater runoff into Prince William Sound using a digital elevation model. Master's thesis, Univeristy of Alaska Fairbanks, Fairbanks, Alaska.

Syvitski, J., Burrell, D. & Skei, J. 1987 *Fjords: processes and products*. New York: Springer-Verlag.

Wang, J., Jin, M., Musgrave, D. & Ikeda, M. 2004 A hydrological digital elevation model for freshwater discharge into the Gulf of Alaska. *Journal of Geophysical Research* **109**, doi:10.1029/2002JC001430.

Wiley, J. & Curran, J. 2003 Estimating annual high-flow statistics and monthly and seasonal low-flow statistics for ungaged sites on streams in Alaska and conterminous basins in Canada. *Tech. Rep.*. United States Geological Survey, water Resources Investigations Report 03-4114.